EFF-DOC-552

Final Report for Contract

ERB 5000

CT 95 0068 NET

Evaluation of all important neutron cross sections for ^{9}Be and evaluation of the secondary neutrons from the interaction of neutrons with Be in the neutron energy range from 10^{-5} eV - 20 MeV

V. Pronyaev, S. Tagesen and H. Vonach

Institut für Radiumforschung und Kernphysik,

Universität Wien

Table of Contents

1. Abstract

Evaluated cross sections and their covariances were derived for the cross sections σ_t, $\sigma_{n,2n}$, $\sigma_{n,\alpha 0}$, $\sigma_{n,p}$, $\sigma_{n,d}$ and $\sigma_{n,t}$ of Be, which form a complete set of basic non-redundant cross sections, for the whole neutron energy range 10^{-5} eV to 20 MeV. The evaluation was performed using the code GLUCS based on the Bayesian approach in the same way as our previous work on ^{56}Fe and ^{52}Cr. In addition to the experimental data base on the mentioned basic cross sections, experimental data on σ_{el}, σ_{nonel} and $\sigma_{He\text{-}prod}$, which can be expressed as linear functions of the basic cross sections were also included in the evaluation.

In addition to the cross section evaluation an evaluation of the energy and angular distribution of the secondary neutrons was also performed. For this purpose the energy and angular distributions of all partial reaction channels contributing to the secondary neutron production (neutron inelastic scattering followed by further neutron decay of ^{9}Be levels, (n,α) reactions followed by two neutron breakup of ^{6}He and various other three-body breakup reactions) were investigated and their energy and angular neutron distributions calculated in the laboratory system. Using this information, the total secondary neutron energy and angular distribution was expressed as sum of the distributions for all reaction channels weighted according to their cross sections, which were used as fit parameters to adjust the calculated distributions to the experimental data existing at three energies (5.9, 10.1 and 14.1 MeV). For this purpose the mentioned code GLUCS, after some modification, could also be used. As a result of this process it was possible to reproduce the experimental data within their uncertainties by our model calculations and to derive a set of partial (n,2n) cross sections and their covariances at the mentioned energies. By suitable inter- and extrapolation procedures (guided by theory) subsequently such partial reaction cross sections were derived for the whole energy range from the (n,2n) threshold to 20 MeV. Using these cross sections the energy and angular distribution of the secondary neutrons was calculated for the whole energy range of the evaluation.

The results of the cross section evaluation were transformed into corresponding ENDF-6 formatted files (file 3 and file 33 for our set of basic cross sections) and the results of the evaluation of the energy-angle distribution of the secondary neutrons were transformed into a file 6 referring to the total (n,2n) cross section (MT 16) as this process is the only source of secondary neutrons for ^{9}Be.

2. Evaluation of the neutron cross sections of ^{9}Be including complete covariance information

2.1. General evaluation procedure

The general principle of our evaluation is essentially the same as used in (Vonach 92). For better understanding of this report we will nevertheless give a short description of this procedure; it is shown schematically in Fig. 1. As the starting point we use either an experimental data set covering the whole energy range of the evaluation or a so-called "uninformative prior" that is a prior, which has negligible influence on the evaluation result due to its very large assigned uncertainties (see next section for details). This constitutes our prior knowledge of the neutron cross sections of Be. For each type of cross section this prior is represented by a cross section vector T and its covariance matrix M. Then Bayes' theorem is used to add successively the experimental data for the various ^{9}Be cross sections to the respective prior. This is done in the following way: If the data are described by a vector R with the covariance matrix V, application of Bayes' theorem results in the following relations for the improved cross sections T' and the covariances M'

$$T' = T + MG^{+}(GMG^{+} + V)^{-1} (R-R_T) \qquad (1)$$

$$M' = M - MG^{+} (GMG^{+} + V)^{-1} GM, \qquad (2)$$

where R_T presents the prior value interpolated at the point where R is given, G is the sensitivity matrix of the new experimental data relative to the prior data with the matrix elements $g_{ij} = \delta R_i/\delta T_j$, and the superscript (+) means transpose and (-1) inverse operation. One of the most important conditions for obtaining these formulae is an absence of correlations between the data vectors T and R. This condition is fulfilled as will be discussed in the next section.

From this procedure (depicted at the left side of Figure 1) we get a set of improved cross sections and their covariances. Cross sections for which no experimental data exist ($\sigma_{n,\gamma}$) remain unchanged. The procedure of independent adjustment of individual reactions is, however, only permitted if there are no known correlations between reactions and, moreover, the reactions under consideration are linear independent. Therefore all data and reactions, which do not fulfill these requirements, have to be considered in a second step. For this

purpose the set of independent cross sections (see Figure 1) is selected as the new prior whereas the remaining redundant cross sections (which can be expressed as linear functions of the basic cross sections) are used as "data" for application of the equations 1 and 2.

Thus the evaluations proceed in the following steps:

1) Establishment of the prior data for all cross sections of interest.

2) Establishment of the experimental data base.

3) Calculations of the improved cross sections T' and covariances M' for all important independent cross sections for which data are available.

4) Performing a constrained least - squares adjustment of the results obtained at step 3 with data which have to be considered redundant. This leads to a final result of the evaluation in form of a cross section vector T' containing a complete set of independent cross sections and one large covariance matrix M' which can be subdivided into covariance matrices for the individual cross sections and covariance matrices between different cross section types (interreaction covariance matrices). In addition full consistency of all data is established and uncertainties of the independent reactions are further reduced.

Technically this procedure is performed by means of the code GLUCS (Hetrick 80) which implements Equ. (1) and (2) and provides output on T' and M' directly in ENDF-6 format. As modified recently (Tagesen 94) it can also be used for the constrained least - squares adjustment of step 4 of our evaluation procedure.

2.2. Establishment of the prior information for all cross sections of interest

In order to rely as much as possible on experimental information we decided to use experimental data sets as prior in all cases where at least one data set of good quality covering the whole energy range of the evaluation was available. In all other cases we decided to use the results of the ENDF/B-VI evaluation which have also been adopted in EFF-2 for our prior cross section vectors, and to combine it with a covariance matrix M corresponding to very high (100%) uncertainties in order to obtain a so-called uninformative prior, that is to have a prior which practically does not influence the evaluation results. In this way the independence of the prior and the data is either guaranteed by the independence of the different experimental data sets or unimportant in the case of the "uninformative" priors. In detail our prior was constructed in the following way:

1) The cross sections σ_t, $\sigma_{n,2n}$, $\sigma_{n,\alpha 0}$, $\sigma_{n,p}$, $\sigma_{n,d}$ and $\sigma_{n,t}$ are used as our set of basic cross sections; all other cross sections (e.g. σ_{el}, σ_{non}) can be derived as linear functions of these basic cross sectons. $\sigma_{n,2n}$ is considered as the cross section for all processes which result in the decay of ^{9}Be + n into 2 neutrons and 2 α-particles thus it includes inelastic scattering as all excited levels of ^{9}Be eventually decay into one neutron and two α-particles.

2) For the cross sections σ_t and $\sigma_{n,t}$ experimental data sets covering the whole energy range and their covariances were used as priors, for $\sigma_{n,2n}$, $\sigma_{n,\alpha 0}$ and $\sigma_{n,p}$ we used the ENDF/B-VI results in form of "uninformative priors" as discussed before; for $\sigma_{n,d}$ we have only one data set covering however the complete energy range. Therefore in this case we directly adopted these results as the evaluated (n,d) cross sections for the first step of the evaluation (see Figure 1).

3) Concerning the energy grid of the evaluation a different procedure was used for the total cross sections and for the rest of the cross sections.

The total cross sections were evaluated in an energy grid of 0.5 MeV energy groups up to 15 MeV and 1 MeV groups between 15 and 20 MeV and the evaluated quantities are the group cross sections averaged within these bins. Above about 4.5 MeV these group cross sections are practically identical to the point cross sections at the center of the energy group. In the low energy range the group cross sections are a rather crude description of the cross section shape because of the existing resonance structure. For this reason in our final evaluated file 3 (see section 2.7.) for σ_{tot} the resonance structure of the cross section is taken into account by using the high-resolution results of (Bilpuch 61) and (Schwartz 71) normalized to the group cross sections derived in this evaluation.

For all other cross section types energy grids were chosen which allow an adequate desciption of the cross section as function of energy by linear interpolation. For this purpose a rather fine energy grid (0.1 - 0.2 MeV) was chosen in those energy ranges where the cross sections exhibit a strong energy dependence and otherwise the standard group structure (0.5 MeV up to 15 MeV and 1 MeV above 15 MeV) was used. Such individual energy grids (see section 2.4.2. and 2.4.3.) were used for $\sigma_{n,2n}$ and $\sigma_{n,\alpha 0}$ in the energy regions between threshold and 3.0 MeV where these cross sections exhibit a strong energy dependence. For the small and less well-known cross sections $\sigma_{n,p}$, $\sigma_{n,d}$ and $\sigma_{n,t}$ only the standard energy grid was used.

2.3. Establishment of the experimental data base including construction of covariance matrices for all data sets

We used the experimental data compiled in EXFOR (Lemmel 86, McLane 88) and supplemented them by very recent ones which were mostly obtained directly from the authors. All data sets were critically reviewed; obviously wrong data were rejected. The accepted data were renormalized if necessary with regard to the standard cross sections or decay data used. In some cases renormalizations were also applied if comparisons of a data set with other data consistenly indicated the need for such renormalizations. Differential elastic scattering cross sections measured over a sufficient angular range were used to derive the total elastic scattering cross sections by means of fits with Legendre polynomials in those cases where the integrations had not been performed by the authors.

For the construction of the covariance matrices of the experimental data sets it is necessary to have detailed information on all uncertainty components of the measurements and the correlation of each component within the data set. As this information is not given for most of the experiments the following approximation had to be used.

We assumed that the covariance matrix of total uncertainties can be split into three matrices of partial uncertainties:

1) a diagonal covariance matrix of partial uncertainties describing short-energy-range (SER) correlation properties such as statistical uncertainties due to a finite number of counts per channel;

2) a covariance matrix of partial uncertainties connected with properties that give rise to medium-energy-range (MER) correlations, such as uncertainties due to the correction for the dead time and to the determination of the detector efficiency, the effect/background separation, multiple scattering and scattering at the collimator, the spectrometer resolution function and neutron source properties. For this covariance matrix the correlations between the uncertainties for different energy groups are described by a linear model of correlation propagation with a certain correlation energy Ec (typical 2 MeV) within which the correlation decreases linearly from 100% to zero.

3) a constant covariance matrix of partial uncertainties connected with properties which induce large-energy-range (LER) correlations, such as systematical uncertainties due to any normalization of the cross sections in order to get absolute values, to the determination of the number of nuclei in a sample, to geometrical sizes and distances and to sample self-absorption

properties for the non-resonance energy region. This means we assume complete correlation over all energy groups for these long-range uncertainty components.

The magnitudes of the described three components were chosen according to the uncertainty information given by the authors; in the assessment of the medium-energy-range correlations (both magnitude of MER uncertainties and correlation energy Ec) also the deviations between the different data sets were taken into account.

All steps deriving the experimental data base according to the procedures outlined here are described comprehensively in section 2.4., where the evaluation of the different types of cross sections is treated in detail. The cross section values and their covariances derived in this way cannot be given in this report, they are, however, available on request at our institute.

2.4. Evaluation of the cross sections for the individual reactions

2.4.1. Total cross sections

A summary on the experimental data base is given in Table 1. The table shows the energy range of each data set, the number of data points* (after averaging into our group structure) and the size of the various uncertainty components assigned to the data for construction of the covariance matrices. The data sets (Bilpuch 61) (0.053 - 5 MeV) and (Schwartz 71) (0.5 - 20 MeV) considered as uncorrelated and covering the whole energy range of the evaluation were used as prior. All data sets, for which this was possible, were averaged over the group structure shown for the evaluation. In addition in the energy range above 5 MeV a number of point cross sections were also accepted for the evaluation as discussed in section 2.2. SER and LER uncertainties were evaluated from the information given in the papers or (if information on LER uncertainties was missing) were assigned by us. The MER uncertainties for each data set were estimated from deviations between the average from all data sets and the given data set both smoothed to a resolution of about 2 MeV. This procedure was also used for the construction of the covariance matrix for all other cross section types described in the next subsections.

* Actually the number of data points means either the number of group cross sections derived from the data or the number of point cross sections for those data sets, which could not be averaged.

2.4.2. (n,2n) cross sections

As already discussed the ENDF/B-VI evaluation was used as prior in an energy bin structure adjusted to the shape of the (n,2n) excitation function (see Table 9 and Fig. 6). The covariance matrix can be considered as uninformative due to the large values of the uncertainties assigned by us.

The experimental data accepted by us are summarized in Table 2. In the energy range above about 3.5 MeV there is good agreement between all existing measurements and also between the direct measurements covered in this section and the redundant cross sections σ_{non} and σ_{el}, discussed later. In the energy range between threshold (1.74 MeV) and 3.5 MeV however there exists a serious discrepancy between the rather accurate measurements of Holmberg and Hansen (Holmberg 69) on the one hand and the later work of Bloser (Bloser 73) and also some measurements of σ_{non} by the sphere transmission method (Eaton 68). From careful study of the papers it appears to us that the results of Holmberg 69 are probably correct within the stated uncertainties, whereas the data of Bloser and also the mentioned sphere transmission results must suffer from large unidentified systematic errors. Accordingly we decided to base our (n,2n) evaluation in the low energy range entirely on the data of Holmberg 69 as apparent from Table 2.

2.4.3. (n,α_0) cross sections

As in the (n,2n) case the ENDF/B-VI evaluation combined with a covariance matrix with very large uncertainties was chosen as uninformative prior. The energy grid for the evaluation was adjusted to the shape of the excitation function so as to allow an adequate description of the cross section by linear interpolation. Accordingly energy steps of 0.1 and 0.2 MeV were used below E_n = 3 MeV and our standard grid above this energy (see Table 13 and Fig. 7).

A summary of the data is given in Table 3. The most important information on the (n,α_0) cross section is the work of Stelson and Campbell (Stelson 57). In this work three relative excitation functions covering the energy range from threshold to 4.43 MeV and six absolute cross section measurements in the energy range 2.26 - 4.41 MeV are reported. As all three measurements of excitation functions are strongly correlated by means of a common neutron flux measuring system (long counter) they were combined into one data set for this evaluation. The short range uncertainties for these relative cross section measurements not given by the

authors were estimated from the fluctuations of the data around a smooth curve and the MER uncertainty was chosen according to our estimation on typical uncertainties in the energy dependence of the efficiency of long counters. Likewise the six absolute measurements of (Stelson 57) were combined into one data set as they do exhibit considerable correlations due to the use of common measuring systems for β-counting and/or neutron fluence measurement. Due to the detailed description of these measurements in the paper it was possible to directly construct a covariance matrix without the approximation of SER, MER and LER uncertainties (see Table 3).

2.4.4. (n,t) cross sections

The ^{9}Be(n,t) cross section was usually measured by extraction of tritium and by measuring its activity. It means that measured values are tritium production cross sections, but not (n,t) cross section in usual understanding. Part of this cross section, at least for E_n > 15 MeV belongs to multiparticle emission such as (n,t(α,t)). The data from EXFOR 22035 (Liskien 88) covering the whole energy region were used by us for the construction of the prior. For this they were transformed into our group structure and a covariance matrix was generated with uncertainties of partials given in Table 4. Six data sets were selected for evaluation (see Table 4). General χ^2 is 0.45.

2.4.5. (n,d) cross sections

Only one experimental data set practically covering the whole energy range up to 20 MeV exists for this reaction (EXFOR 20833, Scobel 70). The data were obtained by the activation method. Because only the ground state is stable relative to particle decay, the (n,d) reaction includes only one partial channel (n,d_0). Therefore the cross section data for this experiment together with the covariance data constructed from the uncertainty information of (Scobel 70) was directly used as the evaluated (n,d) cross section. For the covariance matrix LER and MER uncertainties of both 5% are assumed and 2 MeV correlation linear dumping width.

2.4.6. (n,p) cross sections

An ENDF/B-VI group averaged cross section with a non-informative covariance matrix of uncertainties was taken as prior. Three experimental data sets were selected for the evaluation (see Table 5). The data for EXFOR 10632 (Rosario-Garcia 77) have been obtained by means of a very crude angular distribution integration procedure. Due to the accuracy of the selected experimental data, the final uncertainty for the evaluated data became small only near 14 MeV. The general χ^2 is 0.28.

2.5. Data base for redundant cross sections

Apart from the discussed data for our basic set of independent cross sections there exists a large body of rather accurate experimental data of so-called redundant cross sections. These cross sections (σ_{el}, σ_{non}, $\sigma_{He\text{-}prod}$) are related to our basic cross sections by the relations

(3) $\sigma_{non} = \sigma_{n,2n} + \sigma_{n,\alpha 0} + \sigma_{n,p} + \sigma_{n,d} + \sigma_{n,t}$

(4) $\sigma_{el} = \sigma_{tot} - \sigma_{non}$

(5) $\sigma_{He\text{-}prod} = 2\sigma_{n,2n} + \sigma_{n,\alpha 0}$

Because the (n,2n) cross section is much larger than all other cross sections all the redundant cross sections listed in equ. 3 - 5 give valuable information on the important (n,2n) cross section (especially σ_{non} which has been determined rather accurately by means of the so-called sphere-transmission method). Thus these cross sections were included into the evaluation with the main purpose to improve the quality of the evaluated (n,2n) cross section.

A summary on the existing data for σ_{el} is given in Table 6. Legendre fits by means of the code GPOLFIT (Pavlik 90) were used to integrate differential elastic cross sections for which this integration had not been done by the authors themselves.

Only elastic cross sections for neutron energies above 4.5 MeV were used in the evaluation for the following reason. All measurements of total elastic scattering are point data, thus application of equ. 4 demands that also σ_t is available at the corresponding energy point. Our total cross sections however are evaluated as group cross sections in our 0.5 MeV/1.0 MeV energy grid. As already discussed this difference becomes negligible above 4.5 MeV and the total cross section at any energy can be derived accurately by linear interpolation. Below E_n =

4.5 there is considerable resonance structure in the total cross sections and thus point cross sections in this energy range cannot be derived from the evaluated group cross sections and thus equ. (4) cannot be used.The loss of information due to the neglect of the low-energy elastic data, however, is rather small as in this energy region the elastic cross section is the dominant one. Thus it can be derived more accurately from the total cross sections and the partial reaction cross sections than from the direct measurements of σ_{el}.

The data base for σ_{non} is summarized in Table 7. All data sets existing in the literature were accepted with exception of the results of (Eaton 68) and (Weaver 74) for neutron energies below 3 MeV, as these data strongly contradict the (n,2n) measurements of (Holmberg 69) (see discussion in section 2.4.2.) and also because the sphere transmission method used for the measurement of σ_{non} is subject to large systematic errors in the region of the strong elastic scattering resonances in ^{9}Be (E_n = 2.75 MeV) where these discrepant data points are located. Only one measurement (Kneff 86) exists for $\sigma_{He\text{-}prod}$ at E_n = 14.9 MeV.

2.6. Consistent joint evaluation of all cross sections

As the final step of the evaluation (see right side of Figure 1) an improved evaluation using the information contained in both our basic and redundant cross sections was obtained in the following way: The redundant cross sections (see section 4.2.) were added as „data" of sums or differences of basic cross sections according to equ. 3 - 5 again using the code GLUCS based on equ. 1 and 2 (see section 2). Technically all accepted redundant cross sections (see section 4.3.) of all types were added as one large data vector to the prior consisting of the coupled set of all basic cross sections in one GLUCS run.

Because of the conditions (3 - 5) and the consideration of all basic cross sections as one coupled set the resulting correlation matrix now includes parts which describe correlations between different energy intervals of different cross sections. These correlations are generally small (< 10%), only between total and (n,2n) and (n,2n) and (n,α) they are important and have to be taken into account.

2.7. Results of the evaluation

The main result of this evaluation is a complete non-redundant set of cross sections (σ_{tot}, $\sigma_{n,2n}$, $\sigma_{n,\alpha 0}$, $\sigma_{n,p}$, $\sigma_{n,d}$ and $\sigma_{n,t}$) and their covariances in the neutron energy range 10^{-5} eV - 20 MeV in the group structure discussed in section 2.2. In addition, cross sections and covariances for σ_{el} and σ_{non} were obtained by expressing these cross sections as linear functions of the basic cross sections (see equations 3 - 4). In the Tables 8 - 13 the final results of this evaluation, i.e. the cross sections and their uncertainties, are listed. There is, however, some difference in the meaning of the listed cross section values between σ_{tot} and σ_{el} on the one hand and all the other cross sections. Due to the special evaluation procedure used for σ_{tot} (see section 2.4.1.) the evaluated cross sections are group cross sections averaged over the bins of our 35 bin structure. As σ_{el} was essentially derived as difference between σ_{tot} and all other cross sections, also the listed σ_{el} values are essentially group-averaged cross sections. All other cross sections, however, are point cross sections, as their priors are the point cross sections and also the added data are approximately point cross sections. This difference however is only of importance in the energy range below 4 MeV, for higher energies both σ_{tot} and σ_{el} are smooth functions of energy and the listed values can also be considered as point cross sections at the respective energy bin centers. In the energy region below 4 MeV the known fine structure of the total (and elastic) cross sections was superimposed on our evaluated group cross sections for an accurate description of σ_{tot} in file 3 of our evaluated data file, while retaining our course group structure in the description of the covariances in file 33 (see section 2.8.).

These results are also presented in the Figures 2 - 9. Each figure shows the experimental data base, the evaluated cross sections and their uncertainties and for comparison also the results of the ENDF/B-VI evaluation.

The results of this evaluation may be summarized as follows:

1) The evaluated cross sections will probably meet most requirements of fusion and fission technology. Typical uncertainties are less than 1% for σ_t, $\approx$ 2% for σ_{el}, $\approx$ 3% for $\sigma_{n,2n}$ and $\sigma_{He\text{-}prod}$ at 14.1 MeV and 5% otherwise. The uncertainties derived in this evaluation are conservative estimates for several reasons. The uncertainty estimates given by the authors have been increased whenever there was some doubt that they may have been underestimated. In all steps of the evaluation χ^2 per degree of freedom remained well below unity. Finally we have not made use of the fact that the cross sections (at least in the energy range above 4 MeV) are smooth functions of neutron energy, that is we have used rather weak correlations in

our prior which also leads to an overestimate of the uncertainties. Thus we believe that the stated uncertainties are rather somewhat too large than too small.

2) In general our evaluated cross sections are in very good agreement with the ENDF/B-VI evaluation. For $\sigma_{n,2n}$, $\sigma_{n,\alpha o}$, $\sigma_{n,p}$ and $\sigma_{n,d}$ both evaluations agree well within the uncertainty of our evaluation. For $\sigma_{n,t}$ there is also very good agreement in the practically important range up to 15 MeV, at higher energies our values are about 10-15% higher, due to new data included in our evaluation. Only for σ_t the ENDF/B-VI cross sections do show some deviations (up to 5%) which are well outside the uncertainty band of our evaluation. It also appears (see Fig. 3) that the structures of σ_t in the high energy range of the ENDF/B-VI evaluation may not be real.

3) In spite of the rather satisfactory result of the evaluation new cross section measurements would be desirable for the following reason.

Only one experiment (Holmberg 69) exists for the important (n,2n) cross section near threshold and for $\sigma_{n,\alpha o}$ between threshold and 4 MeV (Stelson 57). Although both experiments have been performed very carefully and are well documented, it does not appear completely safe to base an evaluation on only one data set. Thus new measurements of these specific cross sections should be performed. On the other hand at En = 14.1 MeV where a large number of measurements have been performed for most cross sections it appears unlikely that the uncertainty of the evaluated cross sections could be reduced by additional experiments.

2.8. Construction of files 3 and 33 for the evaluated cross sections

Generally the output of the computer code GLUCS can directly be used for assembling MF3 and MF33. In our ^{9}Be evaluation special treatment was only necessary for the total neutron cross section MT1. In the incident neutron energy range up to 4.5 MeV the cross section exhibits considerable structure, which is well established in the measurements of (Bilpuch 61) and (Schwartz 71). For the least-squares adjustment procedure it is, however, very impractical to treat the full original data sets with several thousand data points each. The adjustment was therefore done with group average values spanning a 500 keV neutron energy range each. Next, the adjustment factors calculated by GLUCS were used to scale the experimental points to the evaluation results. Finally a thinning and smoothing procedure combining at least 5 data points was applied, to get a good representation of the existing structures without reflecting large statistical fluctuations.

Thus the complete excitation function was assembled in the following way:

incident neutron energy range	data source
10^{-5} eV - 10 keV	ENDF/B-VI
24 keV	experimental point (Aizawa 83, Block 75)
55 keV - 490 keV	Bilpuch 61, thinned to 5 keV steps
500 keV - 1.4 MeV	Schwartz 71, thinned to 5 keV steps
1.4 MeV - 3.0 MeV	Schwartz 71, thinned to 10 keV steps
3.0 MeV - 4.5 MeV	Schwartz 71, thinned to 25 keV steps
4.5 MeV - 20 MeV	GLUCS results, .5 MeV group averages

This total cross section is shown in detail in Fig. 10 - 13. As apparent from the figures there are some significant changes compared to ENDF/B-VI.

3. Evaluation of the energy-angle distribution of the secondary neutrons from the interaction of fast neutrons with ^{9}Be

3.1. General outline of the evaluation procedure

The total (n,2n) cross section of ^{9}Be is the sum of a rather large number of reaction channels (s. section 3.3.1.) which have quite different energy- and angular distributions (s. Fig. 15 - 44). For most of these reaction channels the energy and angular distribution in the laboratory system can be calculated reasonably well from some plausible assumptions on the reaction dynamics and the kinematics of the reactions. The cross sections for these partial reaction channels are less well known; only the strongest channel, inelastic scattering to the second excited level has been measured rather accurately, whereas the importance of many other channels, especially three- or four-body breakup processes, is still not known.

Thus it is the obvious procedure, to fit the measured double-differential neutron emission cross sections by a sum of the double-differential cross sections for the individual reaction channels, whereby the shapes of the energy- and angular distributions are kept fixed at their theoretically calculated values and the cross sections for the various reaction channels are used as fit parameters with the constraint that the partial cross sections sum up to the experimentally determined total (n,2n) cross section and also the known experimental information on the cross sections of a few of the channels is taken care of.

Most previous evaluations of the secondary neutron emission cross sections (Perkins 85, Shibata 96) have followed this scheme, however the fitting was mostly done by qualitative inspection of calculated versus experimental double-differential neutron emission cross sections and also the number of reaction channels included in the analysis was often rather restricted (e.g. neglect of all three-body breakup channels). In this evaluation it is attempted to avoid these short-comings by considering all reaction channels which may be important and to derive an optimum set of partial reaction cross sections by a quantitative least-squares fit of the experimental data base to a sum of partial reaction cross sections of given shapes in energy-angle space. For this purpose we first establish a so-called prior that is a set of double-differential partial (n,2n) reaction cross sections

$$(6) \qquad \left(\frac{d^2\sigma}{dE_{n'}d\Omega}(E_{n'},\Theta)\right)_i = \sigma_i f_i(E_{n'},\Theta)$$

whereby the f_i are kept fixed to their theoretically calculated values and a first guess is made for the partial cross sections σ_i from the existing experimental and theoretical information on these channels. This prior is then compared to the experimental data and improved values of σ_i are calculated by minimizing the quantity

$$(7) \qquad \sum_j \left[\frac{d^2\sigma_{exp}}{dE_{n'}d\Omega}(E_{n'},\Theta)_j - \sum_i \sigma_i f_i(E_{n'},\Theta)_j \right]^2$$

whereby $(E_{n'},\Theta)_j$ means a special combination of E_n and Θ and the summation has to be performed over the whole experimentally available range of $E_{n'}$ and Θ. This least-squares fitting is done by means of the code GLUCS based on the Bayesian approach which was originally designed for least-squares fitting of integral cross sections but can also be used for the described task. In the following sections we first describe the experimental data base, general properties of the various reaction channels, the calculation of the neutron energy- and angular distribution for the various channels and the choice of the "prior" set of partial cross sections selected as starting point of the least-squares analysis and finally give the results. According to the availability of experimental data such fits could be obtained for three energies, 5.9, 10.1 and 14.1 MeV and therefore suitable interpolation and extrapolation procedures have been used to obtain the partial cross sections $\sigma_i(E_n)$ for the full range of neutron energies from the respective threshold to 20 MeV.

3.2. Experimental data base

Double differential neutron emission cross sections for the secondary neutrons from the interaction of fast neutrons with ^{9}Be have been measured as function of secondary neutron energy and emission angle at incident energies of 5.9 MeV, 10.1 MeV and 14.1 MeV by the time-of-flight technique (Drake 77, Baba 88, Takahashi 87) using monoenergetic neutron sources. In addition such measurements have been performed at a number of energies in the range 2 to 11 MeV using the white neutron beam at the Geel Linac by means of the unfolding technique of the pulse spectra measured in organic scintillators (De Kempeneer 92). For this evaluation only the data obtained by the time-of-flight method were used as only for those the needed covariances could be estimated easily from the uncertainty information given in the respective papers, whereas the unfolding procedure used in (De Kempeneer 92) probably

created large correlations between the uncertainties for the cross sections for different secondary energies for which we had no information.

Therefore the Geel data were not used directly in the least-squares adjustment procedure, they were however used to check the quality of our results at energies below and between the three energy points of the time-of-flight experiments.

Thus the data base used for the least-squares adjustment process consisted of three data sets of $\delta^2\sigma/\delta En'd\Theta$ values at E_n = 14.1 MeV (Drake 77, Baba 88 and Takahashi 87) and one data set (Drake 77) for both E_n = 10.1 MeV and E_n = 5.9 MeV. Comparison of the three data sets obtained for 14.1 MeV incident neutron energy showed reasonable overall agreement, however also some definite discrepancies.

1) The data of Drake 77 at 25° are considerably larger than both the Baba and Takahashi data, this is probably due to „impurities" in Drake's source spectrum as even small admixtures of low energy neutrons to a monoenergetic neutron beam produce large effects at forward angles (large cross sections for elastic scattering of the „impurity" neutrons). For this reason the data of Drake 77 at 25° were not used.

2) There is a discrepancy between the data of Takahashi and Baba 88 in the energy range $E_{n'}$ = 7 - 9 MeV at several forward angles (see also Fig. 61 - 63). This discrepancy is probably due to the fact that the Takahashi data are too low because of too large corrections for the low energy tail of the source-spectrum, the uncertainty of which was probably underestimated in the uncertainty analysis. Therefore we increased the uncertainties in Takahashi 88 in the discussed $E_{n'}$ range in order to obtain consistency with the other data sets.

In our least-squares procedure we used the double-differential cross sections from the mentioned three data sets in the secondary neutron energy range from 0.5 MeV to the onset of the discrete peak due to neutrons inelastically scattered from the narrow 2.46 MeV level in ^{9}Be (see Figures 45 - 67). Within this energy range the double-differential cross sections were collapsed into a 0.5 MeV group structure in $E_{n'}$. A total number of 378 experimental data points were used at three incident energies of 14.1, 10.1 and 5.9 MeV.

3.3. Preparation of the prior for the evaluation

3.3.1. Summary on the properties of the partial reaction channels contained in the total (n,2n) cross sections

The various reaction channels contributing to the reaction $^{9}Be \rightarrow n + n + \alpha + \alpha$ can be described as chains of sequential two-body and three-body breakup reactions. In principle also four-body breakup into $2n + 2\alpha$ is possible, but its cross section is probably very small. For characterization of such reactions we will use the following notation:

T(a,1 2 ... n) for the reaction of target T with particle a resulting in a breakup into n particles. In our case n will only be 2 (two-body reaction) or 3 (three-body breakup). In case of further decay of one or two of the reaction products the corresponding particle will be replaced by a bracket showing ist decay products e.g. T(a,1(3,4))) which means a two-body reaction followed by further decay of particle 2 into particles 3 and 4. In this way a very complicated sequential tree of reactions can be uniquely characterized.

In our case of $^{9}Be + n$ the following reaction types contribute to the total (n,2n) cross sections:

1) Sequential two-body reactions

a) $^{9}Be(n,n_i'(n''(\alpha\alpha)))$

Neutron inelastic scattering with excitation of i-th level of ^{9}Be with a following neutron decay of this level to a level in ^{8}Be, which subsequently decays to 2 α-particles.

b) $9Be(n,n_i'(\alpha(n''\alpha)))$

Inelastic scattering with excitation of i-th level of ^{9}Be with following emission of an α-particle leaving ^{5}He either in its ground or first excited state with subsequent decay of the ^{5}He into a neutron and α-particle.

c) $^{9}Be(n,(n'\alpha)(n''\alpha))$

Decay of the composite system $^{9}Be + n$ into two ^{5}He nuclei with subsequent two-body breakup of each ^{5}He into a neutron and an α-particle.

d) $^{9}Be(n,\alpha(n'(n''\alpha))$

Reaction to first and higher excited levels of ^{6}He followed by two sequential neutron emissions.

2) Various combinations of two-body and three-body breakup reactions

a) $^{9}Be(n,n'n''(\alpha\alpha))$

Three-body breakup of ^{9}Be + n into two neutrons and ^{8}Be followed by breakup of ^{8}Be into 2 α-particles.

b) ^{9}Be(n,n$_i$'(n'αα))

Inelastic scattering with excitation of i-th level with a following three-body decay of ^{9}Be into one neutron and two α-particles.

c) ^{9}Be(n,n'α(n"α))

Three-body decay into neutron, α-particle and ^{5}He followed by two-body breakup of ^{5}He.

The energy and angular distributions of the neutrons emitted in the listed reactions depend primarily on the properties of the various levels of ^{9}Be, ^{8}Be, ^{6}He and ^{5}He which are populated in these reactions, especially their positions, widths and decay properties. Therefore these quantities have been carefully compiled and evaluated. The level properties chosen in this way for our evaluation are summarized in Tables 15 and 16 and visualized in Fig. 14. Table 15 gives the decay properties for excited levels in ^{9}Be up to an excitation energy of 20 MeV and Table 16 gives the corresponding quantities for ^{8}Be, ^{6}He and ^{5}He and in addition the groundstate Q values for the formation of these residual nuclei from ^{9}Be + n.

The following comments should be taken into account considering the content of Table 15:

1) The Table contains all ^{9}Be levels which can be excited by neutrons with energy up to 20 MeV. But practically, the inelastic scattering cross sections for excitation of some levels at definite energy of neutrons can be negligible.

2) The data have been taken mainly from (Ajzenberg-Selove 88). But because the (Ajzenberg -Selove 88) evaluation does not contain all the needed branching ratios (BR's) and because new data appeared, the reasoning for revision or assigning of missing values is given below under detailed comments.

3) Gamma decay widths known for a few levels are at the level a few eV, which is many orders of magnitude less than "heavy" particle decay widths and for this reason may be excluded from consideration. Gamma production cross section measurements also show their negligible role.

4) α-widths of decaying states of ^{9}Be increase sharply with excitation energy, and as a result, BR for the α-decay modes may be substantial when neutron widths are for any reason small.

5) Neutron widths are definitely small for high l-transitions (l more than 2). Neutron widths for most of s-, p- and d- neutron decays are at the level of a few hundred keV.

6) Because leaving empty spaces (putting zeros) in the table of branching ratios is anyway a very definite assignment we prefer to use the above mentioned simple physical considerations for possible decay widths.

7) Given BRs were determined in different reactions where particular ^{9}Be states are excited and may depend on the involved reaction mechanism and energy.

8) The model cross section calculations may also influence the determination of BRs. They are all based on optical model wave functions or transmission coefficients. This description may fail for some light nuclei due to prominent resonance structure in the cross section up to high energy (non-overlapping resonances). It seems however, that this is not the case for all important ^{9}Be+n reaction channels (large decay widths).
Detailed Comments to Table 15, concerning the choice of the BRs for each level, are given immediately after the table.

3.3.2. Calculation of the partial energy-angle distributions for all reaction channels

The energy and angular distribution of neutrons in any of the partial reaction channels discussed in the preceeding section is determined by the reaction characteristics of each reaction step (e.g. decay of some intermediate reaction product) in its c.m. system and the transformation of these c.m. distributions into the laboratory system according to the relatively complicated kinematics of these sequential reactions.
For the c.m. characteristics of the reaction channels we made the simplest assumption compatible with the existing experimental evidence. In detail we assumed the following:
1) In the first step of the reaction we assume isotropy for all two-body decays of the ^{9}Be + n system except inelastic scattering to the levels of the rotational band (levels No. 2, 7 and 10). For these levels the angular distributions measured for the neutrons inelastically scattered by the second excited level of ^{9}Be (E* = 2.43 MeV) (Hogue 78) (see Table 17) were used.

2) The further two-body decay of any composite particle (e.g. ^{5}He) formed within one of the reaction channels is assumed to be independent of its formation mode, that means isotropy in the c.m. system (in which the decaying particle is at rest) is assumed.

3) The three-body decay of the 2.43 MeV level of ^{9}Be has been studied experimentally and its neutron spectrum has been measured by time-of-flight (Chen 70). Due to the Coulomb interaction between the two low-energy α-particles this spectrum differs considerably from the prediction of the free phase-space model used in previous evaluations. We have therefore used the measured neutron spectrum for this decay.

4) For the other three-body decays (^{9}Be + n → n + n'+ ^{8}Be or ^{9}Be + n → n + α + ^{5}He) we have made the simplest assumption, equal emission probability in the three-body phase space. This seems reasonable in the absence of any experimental information, as Coulomb effects are either absent or at least considerably smaller than in the ^{9}Be* → n + n + α case discussed before because of the larger decay energy.

Assumptions 1 - 4 and the information given in Tables 15 - 17 completely determine the energy and angular distribution of the emitted neutrons and α-particles in the corresponding c.m. systems, where the decaying systems are at rest. The corresponding distributions in the laboratory system are obtained by transferring all these decays into the laboratory system taking into account the velocity distributions of the various intermediate reaction products resulting from the preceding reaction steps.

This transformation was performed using a code originally developped by T.D. Beynon and B.S. Sim (Beynon 88) and extended and modified by one of the authors, which is described in more detail in Appendix 1. Using this code the shapes of the double differential neutron emission cross sections were calculated for all partial reaction channels as function of incident neutron energy. Examples of the double-differential energy/angle distributions from the different processes contributing to the ^{9}Be(n,2n) reaction are shown in Fig. 15 - 44 for 14.1 MeV incident neutron energy.

3.3.3. Choice of the partial reaction cross sections for the prior

At least 26 partial reaction cross sections including more than 40 neutron production channels may contribute to the total neutron spectra at 14.1 MeV incident neutron energy (see section 3.3.1.) and a somewhat smaller, however still rather large number of channels has to be considered in principle at the incident energies 10.1 and 5.9 MeV.

A large number of these reaction channels, however, is expected to be very weak and it is obvious that they cannot be extracted from the fit with any meaningful accuracy. In addition the energy angle distributions for several groups of channels are quite similar (see figures 15 - 44). For these reasons priors limited to the channels expected to be important were constructed for each of the three energies in the following way:

1) In order to reduce the number of fit parameters the branching ratios were fixed to the values given in Table 15, and only the partial cross sections for excitation of the various inelastic levels were used as fit parameters.

2) It is known that only channels with excitation of collective levels in neutron inelastic scattering contribute substantially to incident neutrons with energies as high as 14.1 MeV, whereas for lower neutron energies the excitation of other levels through the statistical mechanism can be appreciable. Accordingly for the neutron energies of 5.9 and 10.1 MeV inelastic scattering to all accessible levels in ^{9}Be was included in our prior, whereas at 14.1 MeV a number of weakly excited levels were neglected.

3) Finally some levels differing only slightly in excitation energy e.g. levels 3 and 4 were combined into one channel with the ratios between the level cross sections fixed and only the sum of the cross sections used as fit parameters. In this way the number of channels used to fit the experimental double-differential emission cross sections was reduced to 9, 11 and 9 for 5.9, 10.1 and 14.1 MeV (see Tables 18 - 20).

The prior cross section values and their uncertainties were assigned for each of these channels in the following way: For inelastic scattering through the strongly excited 2nd level an evaluation of the experimental data (also performed by GLUCS) was used. Furthermore the existing rather incomplete experimental information for the (n,α_1) and (n,α_2) reactions (Kropp 70, Ferenc 89) was used for assigning the prior cross sections for these channels with rather high uncertainties. For all other channels the prior cross sections were assigned by taking into account both the results of previous evaluations and theoretical considerations and also taking into account that the sum of all partial cross sections has to add up to the total (n,2n) cross section as evaluated in section 2.4.2. of this report. An uncertainty of 100% was assigned to all these latter channels. The complete information on these priors is given in Tables 18 - 20.

A special correlation matrix with non-diagonal correlation coefficients equal to 0.95 was assigned to the prior energy-angular distribution for each channel. As result of this we got a large freedom for variation of the integral distribution with a simultaneously fixed shape of the calculated energy-angular distributions for each channel in the least-squares' search. Calculations with a correlation coefficient of 0.99 have confirmed that the results of the least-

squares procedure does not depend on the specific value of this correlation coefficient, as long as it is suffiently large, e.g. 95%.

3.4. Evaluation of the partial reaction cross sections at En = 5.9, 10.1 and 14.1 MeV

We have used the GLUCS code for obtaining the posterior evaluation of partial reaction cross sections for three incident energies. For this purpose the continuous variable "energy" was considered as discrete "pseudo-energy" variable which combined the angle number and secondary neutron energy into an independent variable of the double-differential cross section presentation. The prior evaluated and experimental data have to have the same pseudo-energy values to avoid any meaningless interpolation. To provide all this, the double-differential cross sections calculated for each selected partial channel were averaged (taking into account the resolution function of the given experiment) and reduced to the same group structure in the secondary neutron energy as the experimental data. The secondary neutron energy bins used for spectra presentation had a width of 0.1, 0.25, 0.5 and 1.0 MeV (the same as for experimental data, see section 3.2. above).

The results of the least-squares adjustment of the partial reaction cross sections for these incident energies are given in Tables 18 - 20. Some comments are required to these tables:

1) In some cases, especially for En = 5.9 MeV, the adjustment was done rather for a group of levels than for separate levels.

2) The prior uncertainty for the (n,n'α^5He) channel at 10.1 MeV neutron energy was taken as 5%, because 90 mb is a value close to the value interpolated between 5.9 MeV and 14.1 MeV incident neutron energy. If we give more freedom for this channel the posterior evaluated value will be too low for this channel. Probably there is some drawback in the experimental data for 10.1 MeV neutrons caused by the procedure of separation in the discrete levels contribution made by the author (Drake 77).

3) All uncertainties are reduced after the least-squares adjustment in their absolute values, but in relative values they are sometimes increasing.

4) Appreciable contributions of (n,n'α^5He) and (n,α_2) channels, which have not been considered in many previous evaluations are supported by our least-squares analysis.

5) The values of chi-square per degree of freedom obtained in all cases are about unity (see Table 18 - 20). This indicates that all important reaction channels have been included in our prior.

This is also confirmed by direct comparison of the evaluated double-differential cross sections with the experimental data in figures 45 - 67 for all experimental data included in the evaluation. As demonstrated by the figures there is agreement within experimental uncertainties for the whole range of secondary neutron energy and emission angle for each of the three incident energies.

3.5. Calculation of the evaluated secondary neutron energy and angular distributions from threshold to 20 MeV and representation of the results in ENDF-6, MF 6 format

The cross sections for the neutron producing partial channels evaluated by the least-squares procedure for three initial energy points (5.9, 10.1 and 14.1 MeV) have to be interpolated and extrapolated to cover the whole energy range between 2 and 20 MeV (below 1.8 MeV only elastic scattering, (n,α) and (n,γ) reaction cross sections are important.

For this purpose theoretical model calculations have been done for the whole energy range. These calculations are based on the optical model approach with consideration of the two main mechanisms of nuclear reactions, direct and compound nucleus. Although there is some opinion that the optical model in general is not suitable for light nuclei because of the presence of compound and door-way state resonances up to rather high energies, this objection does not seem to be valid for the ^{9}Be target nucleus. Only one resonance at 2.7 MeV neutron incident energy is observed in the cross sections. The other resonances are well overlapping because of large widths of decay into the continuum.

The number of states open and closed in the continuum is rather limited at not too high neutron energy and we have used the strong channel coupling code ECIS87 with a coupling scheme accounting for all channels strongly coupled with the elastic scattering channel. This is - as known - the rotational band based on the ground state with a deformation parameter β = 1.1 (Satchler 67).

Because of the high contribution of three-body break up channels and channels with emission of α-particles in the first step of the reaction, such as (n,α_0, (n,α_1) and (n,α_2) to the total reaction cross section, it was difficult to organize an automatical search of OM parameters (compound elastic and inelastic scattering contributions to the fitted cross sections have to be renormalized with account of break up and (n,α) channels). The contribution of these reactions explains a relatively high imaginary part of about 3 MeV which is required in the

case when the maximum number of channels strongly coupled with the elastic channel are taken into account. These levels are: 0.0 ($3/2^-$) - 2.4294 ($5/2^-$) - 6.38 ($7/2^-$) - 11.283 ($9/2^-$). The compound nucleus mechanism contribution in elastic and inelastic scattering channels was evaluated also by the ECIS87 code (Raynal 84). The OM parameters were determined by a try-and-see method and are given in Table 21 below. The quality of the description of the elastic angular distributions is good. The TNG code (Fu 88) was used to calculate the contribution of the compound nucleus mechanism to the $n_{\alpha 0}$, $n_{\alpha 1}$ and $n_{\alpha 2}$ cross sections taking into account the competition by the breakup and direct inelastic channels. The results of the model calculations are summarized in Table 22. Cross sections for all break up channels used for renormalization of the compound part of the reaction cross section in model calculations and also given in Table 22 are obtained as preliminary evaluation by interpolation and extrapolation through the posterior values obtained by GLUCS for 5.9, 10.1 and 14.1 MeV.

At the next step of the evaluation, the results of the model calculations (Table 22) were adjusted (renormalized) either to the cross sections evaluated earlier (see Chapter 2) or to the GLUCS posterior values. The final evaluation for the partial reaction cross sections was obtained as a compromise between results of model calculations for the neutron energy between 1 and 20 MeV and the GLUCS posterior evaluation results (see Tables 18 - 20) for 5.9, 10.1 and 14.1 MeV and it is given in Table 23.

In order to prepare the evaluation data file (MF = 6) for secondary neutron energy angular distributions, detailed calculations of double-differential cross sections in the laboratory system were done for all partial reactions and incident energies listed in Table 23. Branching coefficients from Table 15 were used for these calculations. The bin width for secondary neutron energy was chosen as 0.1 MeV and for the cosine of laboratory angle as 0.1. To reduce the size of the file, the partial reaction energy-angular distributions for each incident energy were summed to one distribution representing the total neutron emission energy-angular distribution. The continuum energy-angular distributions (LAW = 1) in ENDF-6 format with cross section for the (n,2n) reaction (or better to say cross section for the production of two neutrons) taken from MT = 16 and multiplicity two were used for the presentation of the evaluated data. This distribution contains the whole complete secondary neutron emission spectrum, including also the rather sharp neutron line due to the (n,n_2x) process. According to the chosen energy grid this line is distributed over an energy region of about 0.1 MeV. In principle this is certainly not correct, however in practice the difference will not be important and the presentation of the whole secondary distribution in one file 6

will make the whole file much easier to process compared to a separate description of the (n,n_2) line in e.g. an additional file MF3 and MF4.

References

Aizawa 83: O. Aizawa et al., J.Nucl.Sci.Technology **20**, 354 (1983)

Ajzenberg-Selove 88: F. Ajzenberg-Selove, Nucl.Phys. A**490**, 1 (1988)

Alburger 63: Alburger, Phys.Rev. **132**, 328 (1963)

Angeli 70: I. Angeli et al., Acta Phys.Hung. **28**, 87 (1970)

Ashby 58: V.J. Ashby et al., Phys.Rev. **111**, 616 (1958)

Auchampaugh 79: G.F. Auchampaugh et al., Nucl.Sci.Eng. **69**, 30 (1979)

Augustson 74: R.H. Augustson and H.O. Menloe, Nucl.Sci.Eng. **54**, 190 (1974)

Baba 78: M. Baba et al., Proc.Int.Conf. on Neutron Physics and Nuclear Data, Harwell, Sept. 1978, 198 (1978)

Baba 88: M. Baba and M. Ishikawa, Proc.Int.Conf. on Nuclear Data for Science and Technology , Mito 1988, 209, (1988)

Ball 58: W. Ball, M.H. Mc Gregor and R. Booth, Phys.Rev. **108**, 726 (1957)

Bass 61: R. Bass, T.W. Bonner and H.P. Haenni, Nucl.Phys. **23**, 122 (1961)

Battat 53: M.E. Battat and F.L. Ribe, Phys.Rev. **89**, 80 (1953)

Beynon 79: T.D. Beynon and A.K. Oalster, Ann.Nucl.Energy **6**, 537 (1979)

Beynon 88: T.D. Beynon, B.S. Sim, Ann.Nucl.Energy **15**, 27 (1988)

Beyster 56: J.R. Beyster, M. Watt and E.W. Salmi, Phys.Rev. **104**, 1319 (1956)

Bilpuch 61: E.G. Bilpuch et al., Report Wash-1034, 10 (1961)

Biro 75: T. Biro et al., J.Inorg. and Nucl. Chemistry **37**, 1583 (1975)

Block 75: R.C. Block et al., J.Nucl.Sci.Technology **12**, 1 (1975)

Bloser 73: M. Bloser, Atomkernenergie **20**, 309 (1973)

Bochkarev 90: O.V. Bochkarev, Yu.O. Vasiliev, A.A. Korsheninnikov et al., Sov.J.Nucl. Phys.**52**, 964 (1990)

Bockelmann 51: C.K. Bockelmann, Phys.Rev. **80**,1011 (1951)

Bödy 75: Z.T. Bödy et al., Proc.Int.Conf. on Nuclear Data for Science and Technology, Antwerpen 1975

Boerker 88: G. Boerker et al., Proc.Int.Conf. on Nuclear Data for Science and Technology, Mito (Japan), 30. May - 3. June 1988, 193, JAERI 1988

Bratenahl 58: A. Bratenahl, J.M. Peterson and J.P. Stoering, Phys.Rev. **110**, 927 (1958)

Cabe 73: Cabe, Report CEA-R-4524 (1973)

Catron 61: H.C. Catron et al., Phys.Rev. **123**, 218 (1961)

Chen 70: Y.S. Chen, T.A. Tombrello and R.W. Kavanagh, Nucl.Phys. A**146**, 136 (1070)

Chen Guan Ren 84: Chen Guan Ren et al., Nucl.Sci.Eng. **86**, 184 (1984)

Cohen 61: A.V. Cohen, J.Nucl.En. Parts A and B **14**, 180 (1961)

Cook 54: C.P. Cook and T.W. Bonner, Phys.Rev. **94**, 651 (1954)

Coon 52: J.H. Coon et al., Phys.Rev. **111**, 250 (1952)

De Kempeneer 92: De Kempeneer, Proc.Int.Conf. on Nuclear Data for Science and Technology, Jülich, 13-17 May 1991, 326, Springer (1992)

Didier 61: D. Didier, J.Phys.Rad. A**22**, 149 (1961)

Didier 63: D. Didier and H. Dillemann, J. de Physique **24**, 805 (1963)

Dixt 91: S. Dixt, W. Bertozzi, T.N. Buti et al., Phys.Rev. C**43**, 1758 (1991)

Drake 77: D.M. Drake , G.F. Auchampaugh, E.D. Arthur et al., Nucl.Sci.Eng. **63**, 401 (1977)

Eaton 68: J.R.P. Eaton and J. Walker, NBS Special Publication 299, U.S. Dep. of Commerce - National Bureau of Standards, 169 (1968)

Ferenc 89: D. Ferenc, B. Antolkovic, G. Paic et al., Nucl.Sci.Eng. **101**, 1 (1989)

Finlay 89: R.W. Finlay et al., Phys.Rev. C**47**, 237 (1989)

Fossan 61: D.B. Fossan et al., Phys.Rev. **123**, 209 (1961)

Foster 71: D.G. Foster and D.W. Glasgow, Phys.Rev. C**3**, 576 (1971)

Fowler 55: J.M. Fowler, S.S. Hanna and G.E. Owen, Phys.Rev. **98**, 249 (1955)

Fowler 59: J.M. Fowler, ORNL-Report 2718, 16 (1959)

Fu 88: C.Y. Fu (the TNG code), Nucl.Sci.Eng. **100**, 61 (1988

Gorbachev 58: Gorbachev, Atomnaya Energia **4**, 191 (1958)

Gorlov 67: G.W. Gorlov, Yad.Fiz. **6**, 910 (1967)

Hetrick 80: D.M. Hetrick and C.Y. Fu, GLUCS: A Generalized Least-Squares Program for Updating Cross Section Evaluations with Correlated Data Sets, ORNL/TM-7341 (1980)

Holmberg 69: M. Holmberg and J. Hansen, Nucl.Phys. A**129**, 305 (1969)

Hogue 78: H.H. Hogue et al., Nucl.Sci.Eng. **68**, 38 (1978)

Hundyadi 68: I. Hundyadi and I. Angeli, Nucl.Phys. A **119**, 525 (1968)

Khaletskij 56: M.M. Khaletskij, Doklady Akad.Nauk. S.S.S.R. **113**, 305 (1956)

Kneff 86: D.W. Kneff et al., Nucl.Sci.Eng. **92**, 491 (1986)

Kropp 70: T. Kropp, Rep. KFK-1190 (1970)

Lemmel 86: H.D. Lemmel, Short Guide to EXFOR, Report IAEA-NDS-1, Rev. 5 (1986)

Liskien 88: H. Liskien et al., Nucl.Sci.Eng. **98**, 266 (1988)

Marion 59: J.B. Marion, J.S. Levin and L. Cranberg, Phys.Rev. **114**, 1584 (1959)

McGregor 57: M.H. McGregor and R. Booth, Phys.Rev. 110, 1392 (1957)

McLane 88: V. McLane, EXFOR Manual, Report IAEA-NDS-103, Rev. 88-1 (1988)

McTaggart 63: M.H. McTaggart and H. Goodfellow, Reactor Science and Technol. **17**, 437 (1963)

Merchez 66: Merchez, Proc. of Conf. on Nuclear Data for Reactors, Paris 1966

Mjachkova 61: Mjachkova, Zhuv. Eksper i Teoret.Fiz. **40**, 1244 (1961)

Nakada 58: Nakada, Phys.Rev. **110**, 1439 (1958)

Nereson 53: Nereson, Phys.Rev. **89**, 775 (1953)

Olsson 89: N. Olsson, B. Trostell and E. Ramström, Nucl.Phys. A**509**, 161 (1989)

Paic 67: G. Paic, D. Readic and P. Tomas, Nucl.Phys. A**96**, 476 (1967)

Pavlik 90: A. Pavlik, Code GPOLFIT, priv. communication (1990)

Perkins 85: S.T. Perkins, E.F. Plechaty, R.J. Howerton, Nucl.Sci.Eng. **90**, 83 (1985)

Perroud 74: J.P. Perroud, Nucl.Phys. A**227**, 330 (1974)

Peterson 60: Peterson, Phys.Rev. **120**, 521 (1960)

Phillips 60: T. Phillips, Report Wash-1028, 29 (1960)

Raynal 84: J. Raynal, in: Mater. of Workshop on Nuclear Model Computer Codes, Jan. 16 - Feb. 3, 1984, ICTP, Trieste, (1984)

Rosario-Garcia 77: Rosario-Garcia, Nucl.Phys. A**275**, 453 (1977)

Rosen 57: L. Rosen et al., Phys.Rev. **107**, 824 (1957)

Roturier 68: J. Roturier, Report NP-17 794 (1968)

Sakisaka 59: Sakisaka, J.Phys.Soc. of Japan **14**, 554 (1959)

Satchler 67: G.R. Satchler, Nucl.Phys. A**100**, 1497 (1967)

Schwartz 71: R.B. Schwartz et al., Bull.Am.Phys.Soc. **16**, 495 (1971)

Scobel 70: W. Scobel and M. Bormann, Zeitschr. f. Naturf. A**25**, 1409 (1970)

Shibata 83: K. Shibata, J.Phys.Soc. of Japan **52**, 3748 (1983)

Shibata 96: K. Shibata, Evaluation of Neutron Nuclear Data for ^{9}Be, Report INDC(JPN)-176/U, 15 (1996)

Smolec 76: W. Smolec et al., Nucl-Phys.A**257**, 397 (1976)

Stelson 57: P.H. Stelson and E.C. Campbell, Phys.Rev. **106**, 1252 (1957)

Sugimoto 89: M. Sugimoto et al., Nucl.Sci.Eng. **103**, 37 (1989)

Tagesen 94: S. Tagesen and D.M. Hetrick, Proc.Int.Conf. on Nuclear Data for Science and Technology, Gatlinburg, 9-13 May 1994

Takahashi 87: A. Takahashi, E. Ichimura, Y. Sasaki and H. Sugimoto, Rep OKTAV-A-87-03 (1987)

Taylor 55: H.L. Taylor et al., Phys.Rev. **100**, 174 (1955)

Templon 85: J.A. Templon et al., Nucl.Sci.Eng. **91**, 451 (1985)

Vasiliev 89: O.Yu. Vasiliev, A.A. Korsheninnikov, I.G. Mukha and L.V. Chulkov, JETP Lett., **49**, 622 (1989)

Vonach 92: H. Vonach et al., Physics Data **13-7** Fachinformationszentrum Karlsruhe (1992)

Weaver 74: D.R. Weaver and J. Walker, J.of Physics D7, 1122 (1974)

Woelfle 90: R. Wölfle et al., Radiochimica Acta **50**, 5 (1990)

Wyman 58: M.E. Wyman, E.M. Fryer and M. Thorpe, Phys.Rev. **112**, 1264 (1958)

Xuan Chuan 59: Xuan Chuan, J.de Physique **20**, 621 (1959)

Zadro 87: M. Zadro et al., Nucl.Sci.Eng. **95**, 79 (1987)

Table 1: Experimental data base for the Beryllium total cross section with assigned maximal uncertainties SER, MER, LER

EXFOR ENTRY	Reference	Number of pts	Energy Range MeV	SER max,%	LER %	MER max,%	χ^2
11011	Bilpuch 61	1	0.053-0.5	0.85l	total		prior
10070	Schwartz 71	34	0.5-20.0	0.03	0.5	1.0	prior
10047	Foster 71	26	2.0-15.0	0.7	1.0	1.5	1.63
10884	Auchampaugh 79	26	1.0-14.0	0.4	1.2	1.8	1.02
11048	Bockelman 51	4	1.5-3.5	0.5	2.0	1.0	0.25
11060	Nereson 53	20	3.0-14.0	5.0	1.0	2.0	0.16
11074	Cook 54	4	14.0-18.0	1.4	1.0	1.0	0.18
11252	Fowler 59	5	2.0-4.5	0.8	1.0	2.0	1.72
11256	Fossan 61	24	3.5-16.0	1.0	1.0	3.7	0.73
13154	Sugimoto 89	20	1.0-11.0	0.3	0.5	2.5	0.86
13569	Finlay 89	24	5.0-20.0	0.2	0.5	1.3	0.61
20480	Cabe 73	2	0.0-1.0	0.2	0.5	5.0	1.21
11155	Bratenahl 58	5	6.83-14.11	1.0	1.0		
11056	Coon 52	1	14.12	2.0	total		
11108	Peterson 60	1	17.5	1.0	total		
30113	Angeli 70	1	14.8	1.4	total		
30173	Hundyadi 73	1	14.25	3.0	total		
40709	Khaletskij 56	1	14.6	2.0	total	χ^2 = 0.87 for the	
62455	Didier 61	1	14.67	2.0	total	whole set of	
88011	Gorlov 67	1	4.0	2.0	total	single point measurements	

Table 2: Experimental data base for the Beryllium (n,2n) cross section with assigned maximal uncertainties SER, MER, LER

EXFOR ENTRY	Reference	Number of pts	Energy Range MeV	SER max,%	LER %	MER max,%
20067	Holmberg 69	8	2.0-6.4	7.0	5.0	
	Takahashi 87	1	14.05			
	Baba 88	1	14.05			
20872	Baba 78		15.4	30.0	5.0	0.0
10678	Drake 77	3	5.9-14.0	5.0	5.0	5.0
11097	Ashby 58	1	1.4.05	20	total	
11111	Catron 61	3	6.55-8.26	15.0	total	
11213	Fowler 55	1	3.7	35.0	total	
11223	Rosen 57	1	14.05*	16.6	total	
20285	Sakisaka 59	1	14.05*	16.7	total	
21416	Xuan Chuan 59	1	14.05*	30.0	total	
40790	Mjachkova 61	1	14.05*	13.0	total	
68010	Cao 62	1	14.05*	30.0	total	

*- all 14 MeV data reduced to one energy E_n = 14.05 MeV to avoid artificial strong energy dependence in the region where the cross section is practically flat.

Table 3: Experimental data base for the Beryllium (n,α_0) cross section with assigned maximal uncertainties SER, MER, LER

EXFOR ENTRY	Reference	Number of pts	Energy Range MeV	SER max,%	LER %	MER max,%
11194	Bass 61	9	4.0-9.0	28.0	5.0	0.0
12222	Stelson 57	6	2.26-4.41	see	text	
12222	Stelson 57**	90	0.88-4.43	30.0		7.0
30300	Smolec 76	1	12.2	23.1	total	
30300	Smolec 76	1	14.1*	21.2	total	
20877	Perroud 74	1	14.1*	7.2	total	
21904	Shibata 83	1	14.1*	5.4	total	
30198	Paic 67	1	14.1*	15.4	total	
11058	Battat 53	1	14.1*	10.0	total	

*- all 14 MeV data reduced to one energy E_n = 14.1 MeV to avoid an artificial strong energy dependence in the region where the cross section is practically flat.

** relative measurement of excitation function

Table 4: Experimental data base for the Beryllium (n,t) cross section with assigned maximal uncertainties SER, MER, LER

EXFOR ENTRY	Reference	Number of pts	Energy Range MeV	SER max,%	LER %	MER max,%	
22035	Liskien 88	13	11.6-20.0	1.3	5.0	5.0	taken as prior
22183	Woelfle 90	3	16.3-19.0	5.0	5.0	9.0	
30818	Bödy 75	3	13.7-14.8	8.5	0.	13.	
11231	Wyman 58	1	14.1	8.3	total		
30271	Biro 75	1	14.7	20.0	total		
30922	Zadro 87	1	14.6	8.3	total		

Table 5: Experimental data base for the Beryllium (n,p) cross section with assigned maximal uncertainties SER, MER, LER

EXFOR ENTRY	Reference	Number of pts	Energy Range MeV	SER max,	LER %	MER max,%
10389	Augustson 74	2	14.5-14.9	8.0	4.9	0.0
11236	Alburger 63	1	15.5	50.0	total	
10632	Rosario-Garcia 77	1	18.5	50.0	total	

Table 6: Experimental data base for the elastic cross section of Beryllium with assigned maximal uncertainties SER, MER, LER

EXFOR ENTRY	Reference	Number of pts	Energy Range MeV	SER max,%	LER %	MER max;%
10550	Hogue 78	9	6.97-14.93	4.9	4.5	0.0
10678	Drake 77	3	5.9-14.2	13.0	0.0	0.0
11207	Phillips 60	2	6.0-7.0	5.7	5.0	0.0
11232	Marion 59	2	5.0-6.0	5.0	5.0	0.0
13154	Sugimoto 89	12	4.5-10.0	2.5	3.0	0.0
20872	Baba 78	4	4.5-15.4	12.9	3.0	3.0
12939	Templon 85	3	10.96-16.88	7.1	1.0	
22113	Boerker 88	1	10.13	3.8	total	
22113	Boerker 88	1	10.131	3.7	total	
11208	Nakada 58	1	14.0	7.3	total	
20599	Roturier 68	1	14.07	6.9	total	
21117	Merchez 66	1	14.1	7.4	total	
30632	Chen Guan-Ren 84	1	14.7	4.5	total	
22127	Olsson 89	1	19.4*	5.6	total	

* extrapolated to this energy from the energy $E_n = 21.6$ MeV for which the measurements were done.

Table 7: Experimental data base for the nonelastic cross section of Beryllium with assigned maximal uncertainties SER, MER, LER

EXFOR ENTRY	Reference	Number of pts	Energy Range MeV	SER max,%	LER %	MER max;%
11257	Ball 58	5	7.0-11.2	6.5	5.0	
11217	Taylor 55	2	12.7-14.1	22	-	
20253	Weaver 74	2	3.7-3.92	4.2	4.2	
20368	Eaton 68	5	3.2-5.2	13.0	6.0	
21501	Didier 63	1	14.2	2.8 tot		
21750	McTaggart 63	1	14.0	8.5 tot		
11226	McGregor 57		14.2	4.0 tot		
21211	Cohen 61		14.08	7.0 tot		
40391	Gorbachev 58		14.0	7.3 tot		
11220	Beyster 56		7.0	6.6 tot		

Table 8: Present evaluation for ^{9}Be: cross sections and uncertainties

	total MT = 1		elastic MT = 2		non-elastic MT = 3	
Neutron energy group (in MeV)	cross section (in barn)	std.dev. of sigma (E) (in barn)	cross section (in barn)	std.dev. of sigma (E) (in barn)	cross section (in barn)	std.dev. of sigma (E) (in barn)
0.00 -0.50	4.4672	±0.0419	4.4672	±0.0419	0.0000	±0.0000
0.50 -1.00	3.7471	±0.0284	3.7471	±0.0284	0.0000	±0.0000
1.00 -1.50	2.7076	±0.0164	2.7033	±0.0164	0.0043	±0.0006
1.50 -2.00	1.7969	±0.0097	1.7692	±0.0099	0.0277	±0.0021
2.00 -2.50	1.9534	±0.0090	1.8837	±0.0095	0.0697	±0.0029
2.50 -3.00	3.3882	±0.0170	3.1755	±0.0193	0.2128	±0.0093
3.00 -3.50	2.6300	±0.0141	2.0953	±0.0269	0.5347	±0.0232
3.50 -4.00	2.0982	±0.0107	1.5068	±0.0281	0.5914	±0.0262
4.00 -4.50	1.9279	±0.0099	1.3413	±0.0323	0.5866	±0.0307
4.50 -5.00	1.8976	±0.0099	1.3017	±0.0289	0.5959	±0.0285
5.00 -5.50	1.8627	±0.0086	1.2338	±0.0284	0.6290	±0.0283
5.50 -6.00	1.8485	±0.0076	1.1969	±0.0306	0.6517	±0.0305
6.00 -6.50	1.8097	±0.0075	1.1622	±0.0256	0.6475	±0.0255
6.50 -7.00	1.7744	±0.0067	1.1472	±0.0249	0.6272	±0.0247
7.00 -7.50	1.7443	±0.0073	1.1118	±0.0189	0.6325	±0.0184
7.50 -8.00	1.7361	±0.0075	1.1109	±0.0269	0.6253	±0.0270
8.00 -8.50	1.7207	±0.0077	1.1250	±0.0216	0.5957	±0.0214
8.50 -9.00	1.7066	±0.0079	1.1261	±0.0338	0.5806	±0.0339
9.00 -9.50	1.6918	±0.0075	1.1182	±0.0271	0.5736	±0.0274
9.50 -10.00	1.6802	±0.0072	1.1127	±0.0261	0.5675	±0.0262
10.00 -10.50	1.6595	±0.0071	1.0918	±0.0223	0.5677	±0.0227
10.50 -11.00	1.6416	±0.0077	1.0607	±0.0564	0.5809	±0.0564
11.00 -11.50	1.6181	±0.0072	1.0576	±0.0255	0.5605	±0.0256
11.50 -12.00	1.5888	±0.0077	1.0475	±0.0513	0.5413	±0.0507
12.00 -12.50	1.5645	±0.0070	1.0247	±0.0341	0.5398	±0.0342
12.50 -13.00	1.5534	±0.0068	1.0184	±0.0560	0.5351	±0.0558
13.00 -13.50	1.5248	±0.0065	0.9915	±0.0419	0.5334	±0.0418
13.50 -14.00	1.5054	±0.0069	0.9837	±0.0552	0.5219	±0.0552
14.00 -14.50	1.4905	±0.0070	0.9969	±0.0137	0.4938	±0.0123
14.50 -15.00	1.4670	±0.0078	0.9741	±0.0320	0.4929	±0.0311
15.00 -16.00	1.4423	±0.0080	0.9382	±0.0379	0.5041	±0.0376
16.00 -17.00	1.4255	±0.0077	0.9565	±0.0513	0.4690	±0.0510
17.00 -18.00	1.3942	±0.0064	0.9392	±0.0425	0.4550	±0.0423
18.00 -19.00	1.3494	±0.0081	0.8994	±0.0547	0.4500	±0.0544
19.00 -20.00	1.3211	±0.0092	0.8872	±0.0380	0.4339	±0.0381

Table 9: Present evaluation for ^{9}Be: cross sections and uncertainties
(n,2n) MT = 16

	Neutron energy (in MeV)	cross section (in mbarn)	std.dev. of sigma (E) (in mbarn)			Neutron energy (in MeV)	cross section (in mbarn)	std.dev. of sigma (E) (in mbarn)	
1	1.75	0.0000	0.000		21	8.00	572.60	22.16	3.8%
2	2.00	2.2747	0.254	11.1%	22	8.50	564.59	34.63	
3	2.20	8.4563	0.784		23	9.00	548.63	27.75	
4	2.40	17.622	1.139		24	9.50	554.99	26.96	
5	2.60	27.545	1.625		25	10.0	539.60	22.76	4.2%
6	2.70	36.555	2.504		26	10.5	558.49	55.84	
7	2.80	196.06	10.18		27	11.0	569.07	27.01	4.8%
8	3.00	341.61	22.87	6.7%	28	11.5	520.80	50.27	
9	3.20	424.12	22.42		29	12.0	530.34	34.85	6.6%
10	3.40	469.93	27.77		30	12.5	512.87	55.81	
11	3.60	486.16	25.43		31	13.0	512.22	42.30	8.3%
12	3.80	504.59	25.87		32	13.5	500.54	55.87	
13	4.00	505.34	30.46	6.0%	33	14.0	488.09	12.93	2.7%
14	4.50	514.88	27.73		34	14.5	442.40	30.06	
15	5.00	545.28	27.40		35	15.0	476.81	38.52	
16	5.50	594.87	30.50		36	16.0	454.00	53.55	
17	6.00	610.02	26.03		37	17.0	409.42	42.16	
18	6.50	600.25	25.26		38	18.0	413.32	55.83	
19	7.00	581.30	18.67	3.2%	39	19.0	390.79	38.41	
20	7.50	616.46	28.30		40	20.0	380.15	37.39	

Table 10: Present evaluation for ^{9}Be: cross sections and uncertainties
(n,p) MT = 103

	Neutron energy (in MeV)	cross section (in mbarn)	std.dev. of sigma (E) (in mbarn)
1	14.27	0.0000	0.0000
2	14.75	0.1121	0.0102
3	15.50	0.5944	0.0572
4	16.50	0.8834	0.4083
5	17.50	1.0330	0.5015
6	18.50	1.0255	0.3667
7	19.50	1.2026	0.6372

Table 11: Present evaluation for ^{9}Be: cross sections and uncertainties (n,d) MT = 104

	Neutron energy (in MeV)	cross section (in mbarn)	std.dev. of sigma (E) (in mbarn)		Neutron energy (in MeV)	cross section (in mbarn)	std.dev. of sigma (E) (in mbarn)
1	16.301	0.0000	0.0000	11	17.820	8.1989	0.6477
2	16.560	0.09998	0.01071	12	17.960	8.8988	0.7030
3	16.700	0.55989	0.05995	13	18.100	9.1987	0.7345
4	16.840	1.3797	0.1477	14	18.240	9.7986	0.7824
5	16.980	2.7294	0.2923	15	18.380	9.8986	0.7904
6	17.120	4.0594	0.3207	16	18.520	9.9986	0.7984
7	17.260	5.8792	0.4644	17	18.660	10.499	0.8383
8	17.400	6.4991	0.5134	18	18.800	10.898	0.8702
9	17.540	6.9990	0.5529	19	19.500	11.895	1.637
10	17.680	7.7989	0.6161	20	20.000	12.395	1.704

Table 12: Present evaluation for ^{9}Be: cross sections and uncertainties (n,t) MT = 105

	Neutron energy (in MeV)	cross section (in mbarn)	std.dev. of sigma (E) (in mbarn)
1	11.608	0.0000	0.000
2	12.250	4.3430	0.5087
3	12.750	10.233	0.7818
4	13.250	15.767	0.8581
5	13.750	17.298	0.8059
6	14.250	18.906	0.7945
7	14.750	23.976	1.066
8	15.500	29.569	1.594
9	16.500	28.728	1.614
10	17.500	28.936	1.583
11	18.500	30.920	1.738
12	19.500	29.933	1.734

Table 13: Present evaluation for ^{9}Be: cross sections and uncertainties
(n,α_0) MT = 107

	Neutron energy (in MeV)	cross section (in mbarn)	std.dev. of sigma (E) (in mbarn)		Neutron energy (in MeV)	cross section (in mbarn)	std.dev. of sigma (E) (in mbarn)
1	0.66715	0.0000	0.000	24	7.00	34.02	5.811
2	0.83360	0.0805	0.3230	25	7.50	32.28	5.711
3	0.90	0.4519	0.2986	26	8.00	28.03	5.838
4	1.00	0.6693	0.7955	27	8.50	25.37	6.015
5	1.10	0.0355	0.1271	28	9.00	22.81	5.929
6	1.20	3.2363	0.4240	29	9.50	20.70	5.568
7	1.30	5.3744	0.5937	30	10.00	19.89	5.208
8	1.40	8.8067	0.9379	31	10.50	17.74	4.798
9	1.60	18.61	1.420	32	11.00	16.30	4.347
10	1.80	30.47	1.909	33	11.50	14.23	3.923
11	2.00	42.52	2.496	34	12.00	14.55	3.111
12	2.20	55.09	2.628	35	12.50	13.45	2.992
13	2.40	69.83	3.330	36	13.00	11.94	2.953
14	2.60	85.40	4.422	37	13.50	10.58	2.752
15	2.80	100.9	5.270	38	14.00	9.7548	0.6929
16	3.00	102.0	4.665	39	14.50	9.4344	2.293
17	3.50	95.02	5.058	40	15.00	8.9771	2.538
18	4.00	87.10	4.607	41	16.00	7.9922	2.434
19	4.50	65.41	3.395	42	17.00	7.1869	2.258
20	5.00	65.43	7.077	43	18.00	6.4277	2.026
21	5.50	52.90	6.304	44	19.00	5.5740	1.757
22	6.00	46.72	6.509	45	20.00	5.1448	1.626
23	6.50	38.35	6.219				

Table 14: Summary on the experimental data for double-differential neutron cross sections used in the evaluation

Incident En (MeV)	Em. angle (degree)	Range in En' for Data set (MeV)		
		Baba 88	Takahashi 88	Drake 79
14.1	15		0.5 - 9	
	30	0.5 - 9	0.5 - 9	
	35			0.5 - 9
	45	0.5 - 8		0.5 - 8
	60	0.5 - 9	0.5 - 9	0.5 - 8
	80	0.5 - 10	0.5 - 10	0.5 - 8
	100	0.5 - 9	0.5 - 9	0.5 - 8
	120	0.5 - 9	0.5 - 9	
	125			0.5 - 7
	145			0.5 - 6
	150	0.5 - 8	0.5 - 6	
10	25			0.5 - 6
10.1	25			0.4 - 6
	35			0.4 - 5
	45			0.4 - 5
	60			0.4 - 5
	80			0.4 - 4
	100			0.4 - 4
	125			0.4 - 4
5.9	25			0.5 - 1.5
	35			0.4 - 1.5
	45			0.4 - 1.5
	60			0.4 - 1.5
	80			0.4 - 1.5
	100			0.4 - 1.5
	110			0.4 - 1.5
	125			0.4 - 1.25

TABLE 15

Characteristics of ^{9}Be excited states and branching ratios (BR) for their decay to ^{8}Be states ($(n,n'_i(n''_j(\alpha\alpha)))$ reaction), ^{5}He states ($((n,n'_i(\alpha(n''\alpha)))$ reaction) and three-body break up ($((n,n'(n\alpha\alpha))$ reaction) after inelastic scattering with excitation of

N	Elev, MeV	Jp	Γ_{tot}, MeV	Branching Ratio for decay to final state				
				^{8}Be g.s. BR1	^{8}Be 1-st BR2	^{5}He g.s. BR3	^{5}He 1-st BR4	$(n\alpha\alpha)$-3-body BR5
0	0.0 (g.s.)	3/2-	0.0(stable)	0.0	0.0	0.0	0.0	0.0
1	1.684	1/2+	0.217	1.00	0.0	0.0	0.0	0.0
2	2.4294	5/2-	0.00077	0.07	0.0	0.0	0.0	0.93
3	2.78	1/2-	1.08	1.00	0.0	0.0	0.0	0.0
4	3.049	5/2+	0.282	0.87	0.13	0.0	0.0	0.0
5	4.704	3/2+	0.743	0.13	0.87	0.0	0.0	0.0
6	5.59	3/2-	1.33	0.5	0.5	0.0	0.0	0.0
7	6.38	7/2-	1.21	0.02	0.55	0.43	0.0	0.0
8	6.76	9/2+	1.33	0.0	1.0	0.0	0.0	0.0
9	7.940	1/2-	1.00	0.5	0.5	0.0	0.0	0.0
10	11.283	9/2-	1.10	0.02	0.14	0.84	0.0	0.0
11	11.81	5/2+	0.400	0.20	0.80	0.0	0.0	0.0
12	13.79	5/2-	0.590	0.0	1.0	0.0	0.0	0.0
13	14.392	3/2-	0.000381	0.049	0.386	0.565	0.0	0.0
14	14.4	1/2-	0.8	0.5	0.5	0.0	0.0	0.0
15	15.1	7/2-	0.35	0.0	1.0	0.0	0.0	0.0
16	15.9	5/2-	0.31	0.0	1.0	0.0	0.0	0.0
17	16.672	5/2+	0.041	0.0	0.0	1.0	0.0	0.0
18	16.975	1/2-	0.00049	0.07	0.0	0.0	0.0	0.93
19	17.298	5/2-	0.20	0.0	1.0	0.0	0.0	0.0
20	17.493	7/2+	0.047	0.0	0.0	1.0	0.0	0.0

The Q value for the two-body break up $^{9}Be(n,^{5}He^{5}He)$ is equal to -3.350 MeV, for the two-body break up of ^{5}He in neutron and α-particle is equal to +0.890 MeV. The Q-value for the three-body break up reaction $^{9}Be(n,n\alpha^{5}He)$ is equal to-2.640 MeV.

The branching ratios given in the table are based on the following considerations, whereby the remarks refer to the level numbers given in column 1 of the table:

1) The level is much below the position of the 1-st excited level in ^{8}Be at which d-neutron transition having a maximal energy 19 keV may occur. It may have a very low probability and explains why BR=1 for the s-transition to ^{8}Be g.s..

2) This level is a member of the 3/2- ground state rotational band and is strongly excited by the direct reaction mechanism in inelastic scattering. It contributes between 50% at low energy and 20% at high neutron energy to the total neutron production cross section of ^{9}Be. Due to this the importance of the knowledge of it´s decay modes is evident. The level has a total width of only 770 eV and a well established BR = 0.07 for the decay to the g.s. of ^{8}Be. No other neutron decays to ^{8}Be levels are observed. The results of kinematically complete measurements (Vasiliev 89, Bochkarev 90) for inelastic scattering of ^{3}He and ^{2}H with excitation of this level and its subsequent decay with α-particle emission have shown that BR=0.93 has to be assigned to three-body decay (n"α'α"). The direct measurements of the neutron decay modes of this level (Chen 70) populated through β-decay of the ^{9}Li ground state also support these branchings.

3) The level is much below the position of the 1-st excited state of ^{8}Be. α-widths are probably small in comparison with Γ_{tot} = 1.08 MeV. It explains why BR = 1 for decay to ^{8}Be g.s..

4) BR = 0.87 for decay to ^{8}Be g.s. is given at (Ajzenberg-Selove 88). BR = 0.13 is assigned for decay to ^{8}Be 1-st excited state because no α-decays are observed.

5) Similar consideration as for level 4.

6) The position of the level, its spin and parity as well as total width are taken from (Dixt 91). Equal BR = 0.5 for the decay to the ^{8}Be g.s. and 1-st excited state are assigned for the reason, that p-wave neutrons are responsible for decay in both cases and α-widths are possibly small in comparison with the total width.

7) This level is considered by (Dixt 91) as a member of the 3/2- rotational band (6.76 MeV level at (Ajzenberg-Selove 88)). It is strongly excited in neutron inelastic scattering. The neutron decay properties are taken from (Ajzenberg-Selove 88) (6.86 Mev level at (Ajzenberg-Selove 88)). This is due to the fact that most experimental data for the BR determination were obtained at rather high energies in the reactions where only the direct mechanism with excitation of rotational states members may contribute. It means that all decay properties assigned at (Ajzenberg-Selove 88) to the 6.76 MeV level belong to the level with Jp = 7/2-. BR = 0.43 is assigned by us to α_0 decay.

8) The spin and parity of this level (9/2+) are determined at (Dixt 91) (former 7/2- level at (Ajzenberg-Selove 88)). A high total width may be explained by the decay to ^{8}Be 1-st excited state through d3/2 neutron emission with BR = 1 for this process. The probability of g9/2 neutron emission for decay to ^{8}Be g.s. should be small.

9) The analysis has shown that for 10 MeV incident neutrons there is kinematical overlapping in lab system energy angular distributions of sccondary particles emitted in (n,n'$_2$) reaction and second neutron from (n,n'$_9$,n"$_0$) reaction. This overlapping possibly leads to the appearing of a peak in the experimental data for excitation function of the 2-nd level around 10 MeV. BR = 0.5 were assigned for two neutron decay channels because both decays have p-wave contribution and the level has a large width (1.0 MeV).

10) The level is considerably excited in the (p,p') reaction at Ep = 180 MeV. A spin value of 9/2 is assigned by us because it is probably a member of the 3/2- rotational band. BR for neutron decay modes taken from (Ajzenberg-Selove 88). BR = 0.84 assigned to α_0 decay.

11) The same analysis as was done for 7.94 MeV level shows that for 14 MeV incident neutrons there is kinematical overlapping in laboratory system of the energy angular distributions of secondary particles emitted in (n,n'$_2$) reaction and second neutron from (n,n'$_{11}$,n"$_0$) reaction. This overlapping possibly leads to the appearing of the peak in the experimental data of the excitation function of 2-nd level around 14 MeV. Basing on this peculiarity and the value of the total width of the level, the assignement of spin and BRs was made. This is a level which still can be excited by 14-MeV neutrons.

12) It was guessed that neutron decay to the first excited state in ^{8}Be contributes mainly to the total width of 0.59 MeV. 5/2- spin and parity was assigned to this level (Dixt 91).

13) All characteristics were taken from (Ajzenberg-Selove 88).

14) 1/2- spin and parity were assigned by us with equal BR = 0.5 for two neutron decay channels.

15) Spin and branching ratio are assigned based on speculations about total width obtained at (Dixt 91).

16) Spin, parity and width of the level were taken from (Dixt 91). Same speculation for BR assignment as in 15.

17) Total width is 41 keV and assigned completely to the α_0 decay channel (no neutron decays observed (Ajzenberg-Selove 88)).

18) This level has very small total width (490 ev). Possibly the main mode of decay is a three-body break up after inelastic scattering with excitation of this level. BR = 0.93 is assigned to this process.

19) Decay with an emission of n, p, d, a was observed (Ajzenberg-Selove 89). BR = 1.0 is assigned for a neutron decay to the 1-st excited state because of possible p-neutron transitions.

20) Probably α_0 decay because a total width is low and neutron decay to ^{8}Be g.s. needs a g7/2 transition which has low probability.

TABLE 16:

Characteristics of ^{8}Be, ^{5}He and ^{6}He states and Q-values between ^{9}Be ground state and ground state of product nucleus or nuclei

Nucleus	Nlev	Q, MeV	Elev,MeV	Jp	Γ_{tot}, MeV
^{8}Be	0	-1.6654	0.0	0+	0.0000068
^{8}Be	1		3.040	2+	1.50
^{8}Be	2		11.40	4+	3.5
^{5}He	0	-2.460	0.0	3/2-	0.60
^{5}He	1		4.0	1/2-	4.0
^{6}He	0	-0.600			
(nαα)	0	-1.5700			

Table 17:

Legendre coefficients for the description of inelastic scattering angular distributions with excitation of the levels having high direct reaction components (Hogue 78).

Energy	Legendre coefficients		
(MeV)	α_1	α_2	α_3
5.9	0.09892	-0.00041	0.049
6.97	0.0866	-0.0003	0.0429
7.97	0.1136	0.0008	0.0333
8.96	0.1301	0.0060	0.0282
9.96	0.1626	0.0164	0.0176
10.1	0.1650	0.0167	0.0179
10.95	0.1819	0.0171	-0.0024
12.04	0.2270	0.0250	0.0081
12.94	0.2150	0.0176	0.0146
13.94	0.2432	0.0288	0.0148
14.1	0.2434	0.02874	0.01472
14.94	0.2432	0.0288	0.0148

Table 18:

Input and Output of the least-squares adjustment of the different partial reaction cross sections to the experimental double-differential neutron emission cross sections at E_n = 5.9 MeV (cross sections in mb, uncertainties in percent), chi-square = 0.95

Channel	Prior c.s.	Posterior c.s.
(n,n'1)		
(n,α2)	25.1 (100.)	50.7 (49.)
(n,n'2)	271 (5.)	258 (4.6)
(n,n'(3+4)	58.8 (100.)	0
(n,n'5)	16.4 (100.)	18.4 (78.)
(n,α1)	62.6 (50.)	45 (40.)
(n,^{5}He^{5}He)	31 (100.)	44.6 (60.)
(n,n'n"^{8}Be)	27 (100.)	31.2 (80.)
(n,n'α^{5}He)	30 (100.)	57.8 (48.)

Table 19:

Input and Output of the least-squares adjustment of the different partial reaction cross sections to the experimental double-differential neutron emission cross sections at E_n = 10.1 MeV (cross sections in mb, uncertainties in percent), chi-square = 1.05

Channel	Prior c.s.	Posterior c.s.
(n,n'1)		
(n,n'2)	210 (22.)	210 (8.1)
(n,n'(3+4)	15 (100.)	9.7 (121.)
(n,n'5)	15 (100.)	15.3 (61.)
(n,n'6)		
(n,n'7)	35.0 (100.)	39.5 (58.)
(n,n'8)	80.0 (100.)	11.0 (234.)
(n,n'9)	45.0 (100.)	8.6 (211.)
(n,α1)	32.0 (20.)	33.3 (19.)
(n,α2)	35.0 (100.)	63.1 (40.)
(n,^{5}He^{5}He)	20 (100.)	28.4 (65.)
(n,n'n"^{8}Be)	36 (100.)	32.6 (63.)
(n,n'α^{5}He)	90 (5.)	90 (4.9)

Table 20:

Input and Output of the least-squares adjustment of the different partial reaction cross sections to the experimental double-differential neutron emission cross sections at E_n = 14.1 MeV (cross sections in mb, uncertainties in percent), chi-square = 1.22

Channel	Prior c.s.	Posterior c.s.
(n,n'1)		
(n,n'2)	133 (17.2)	133 (5.6)
(n,n'(5+6+7))	45.0 (100.)	47.3 (34.)
(n,n'8)	70.0 (100.)	39.6 (52.)
(n,n'9)	20.0 (100.)	19.1 (36.)
(n,n'10)		
(n,n'11)		
(n,α1)	17.0 (20.)	17.8 (18.6)
(n,α2)	25.0 (100.)	30.5 (63.6)
(n,^{5}He^{5}He)	20 (100.)	10.1 (137.)
(n,n'n"^{8}Be)	51 (100.)	43.8 (40.3)
(n,n'α^{5}He)	81 (100.)	150.2 (20.4)

Table 21:

Optical potential parameters for a strong coupling scheme between members of ground state rotational band $3/2^-$, $5/2^-$, $7/2^-$, $9/2^-$ with a ground state quadrupole deformation parameter β_2 = 1.1 in ^{9}Be

En (MeV)	V_0 (MeV)	W_s (MeV)	$r_0 = r_s$ (fm)	$a_0 = a_s$ (fm)	V_{so} (MeV)	r_{so} (fm)	a_{so} (fm)
2.0	35.0*	3.0	1.50	0.33*	6.2*	1.12*	0.47*
3.0		3.0	1.49				
4.0		3.0	1.47				
5.0		3.0	1.45				
5.9		3.0	1.44				
7.0		3.1	1.42				
8.0		3.2	1.40				
9.0		3.3	1.37				
10.1		3.04	1.34				
11.0		3.6	1.33				
12.0		3.7	1.32				
13.0		3.9	1.30				
14.1		4.0	1.28				
15.0		4.1	1.26				
17.0		4.4	1.26				
20.0		4.8	1.26				

* independent of energy

Table 22:

Results of ECIS-TNG calculations of cross sections in different channels (E_n are given in MeV and cross sections are given in mb)

En	2.0	3.0	4.0	5.0	5.9	7.0	8.0	9.0	10.1	11.0	12.0	13.0	14.1	15.0	17.0	20.0
tot	2102	2005	1885	1842	1798	1754	1733	1722	1676	1640	1584	1528	1473	1436	1375	1315
ela	2010	1700	1389	1295	1218	1170	1135	1117	1094	1065	1037	1006	971	949	912	870
non	92	305	496	547	580	584	598	605	582	575	547	522	502	487	463	445
n,n1	31.3	46.9	38.0	36.0	31.5	24.1	19.8	15.5	11.6	9.90	8.17	6.98	5.43	4.63	3.45	2.06
n,n2		122	212	252	271	272	249	236	215	198	180	158	140	129	112	102
n,n3			23.6	22.6	21.5	19.2	18.8	15.8	12.0	10.3	8.53	7.23	5.43	4.60	3.73	2.60
n,n4			49.2	46.9	42.5	39.6	35.6	31.2	25.0	22.8	19.3	16.6	12.9	11.0	9.21	6.73
n,n5					16.4	16.9	17.4	16.7	14.7	14.4	12.9	11.6	9.19	7.94	6.47	4.69
n,n6						11.9	13.5	13.4	12.4	12.8	12.0	11.3	9.03	7.83	6.58	5.08
n,n7							50.1	65.2	72.1	79.7	82.1	79.0	77.6	75.1	70.5	64.7
n,n8							7.20	9.33	9.15	9.93	10.0	9.65	8.61	8.03	7.97	7.13
n,n9								1.49	3.68	3.67	3.59	3.59	3.31	3.14	2.88	2.46
n,n10												3.15	6.98	8.34	10.9	12.4
n,n11													4.50	4.69	4.55	5.05
n,n12															3.42	3.48
n,n13															1.89	2.31
n,n14															0.91	1.16
n,n15															0.80	3.62
n,n16																2.65
n,n17																2.27
n,n18																0.70
n,n19																1.59
n,n20																1.34
n,α0	45	105	85	65	50	35	28	22	19	17	15	13	11	10	8	5
n,α1		1.50	55.4	70.0	62.6	53.4	40.4	33.5	32.2	27.4	23.9	21.3	18.6	17.1	13.6	9.24
n,α2				4.2	25.1	36.4	32.1	31.1	34.0	30.8	28.3	26.6	24.5	23.3	19.5	14.4*
n,^{5}He^{5}He			5.0	22.0	31.0	37.0	36.0	33.0	28.0	24.0	19.0	14.0	10.0	8.0	5.0	5.0*
n,nn^{8}Be		16.0	22.0	25.0	27.0	29.0	31.0	33.0	34.0	36.0	37.0	38.0	39.0	40.0	41.0	42.0*
n,nα^{5}He					3.0	11.0	20.0	48.0	60.0	78.0	88.0	102	115	124	131	136*

* estimated by interpolation and extrapolation of the GLUCS results at 5.9, 10.1 and 14.1 MeV

Table 23:

Values of the cross sections for all partial reaction channels used in the final calculation of the evaluated double-differential neutron emission cross sections (E_n in MeV and cross sections in mb)

En	2.0	3.0	4.0	5.0	5.9	7.0	8.0	9.0	10.1	11.0	12.0	13.0	14.1	15.0	17.0	20.0
n,n1	19.5	82.6	46.7	40.3	35.0	24.3	20.0	14.6	10.9	10.3	8.2	6.9	5.3	4.6	3.1	1.8
n,n2		214.	260.	282.	301.	275.	252.	222.	202.	206.	180.	156.	137.	128.	100.	89.
n,n3			20.3	14.6												
n,n4			42.3	30.2												
n,n5					18.2	18.6	17.6	15.7	14.3	15.0	12.9	11.5	9.1	7.9	5.8	4.1
n,n6						3.8	4.3	7.9	8.6	11.7	10.9	11.2	9.6	8.7	6.3	5.1
n,n7							16.2	38.3	50.0	73.2	74.6	78.2	82.5	83.6	74	64.8
n,n8							2.3	5.5	6.4	9.1	9.1	9.5	9.1	8.9	7.7	7.1
n,n9								0.8	2.5	3.3	3.3	3.6	3.5	3.5	2.8	2.4
n,n10												3.1	7.4	9.3	10.5	11.4
n,n11													4.8	5.2	4.4	5.0
n,n12															3.3	3.5
n,n13															1.8	2.3
n,α1		3.5	61.5	52.1	51.1	42.4	38.4	32.9	31.2	28.5	23.9	21.5	18.2	16.9	12.1	8.0
n,α2				4.7	55.5	71.7	73.7	63.9	58.2	54.1	45.0	37.4	29.4	25.7	17.8	12.2
n,^{5}He^{5}He			8.6	35.9	50.0	47.5	43.4	36.7	33.0	29.1	22.0	16.2	10.8	7.9	4.5	4.3
n,nn^{8}Be	3.1	35.2	32.0	32.5	34.4	32.3	33.3	32.0	34.0	37.4	37.0	38.4	38.2	39.6	36.5	36.5
n,nα^{5}He		5.3	33.2	48.2	62.2	65.7	74.7	78.0	88.3	102	104	113	115	123	119	123

Appendix 1: Modifications and extensions of the Beynon/Sim code performed for this evaluation

1) A narrower step (0.1 MeV) of the excitation energy was used for the presentation of levels having a large width. The procedure used by Sim for the presentation of levels with a width was replaced by a new one. This allows to obtain smoother secondary neutron energy-angular distributions and to remove unphysical discontinuities in the distributions caused by a too wide step in the excitation energy at least for selected steps of secondary neutron energy.

2) A few procedures which allow to describe:

a) a sequential three-body decay after inelastic scattering (^{9}Be(n,n'$_2$(n"α'α")))

b) a channel (^{9}Be(n,n'α'(n"α"))) with two sequential three-body and two-body decays was added.

The numerical method was used for the transformation of energy-angular distributions of reaction products from the center of mass into laboratory system. This method can be implemented with the required accuracy only for high speed computers. Free space kinematic for three-body decay was used in all cases where we had no direct experimental information on the products center of mass energy-angular distributions. Coulomb distortion of neutron spectra in the center of mass is very important for case a) where kinetic energy of the products, - neutron and two α-particles - is very low, but probably is less important for case b) where kinetic energy of the products, - neutron, α-particle and ^{5}He - is much higher.

Figure 1: ^{9}Be evaluation-flow chart
(integral cross sections)

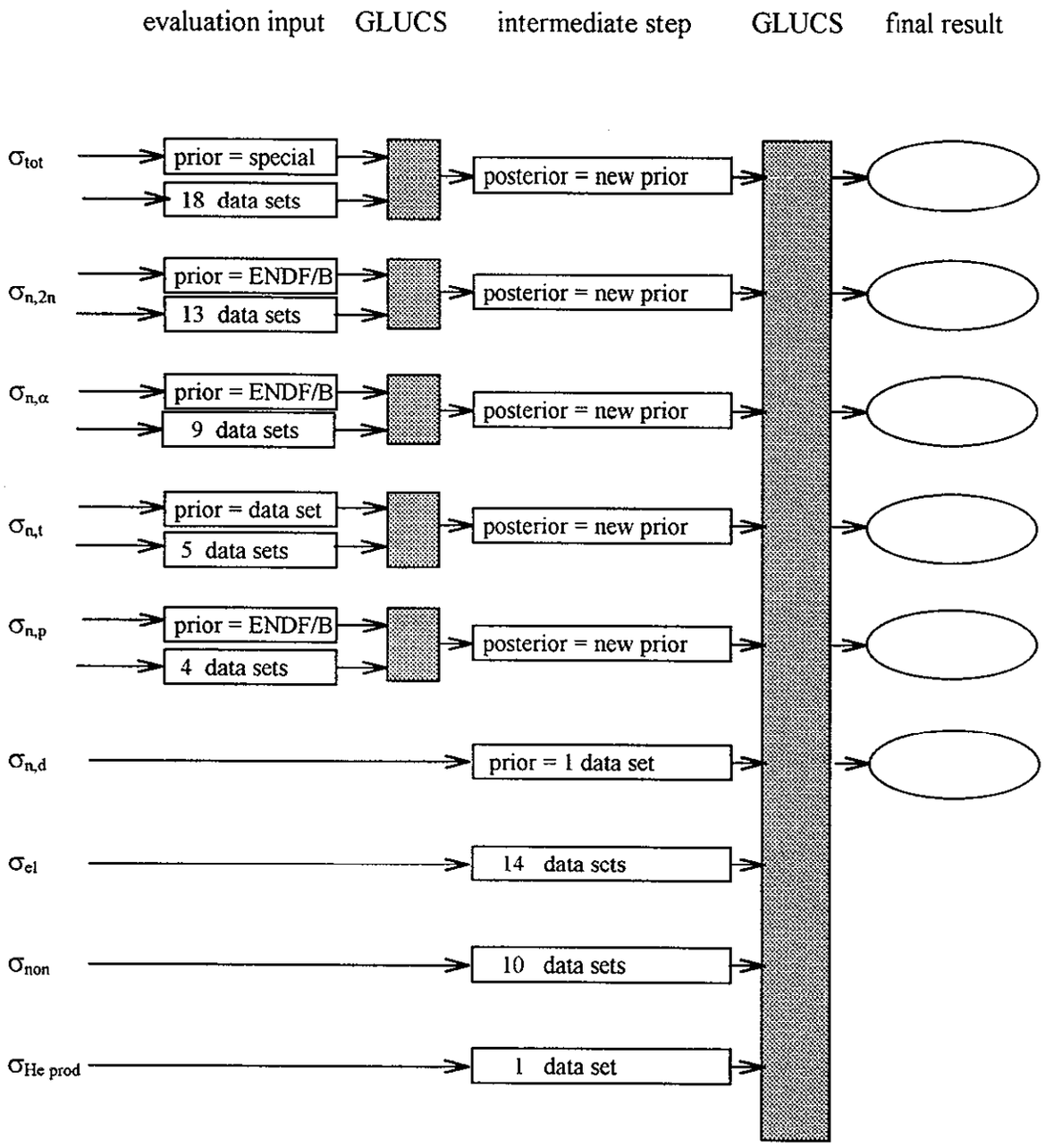

Figure 2: ^{9}Be (n,total) final evaluated cross section

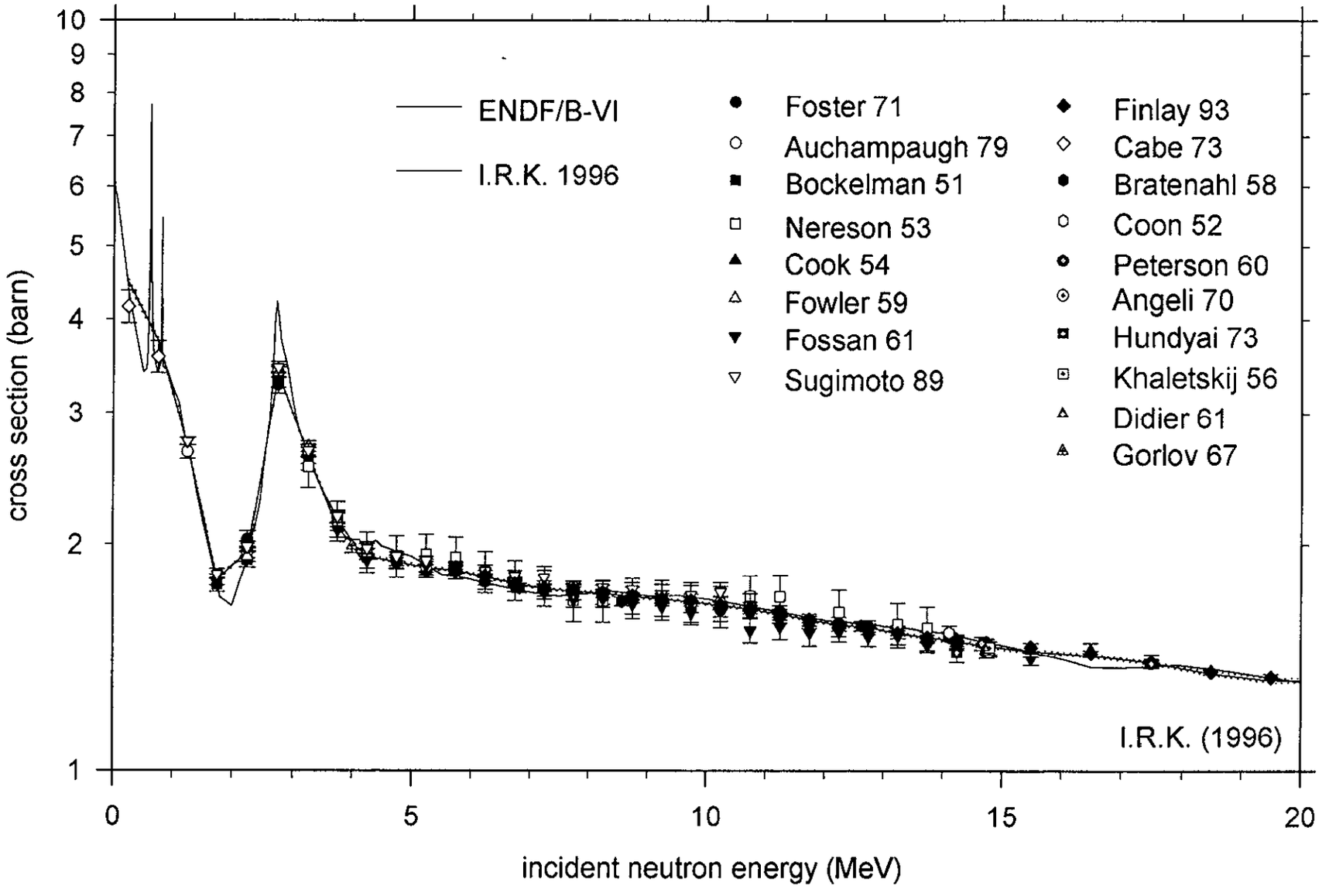

Figure 3: **^{9}Be (n,total) final evaluated cross section**

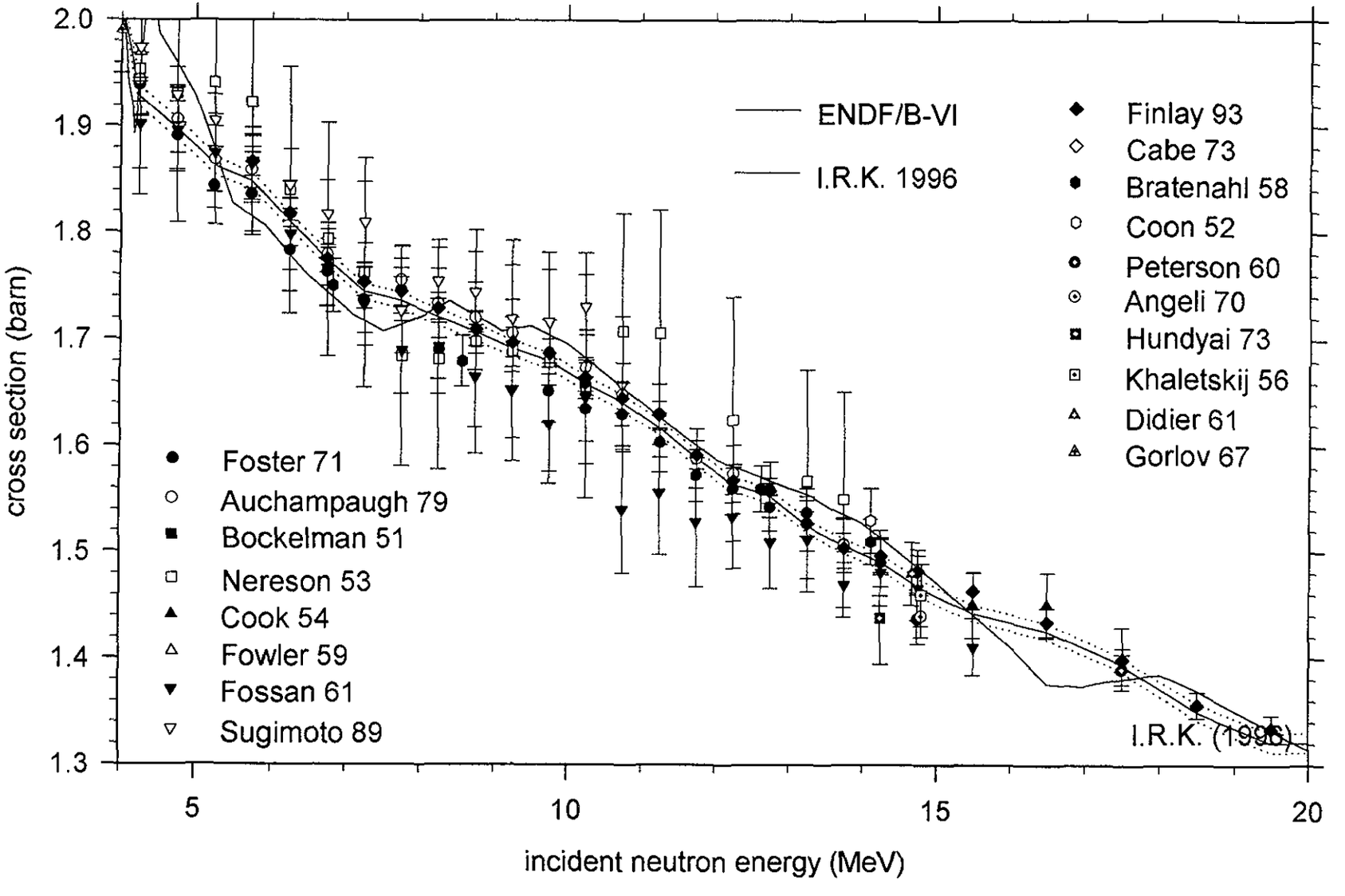

Figure 4: **^{9}Be (n,elastic) final evaluated cross section**

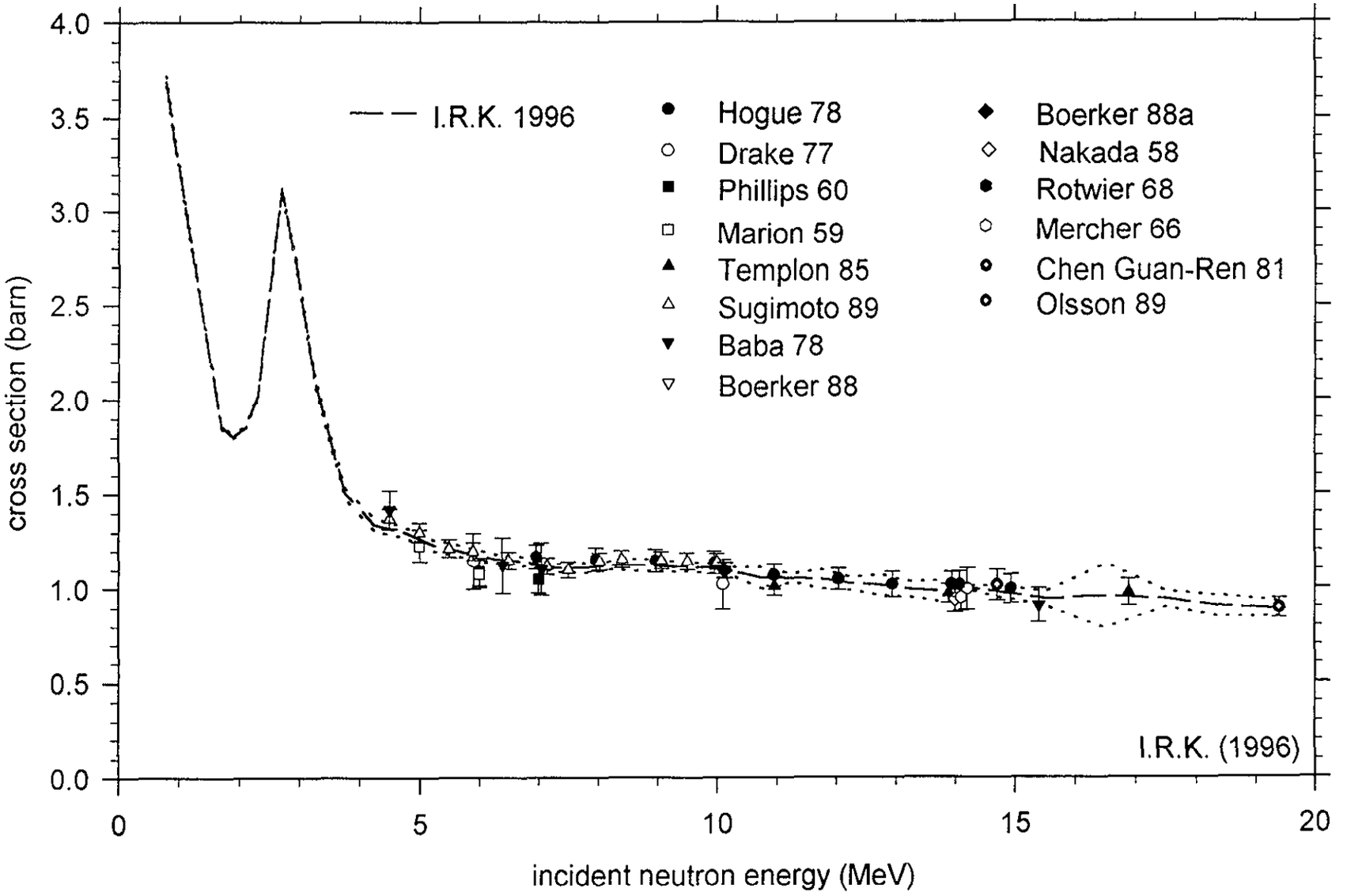

Figure 6: ^{9}Be (n,2n) final evaluated cross section

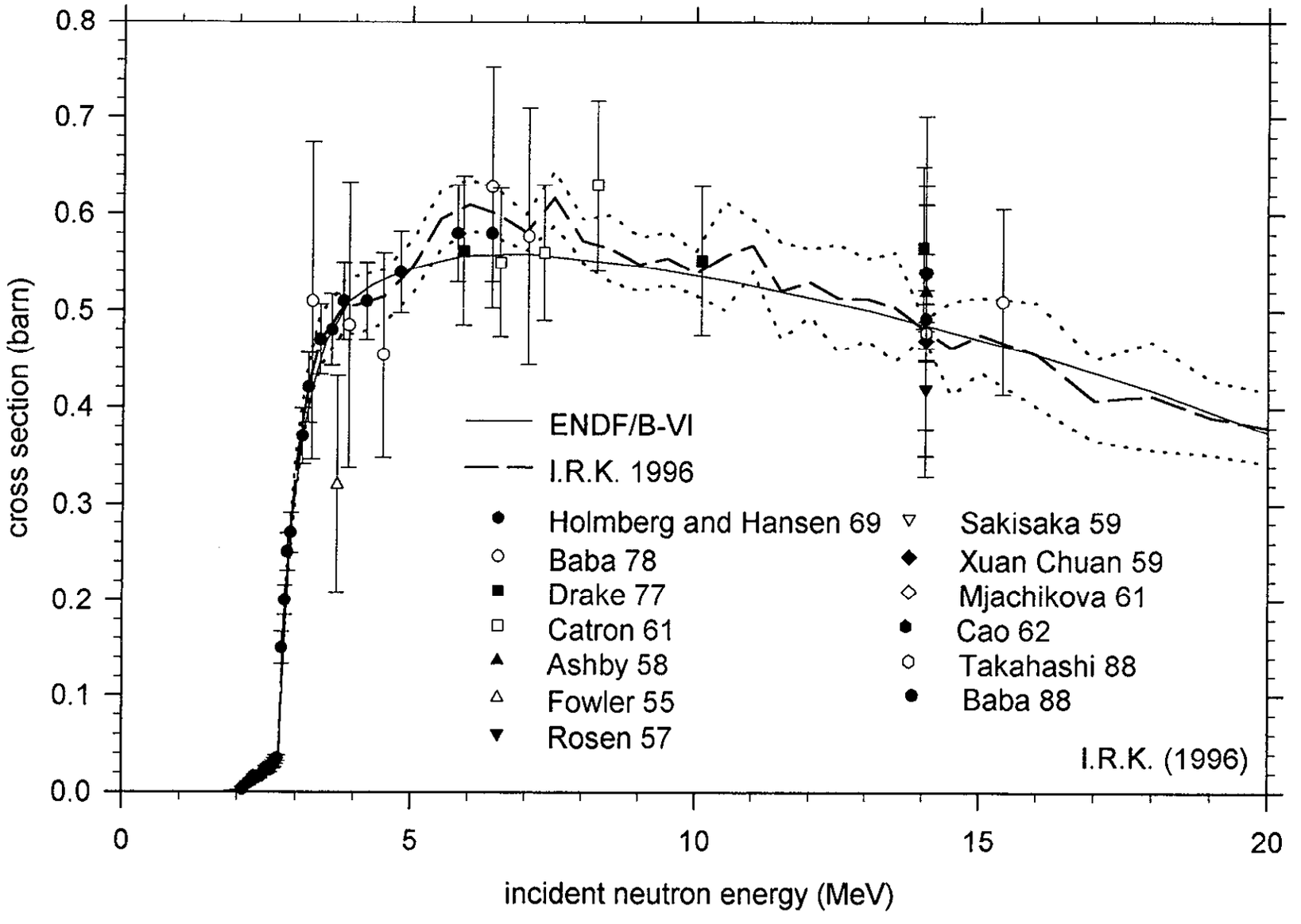

Figure 5: ^{9}Be (n,nonelastic) final evaluated cross section

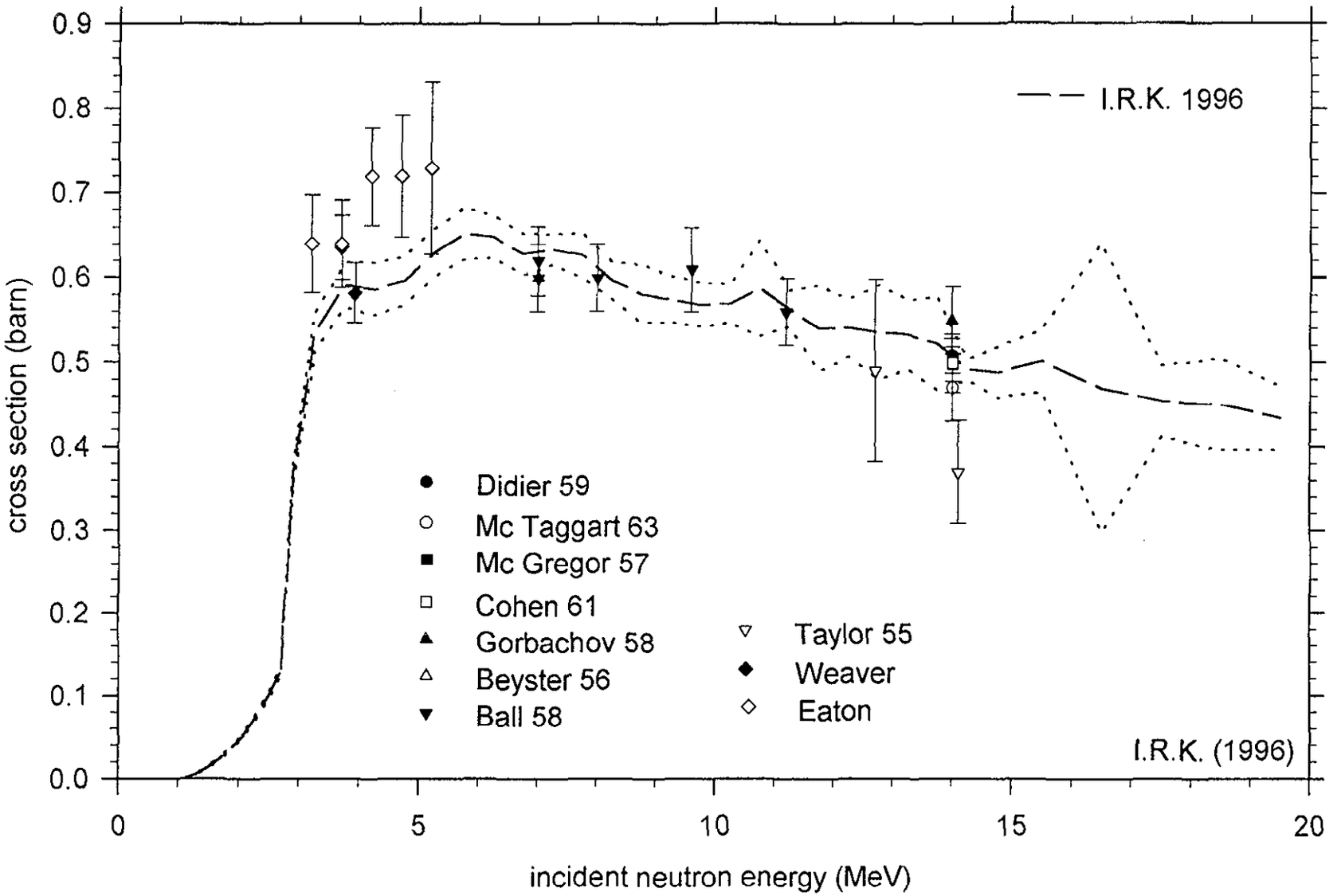

Figure 7: ^{9}Be (n,α) final evaluated cross section

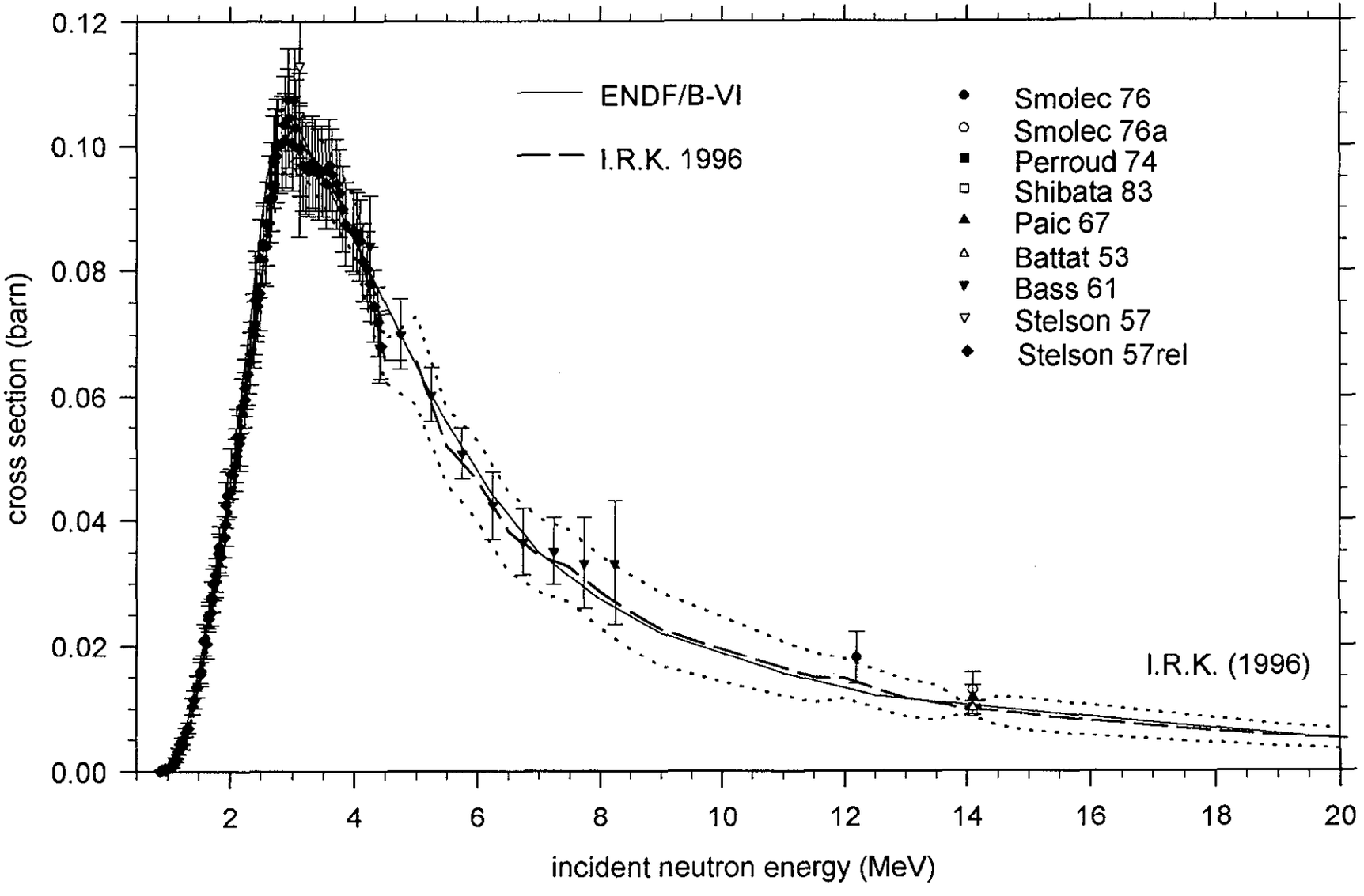

Figure 7a: ^{9}Be (n,α) final evaluated cross section

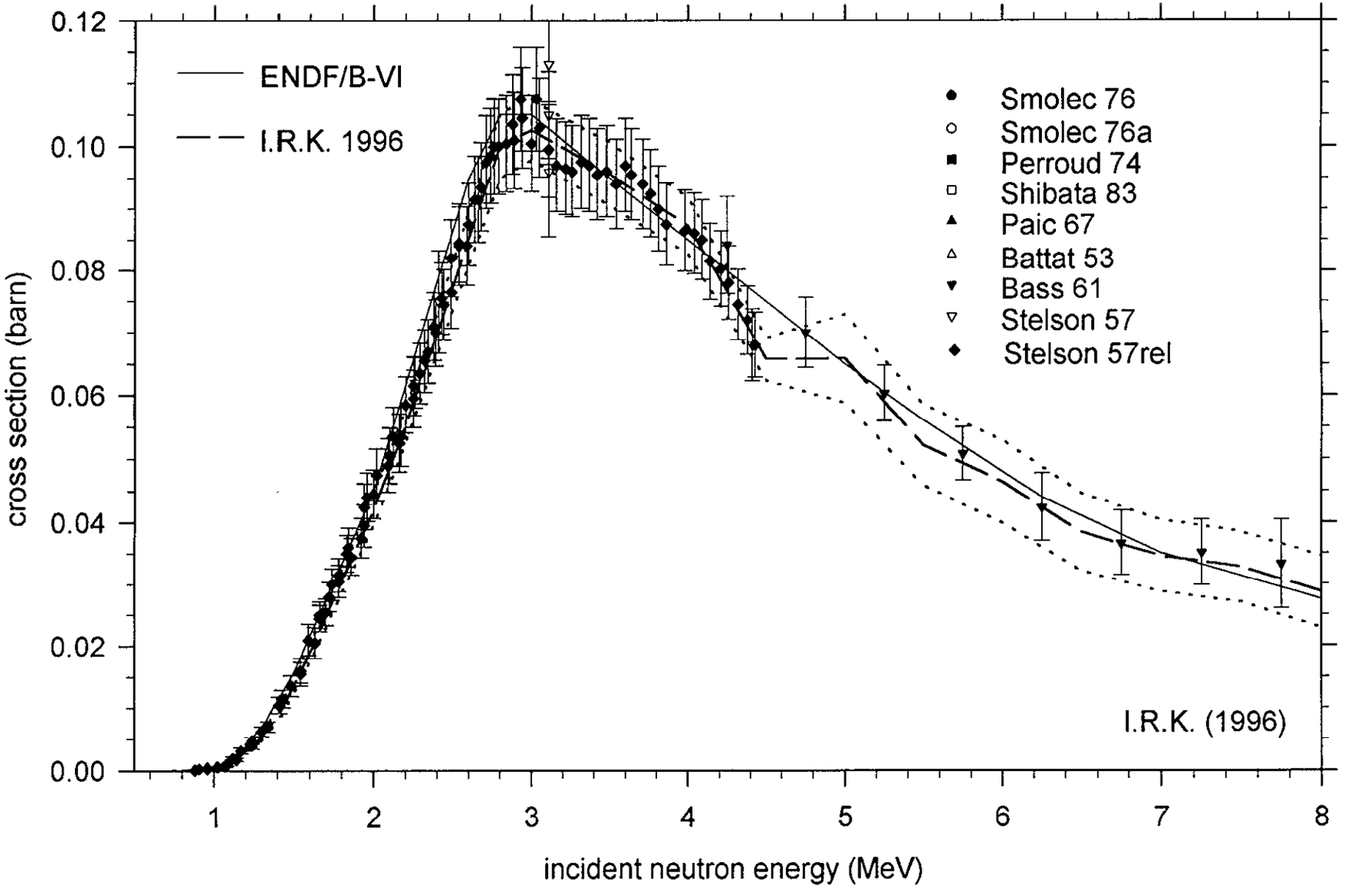

Figure 8: ^{9}Be (n,p) final evaluated cross section

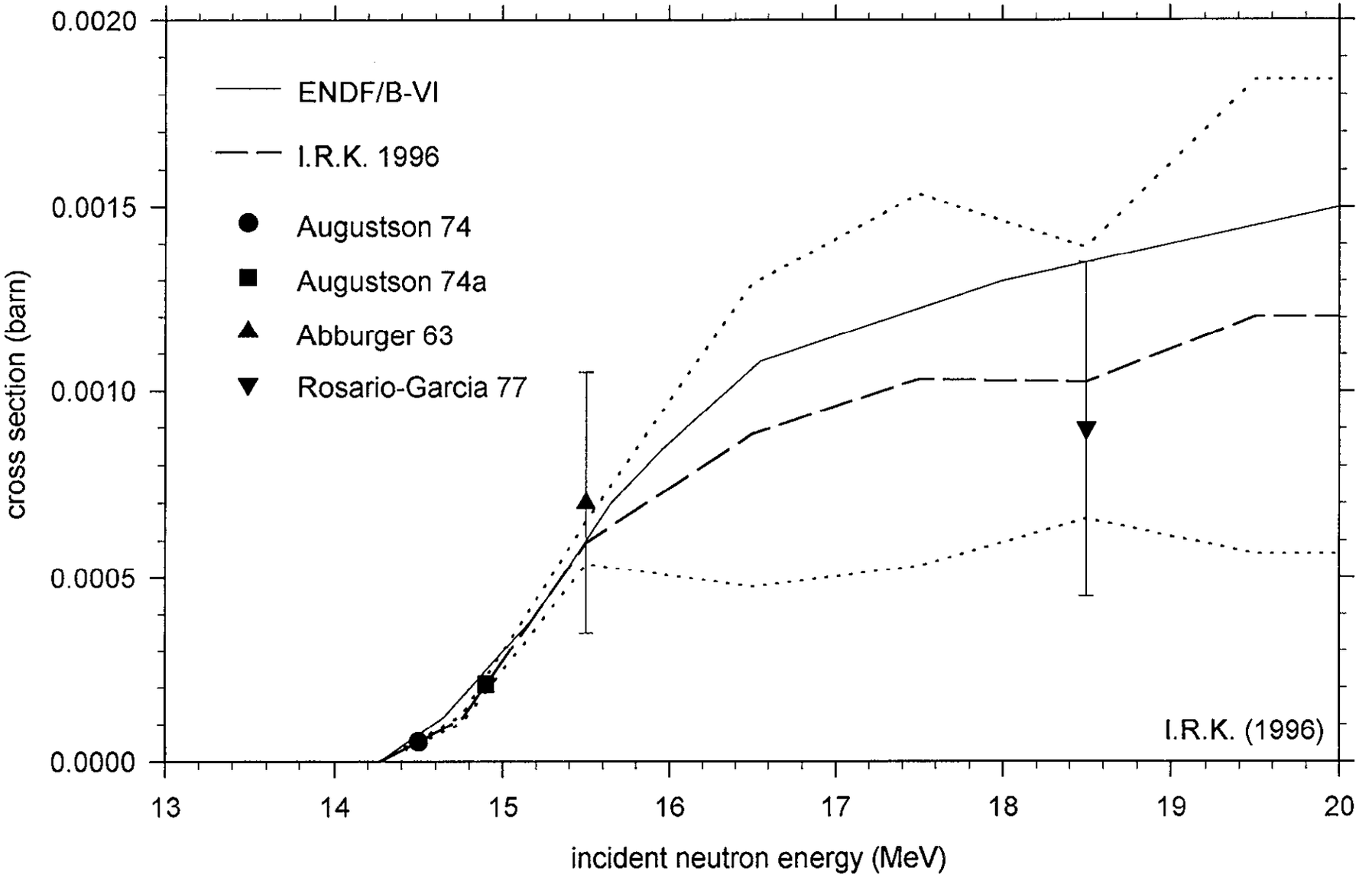

Figure 9: ^{9}Be (n,t) final evaluated cross section

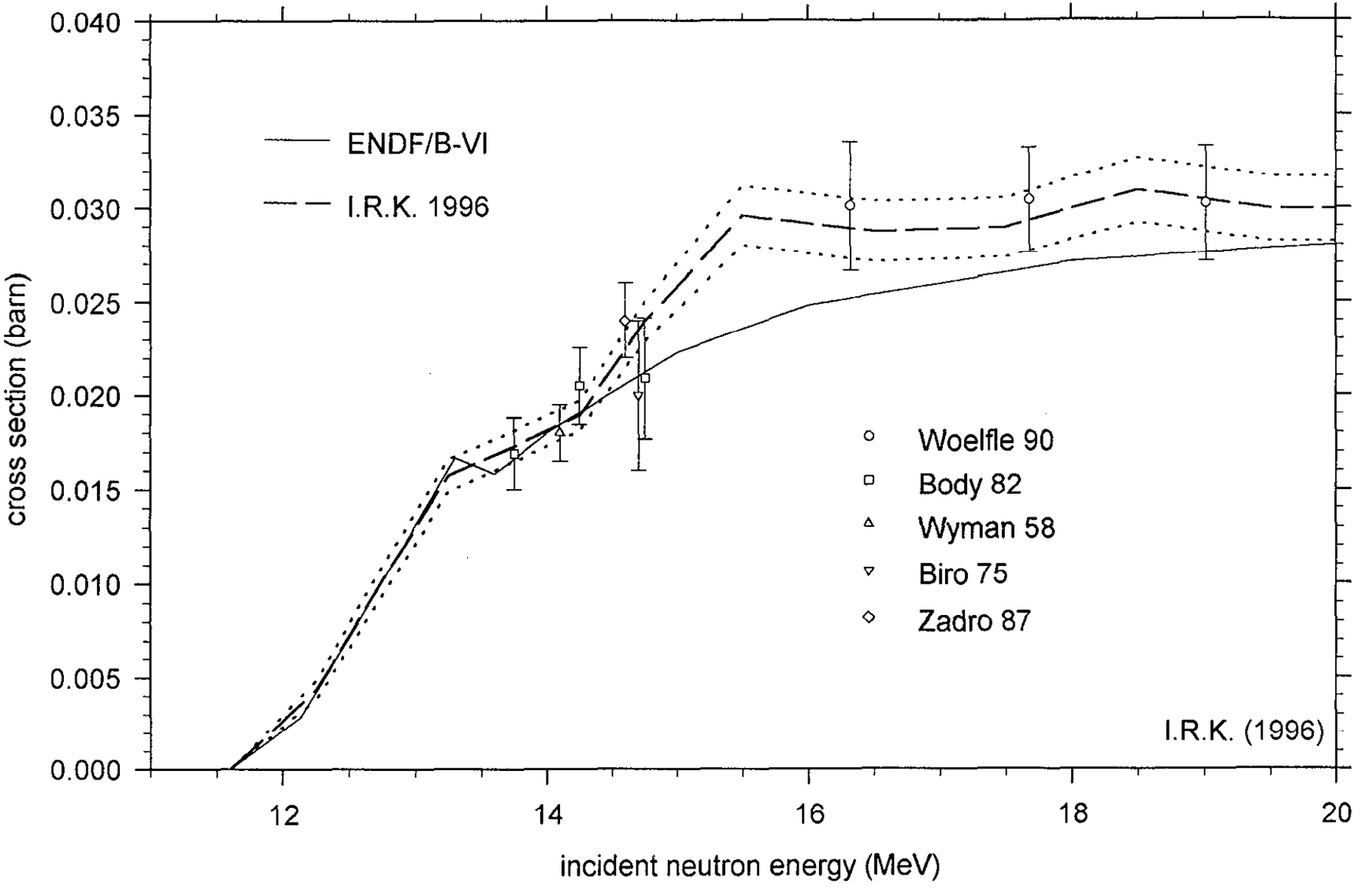

Figure 10: **^{9}Be total neutron cross section**

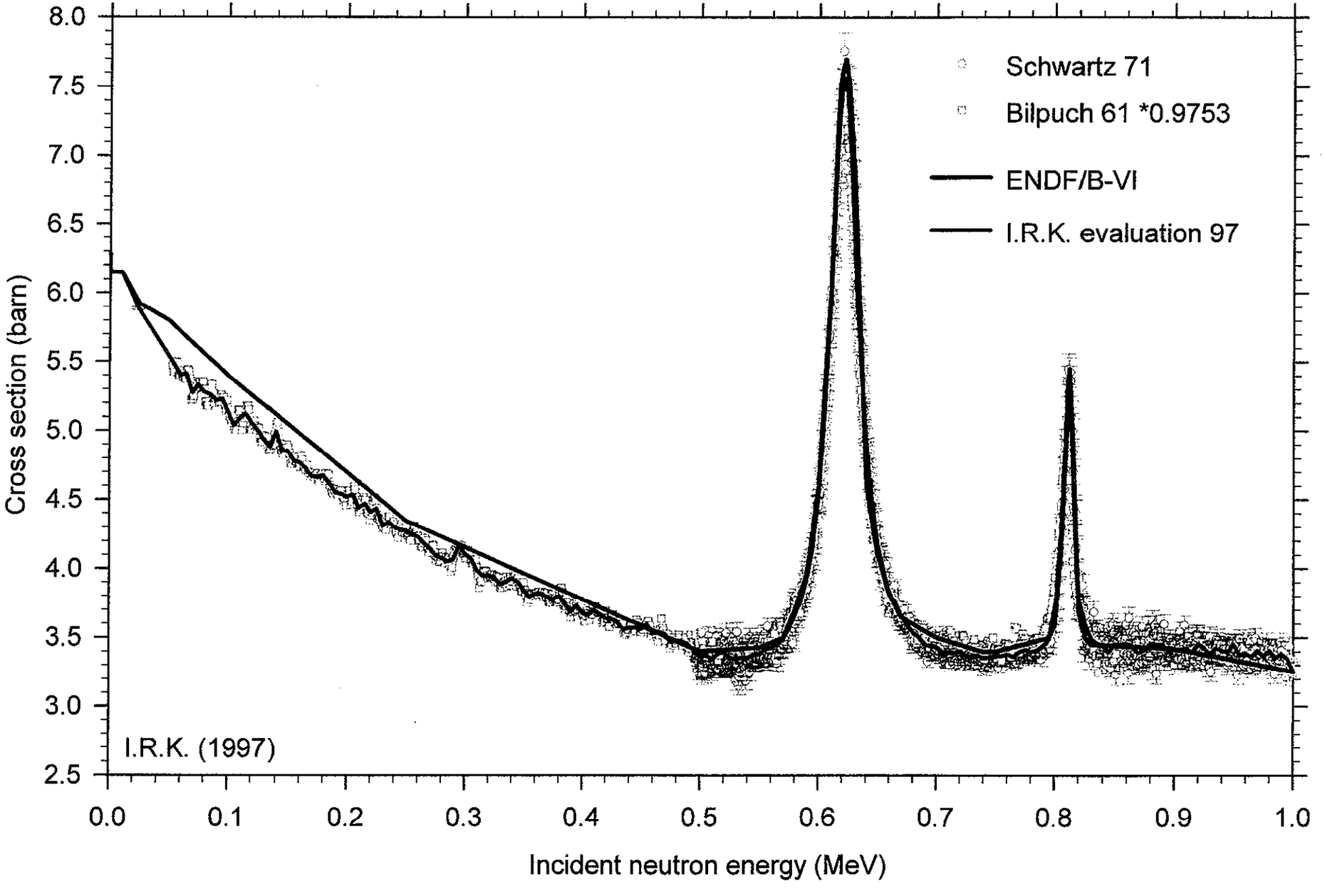

Figure 11: **^{9}Be total neutron cross section**

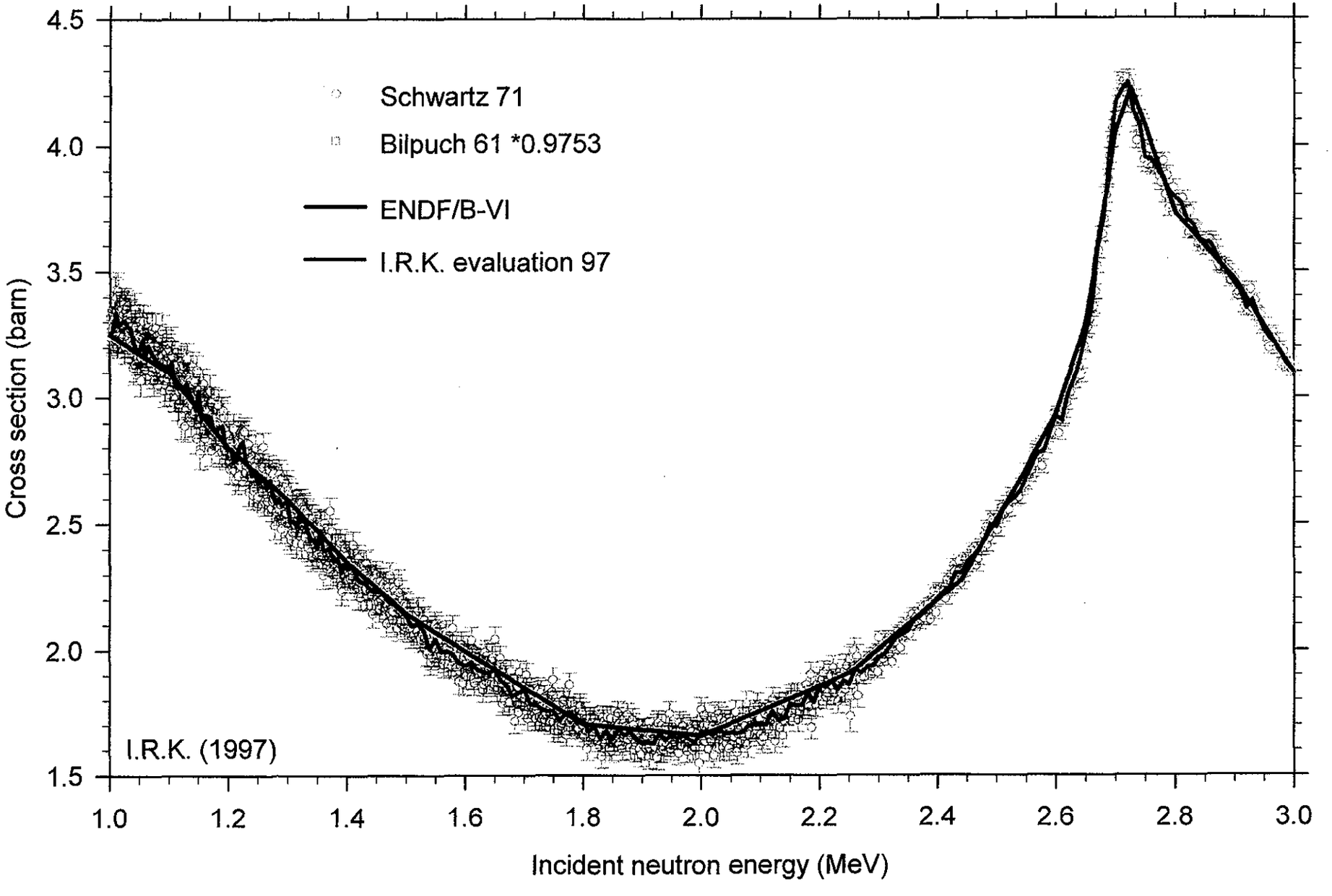

Figure 12: **^{9}Be total neutron cross section**

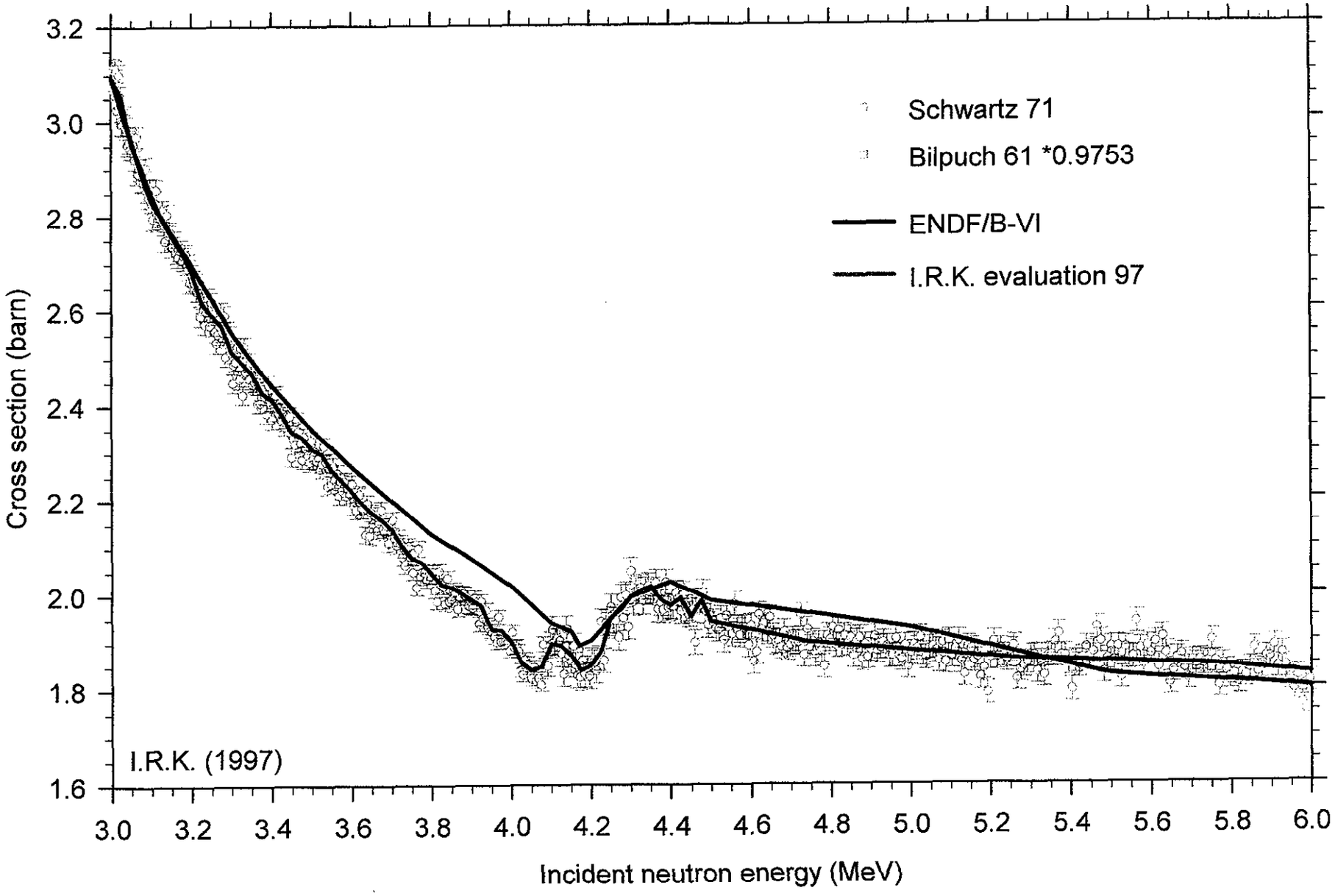

Figure 13: **^{9}Be total neutron cross section**

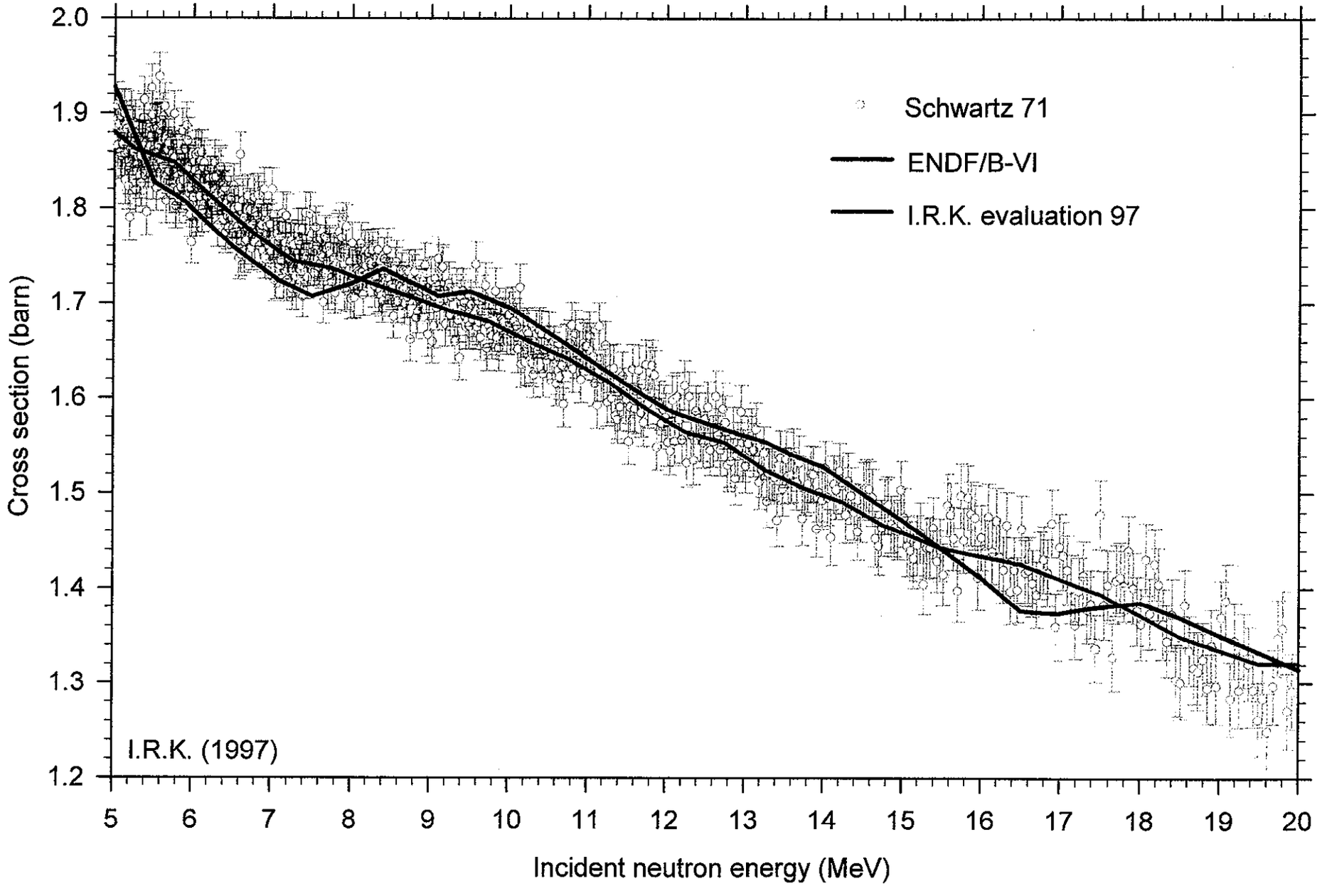

Figure 14: Reaction channels for the ^{9}Be + n system

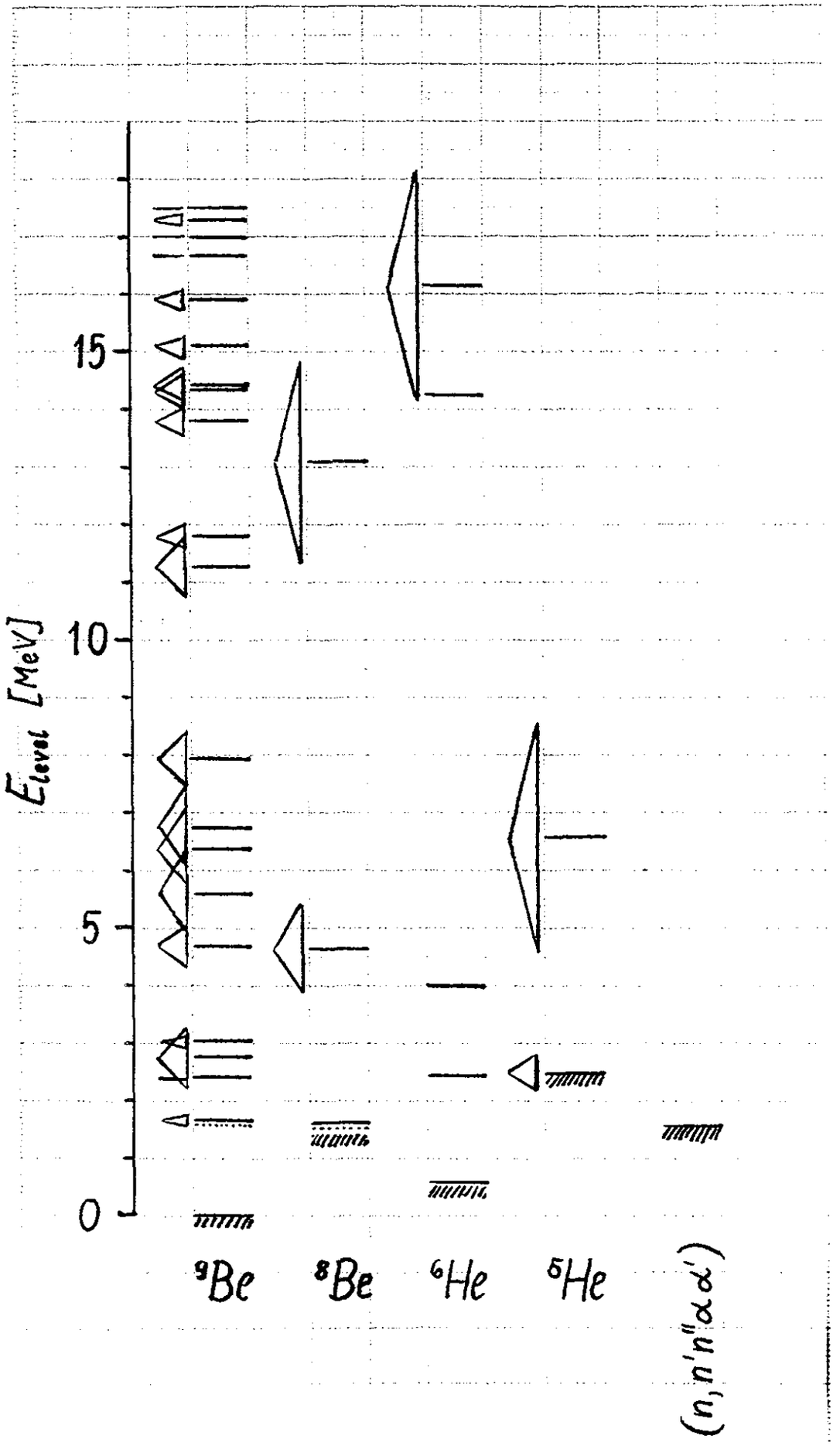

Figure 15: Energy-angular distribution of ^{9}Be(n,2n) secondary neutrons

Incident neutron energy 14.1 MeV, reaction component: (n,n'$_1$)

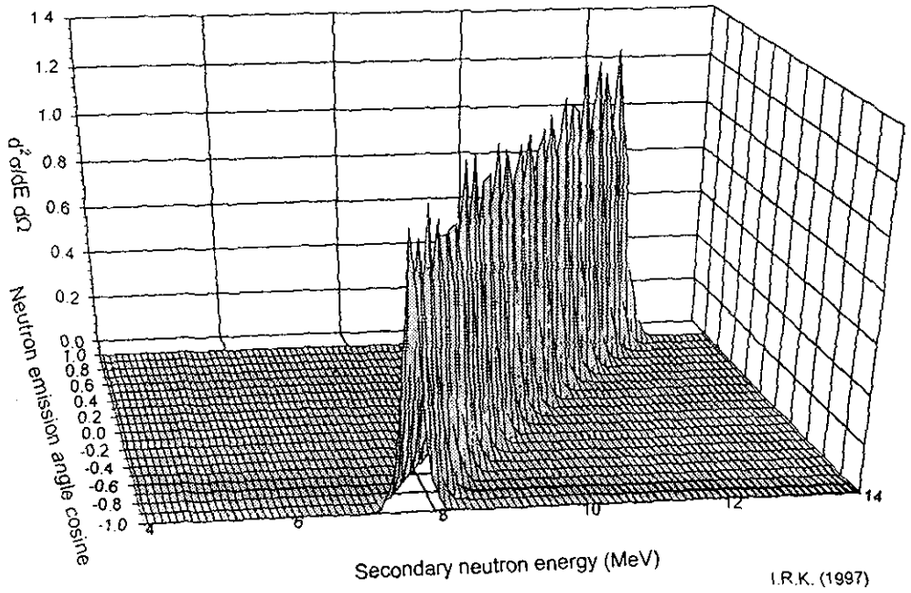

Figure 16: Energy-angular distribution of ^{9}Be(n,2n) secondary neutrons

Incident neutron energy 14.1 MeV, reaction component: (n,n'$_1$(n"$_0$ ^{8}Be))

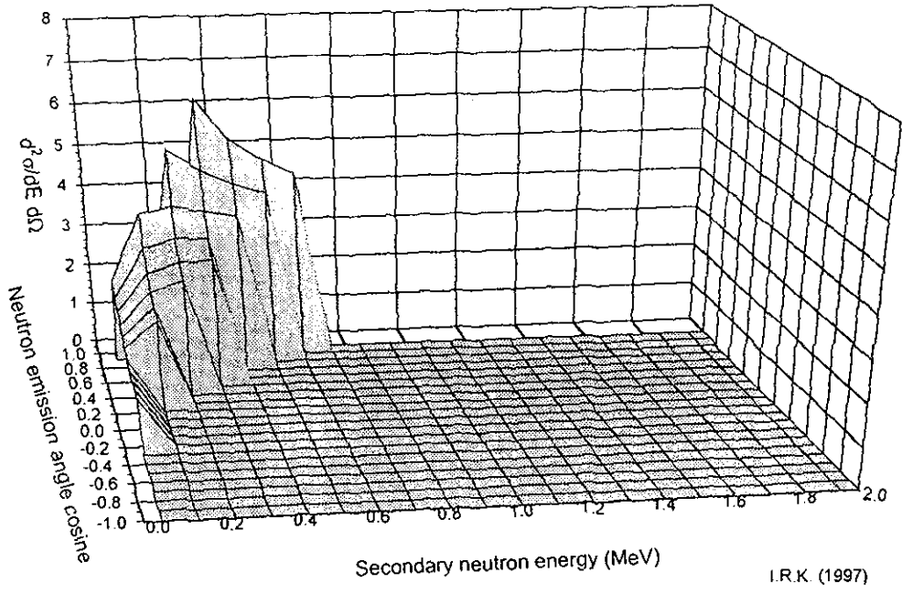

Figure 17: Energy-angular distribution of ^{9}Be(n,2n) secondary neutrons

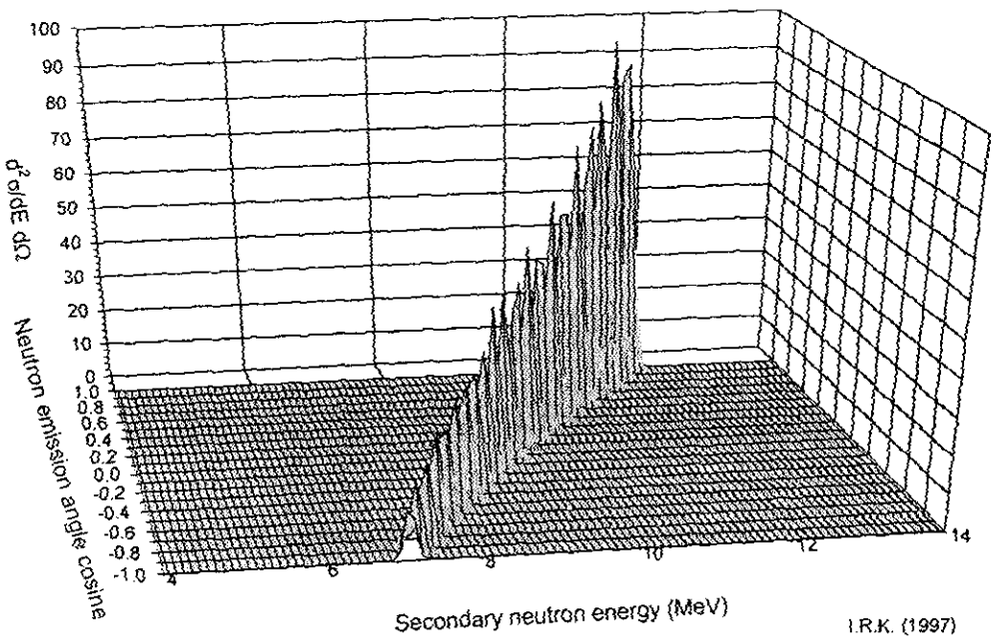

Figure 18: Energy-angular distribution of ^{9}Be(n,2n) secondary neutrons

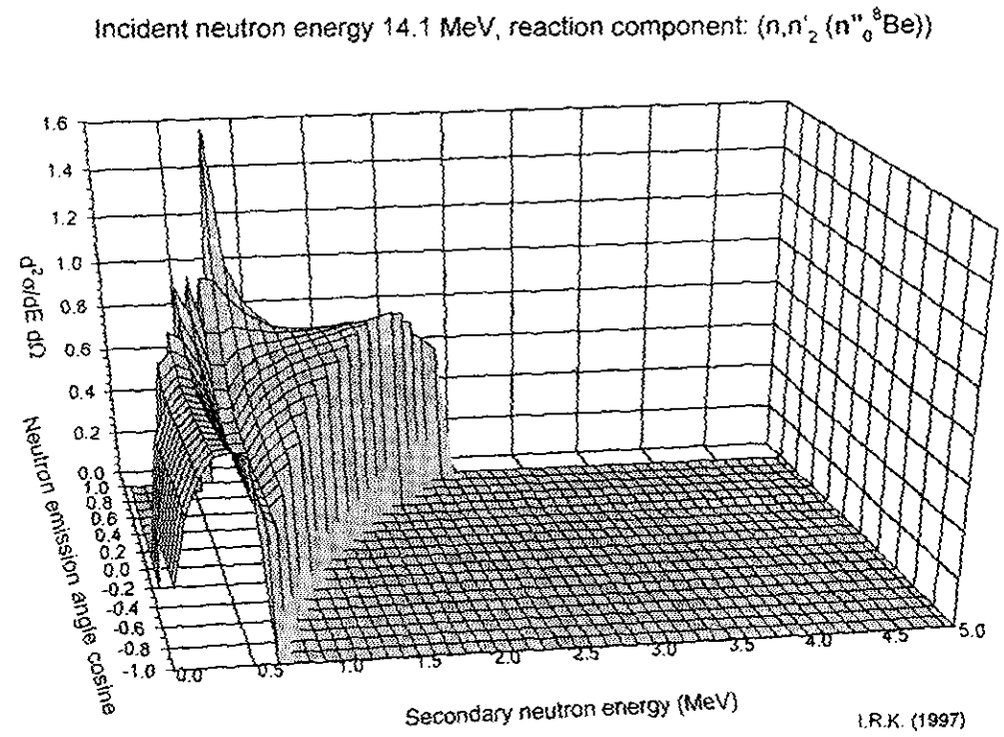

Figure 19: Energy-angular distribution of ^{9}Be(n,2n) secondary neutrons

Incident neutron energy 14.1 MeV, reaction component: (n,n'_5)

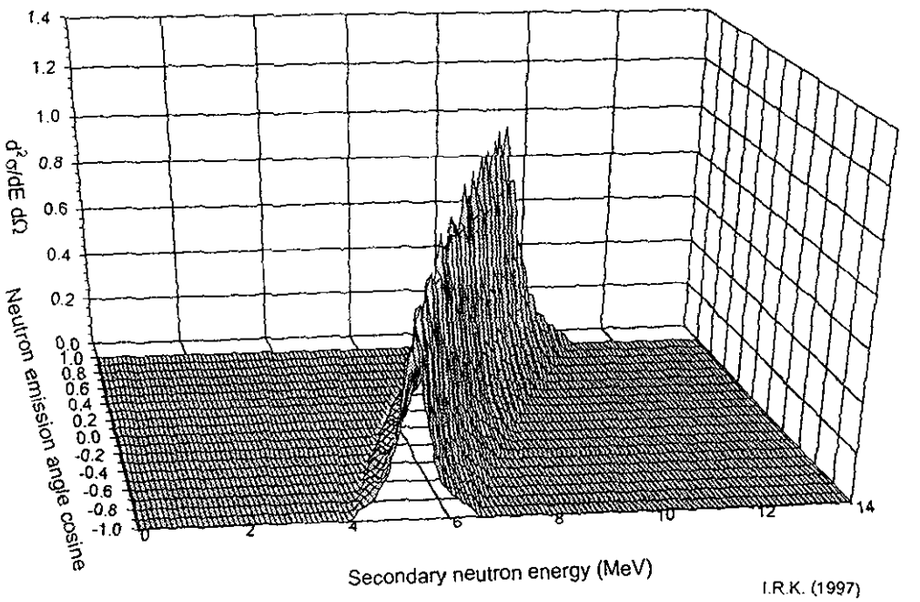

Figure 20: Energy-angular distribution of ^{9}Be(n,2n) secondary neutrons

Incident neutron energy 14.1 MeV, reaction component: (n,n'_6)

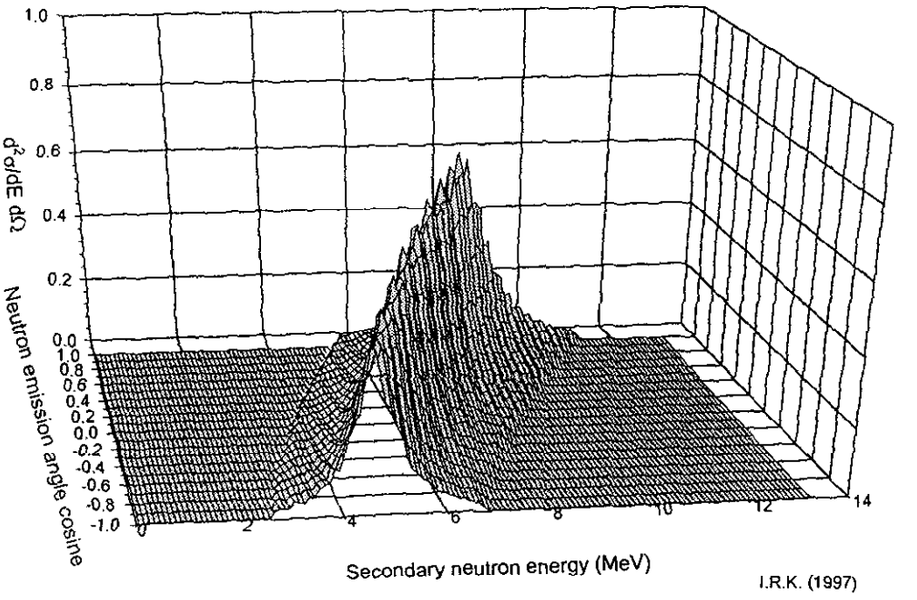

Figure 21: Energy-angular distribution of ^{9}Be(n,2n) secondary neutrons

Incident neutron energy 14.1 MeV, reaction component: (n,n'_5 ($\mathbf{n''}_0$ ^{8}Be))

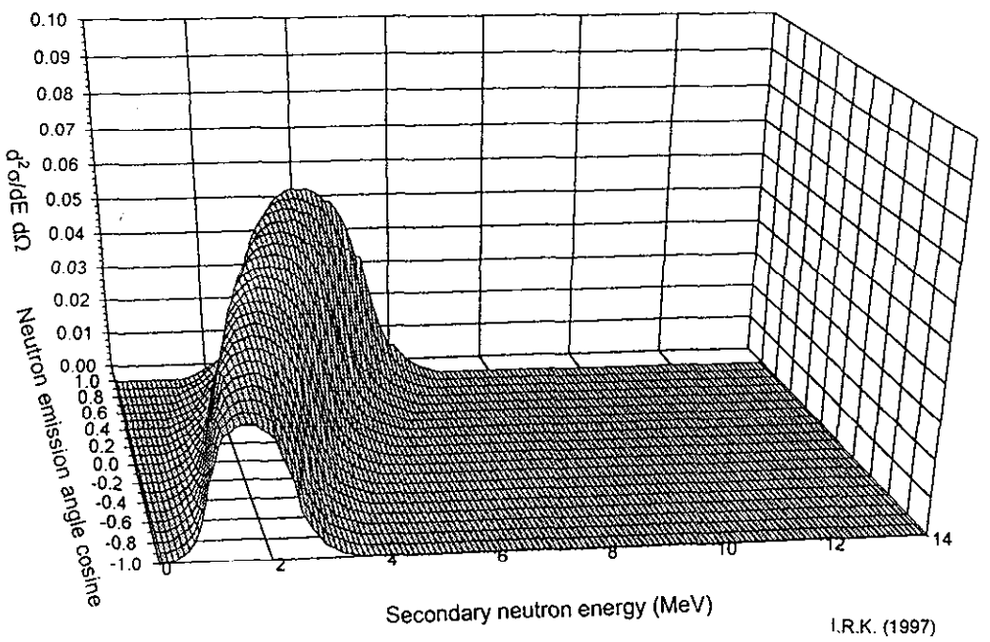

Figure 22: Energy-angular distribution of ^{9}Be(n,2n) secondary neutrons

Incident neutron energy 14.1 MeV, reaction component: (n,n'_5($\mathbf{n''}_1$ ^{8}Be))

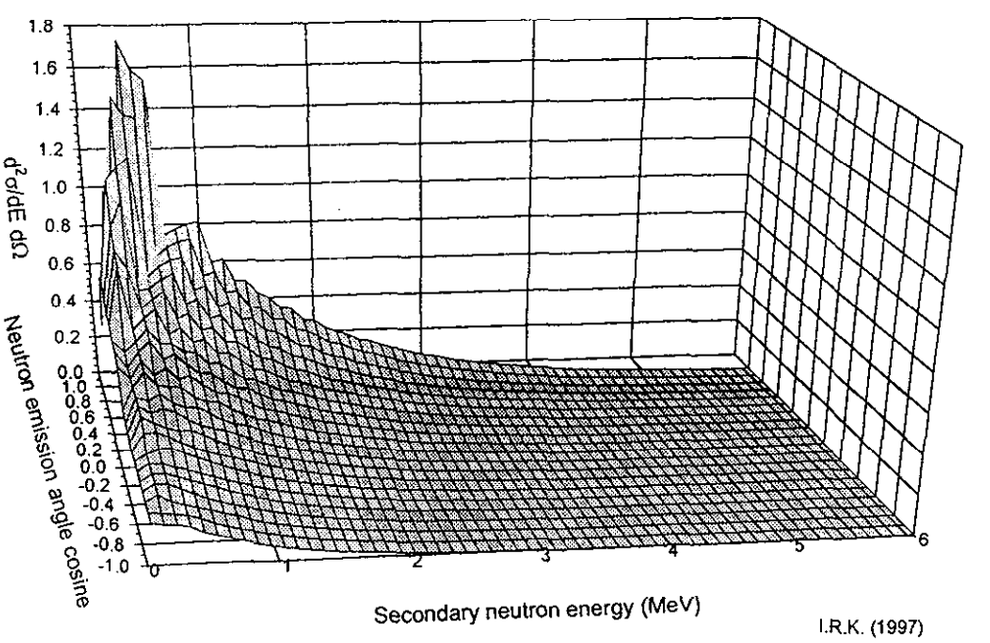

Figure 23: Energy-angular distribution of $^{9}Be(n,2n)$ secondary neutrons

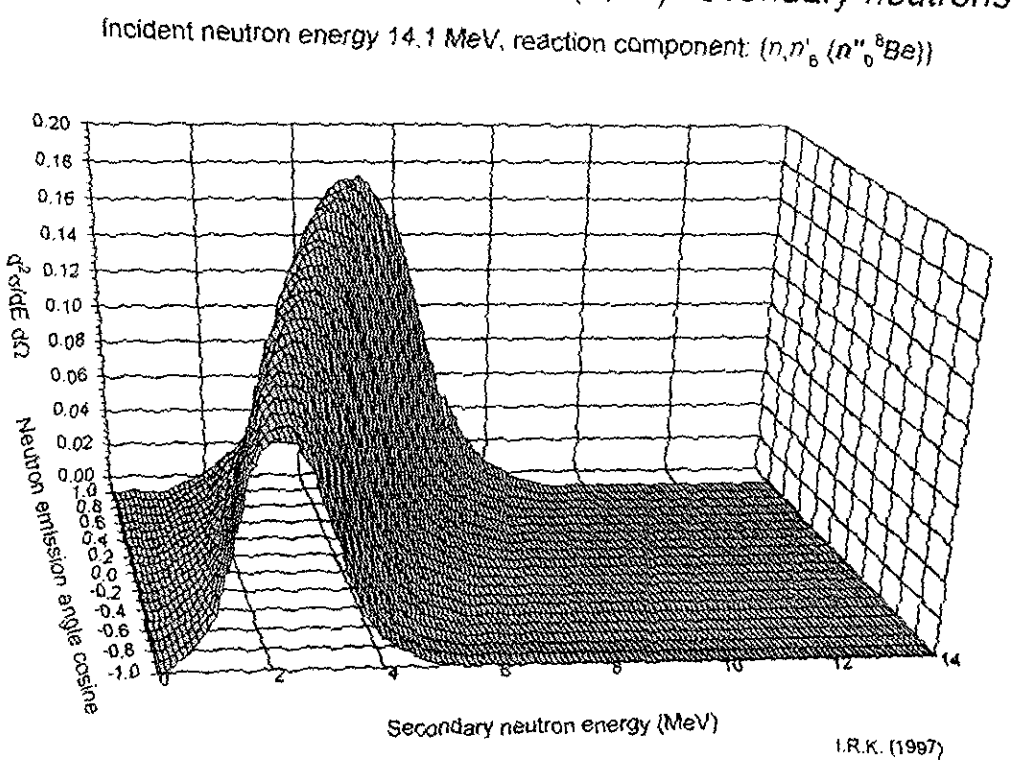

Figure 24: Energy-angular distribution of $^{9}Be(n,2n)$ secondary neutrons

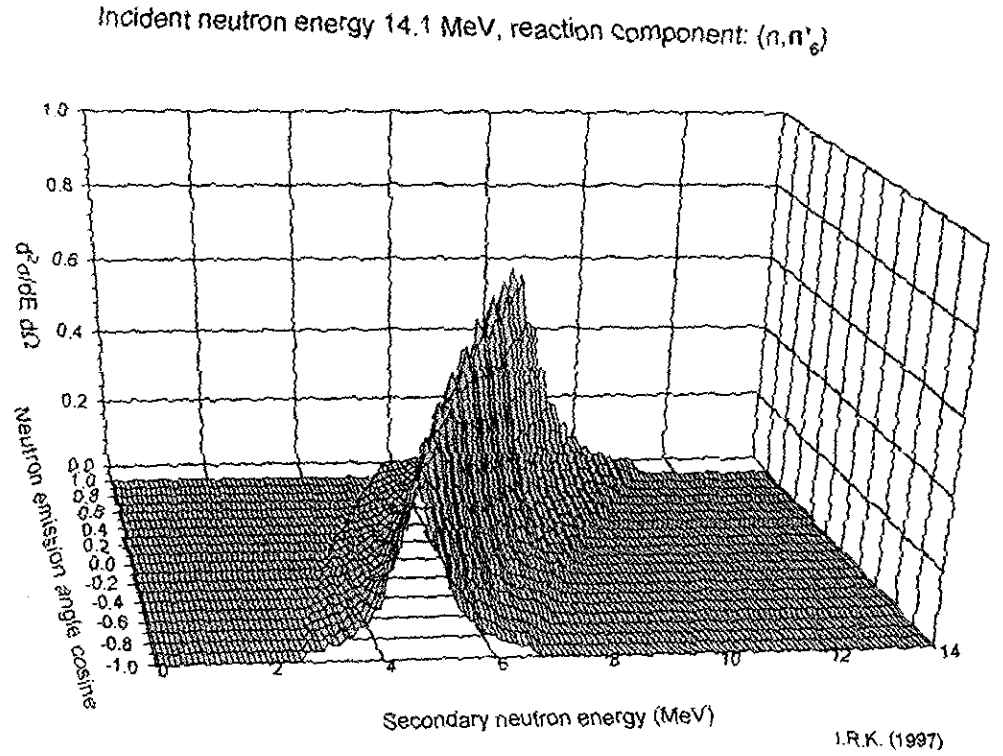

Figure 25: Energy-angular distribution of ^{9}Be(n,2n) secondary neutrons

Incident neutron energy 14.1 MeV, reaction component: (n,n'_7)

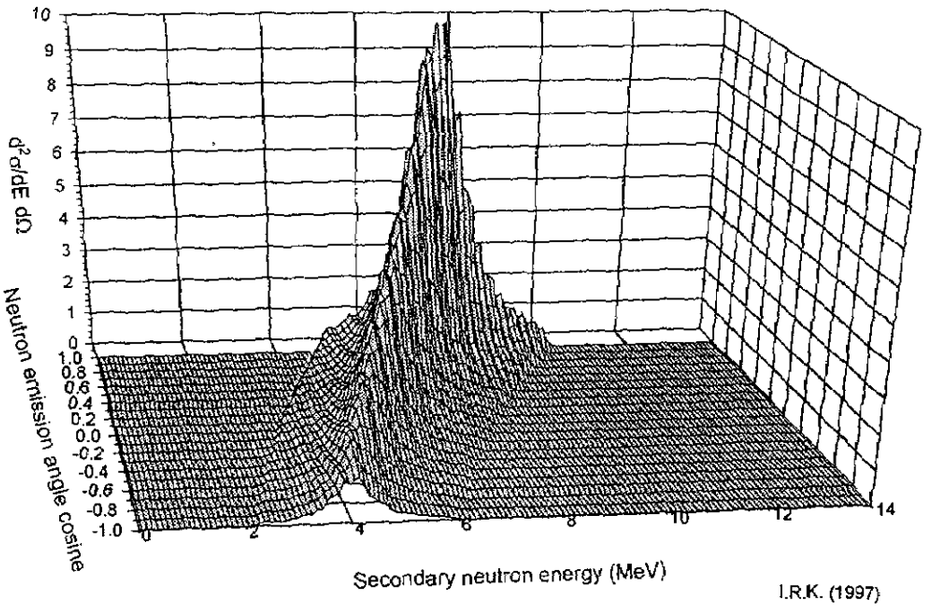

Figure 26: Energy-angular distribution of ^{9}Be(n,2n) secondary neutrons

Incident neutron energy 14.1 MeV, reaction component: (n,n'_8)

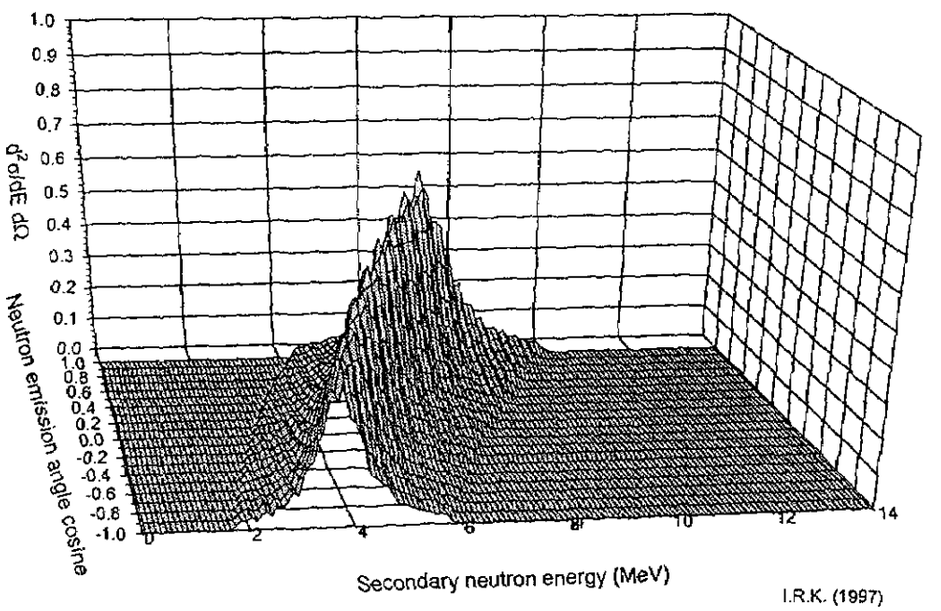

Figure 27: Energy-angular distribution of ^{9}Be(n,2n) secondary neutrons

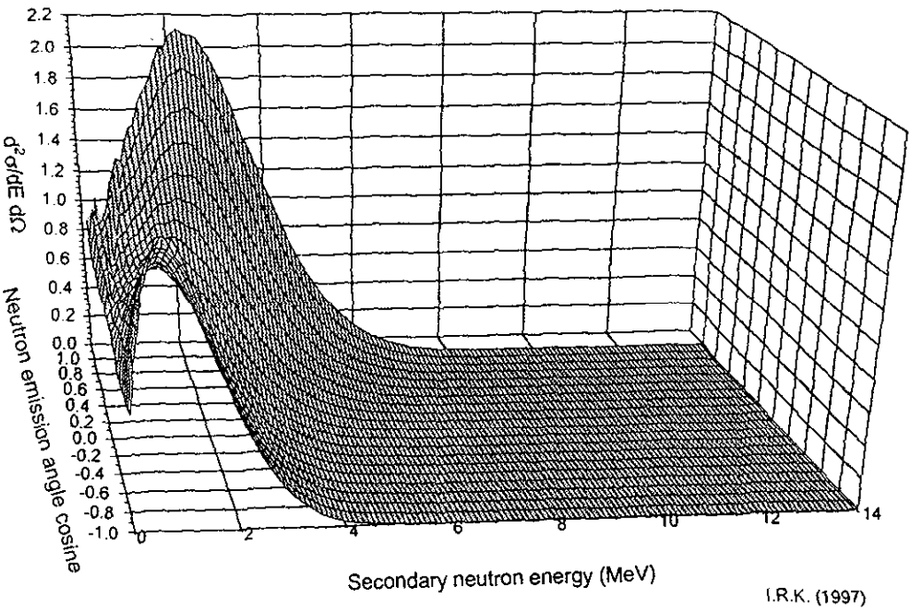

Figure 28: Energy-angular distribution of ^{9}Be(n,2n) secondary neutrons

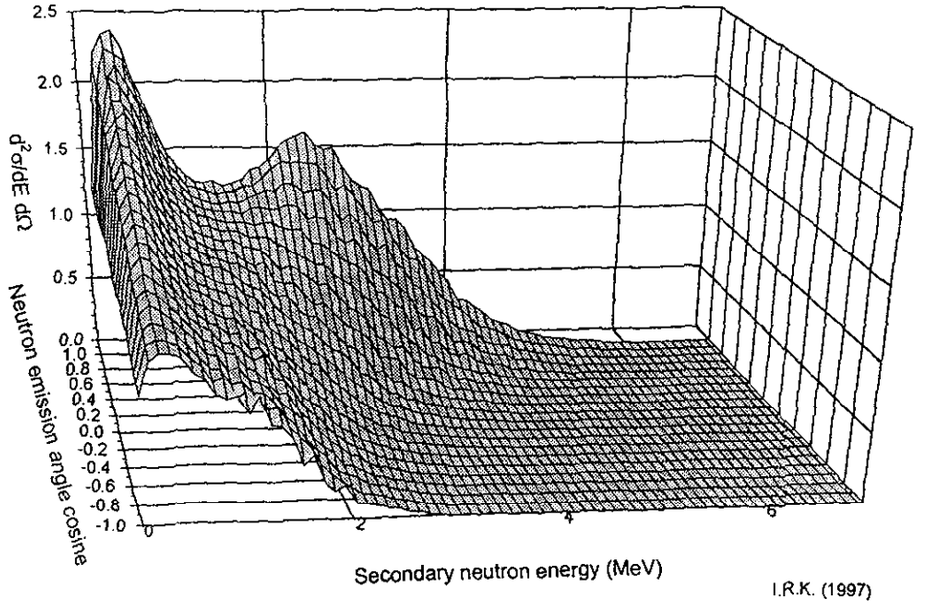

Figure 29: Energy-angular distribution of $^{9}Be(n,2n)$ secondary neutrons

Incident neutron energy 14.1 MeV, reaction component: (n,n'_9)

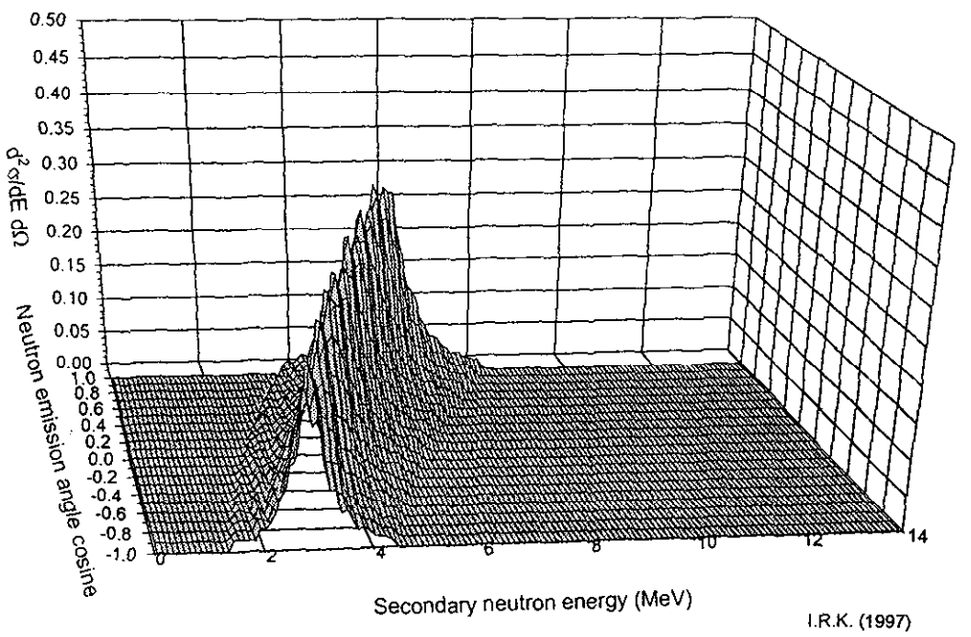

Figure 30: Energy-angular distribution of $^{9}Be(n,2n)$ secondary neutrons

Incident neutron energy 14.1 MeV, reaction component: (n,n'_{10})

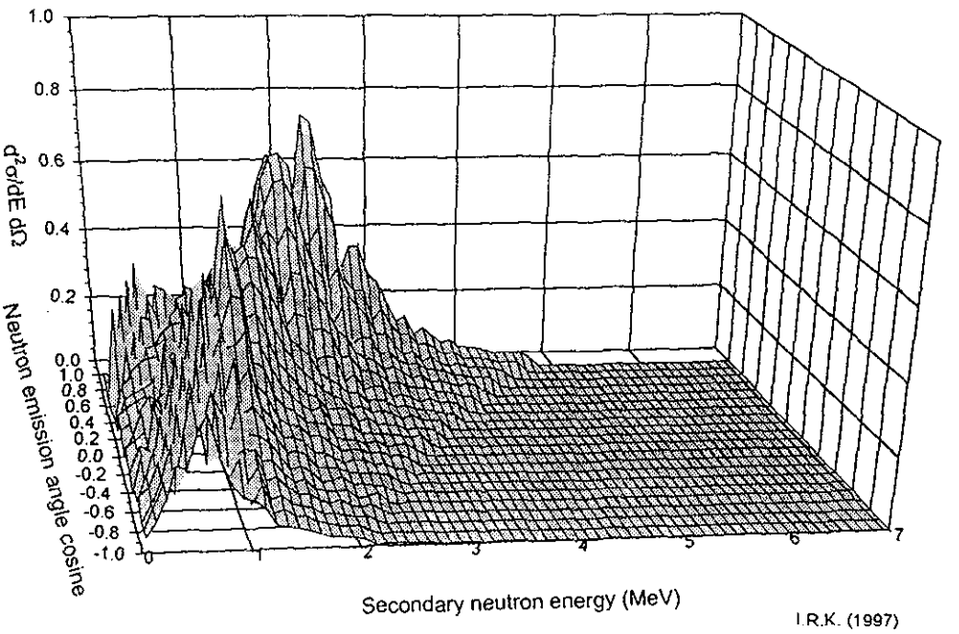

Figure 31: Energy-angular distribution of $^{9}Be(n,2n)$ *secondary neutrons*

Incident neutron energy 14.1 MeV, reaction component: $(n,n'_9\ (n''_0\ ^{8}Be))$

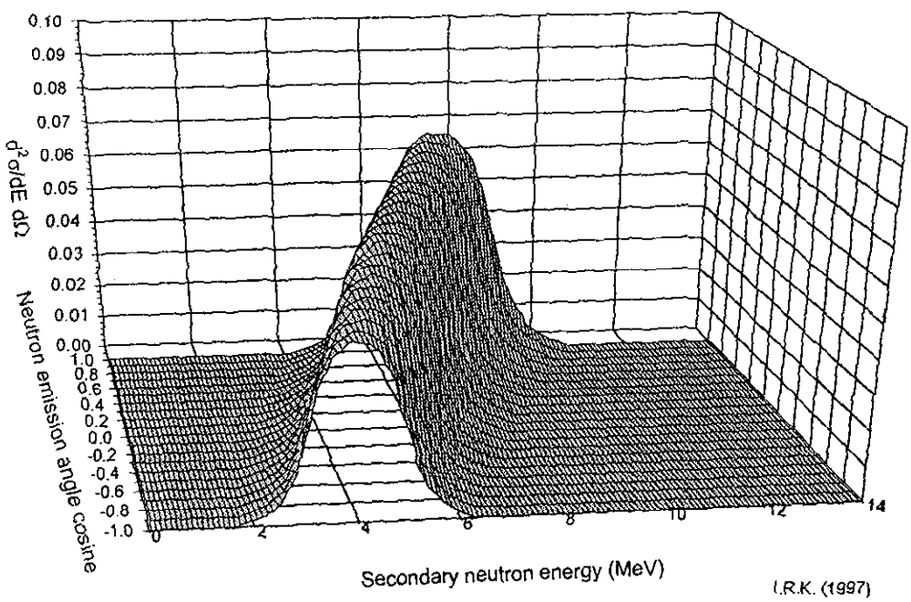

Figure 32: Energy-angular distribution of $^{9}Be(n,2n)$ secondary neutrons

Incident neutron energy 14.1 MeV, reaction component: $(n,n'_9\ (n''_1\ ^{8}Be))$

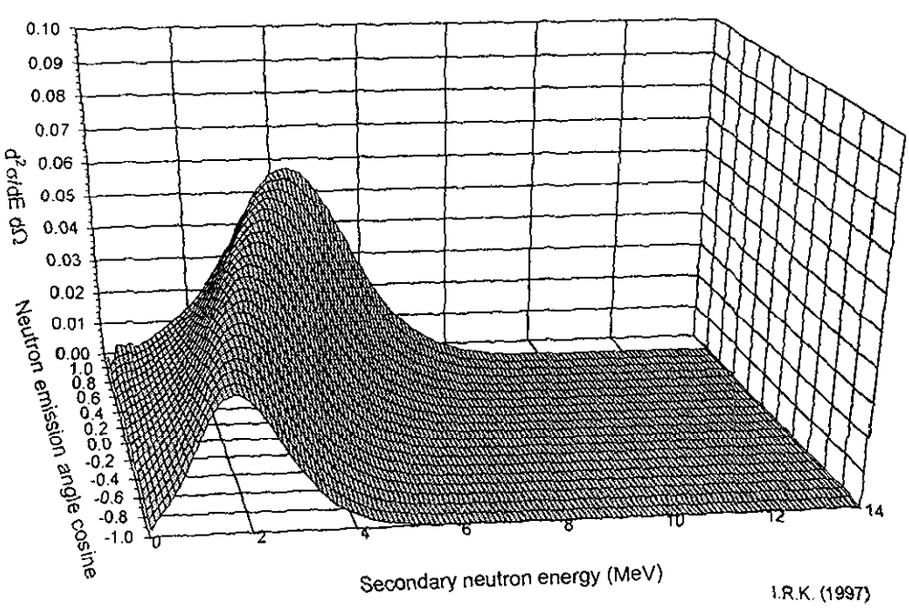

Figure 33: Energy-angular distribution of ^{9}Be(n,2n) secondary neutrons

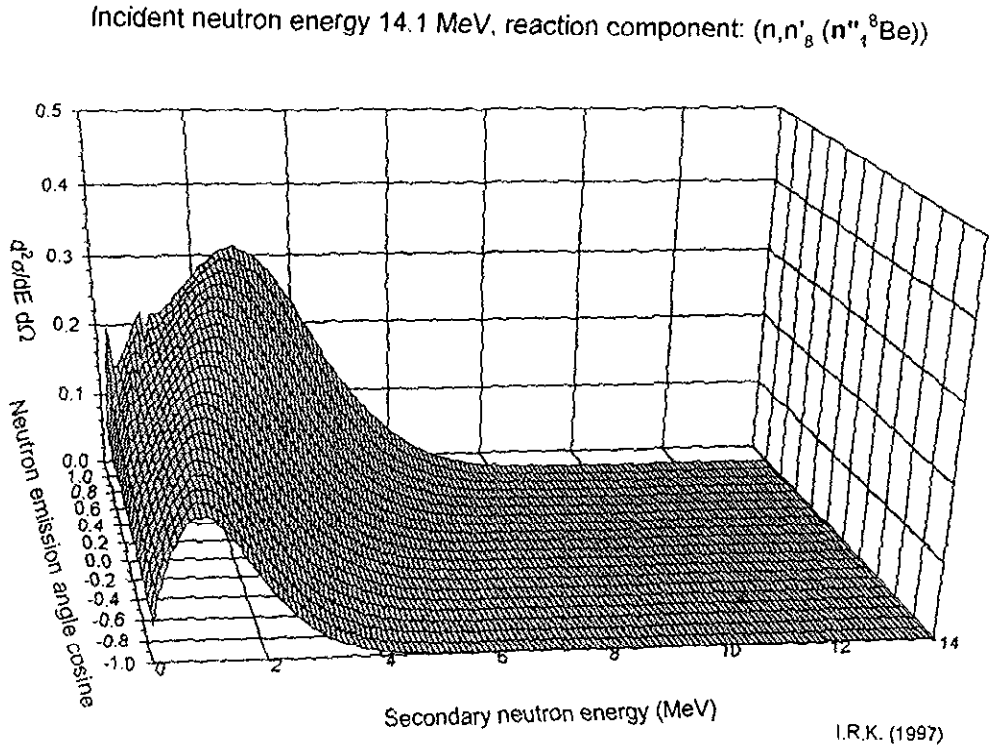

Figure 34: Energy-angular distribution of ^{9}Be(n,2n) secondary neutrons

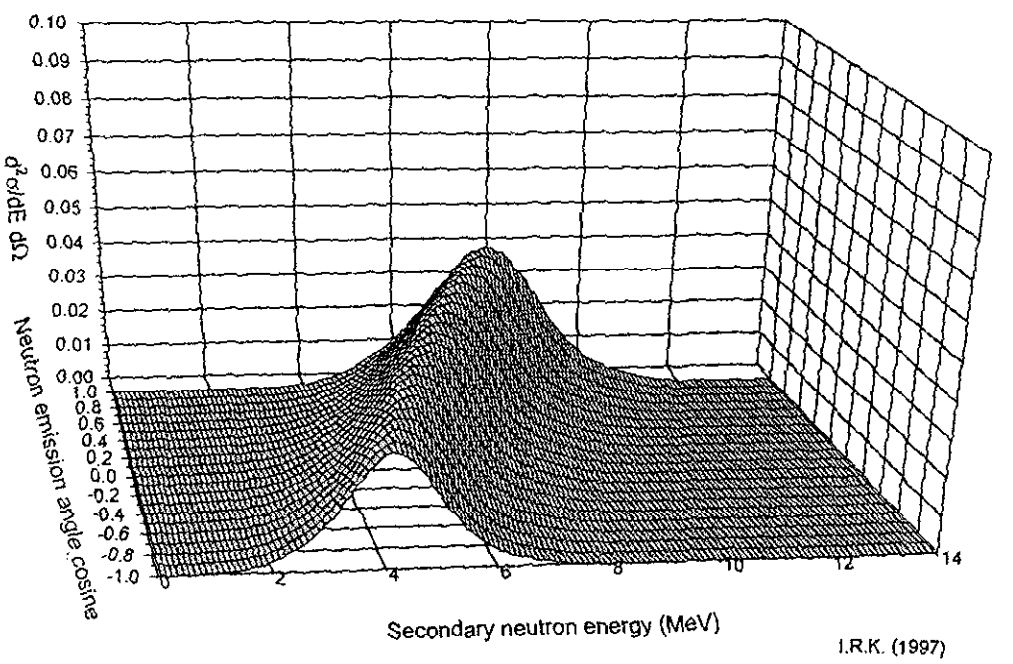

Figure 35: Energy-angular distribution of ^{9}Be(n,2n) secondary neutrons

Incident neutron energy 14.1 MeV, reaction component: (n,n'$_{10}$ (α'_0 (n"α"))

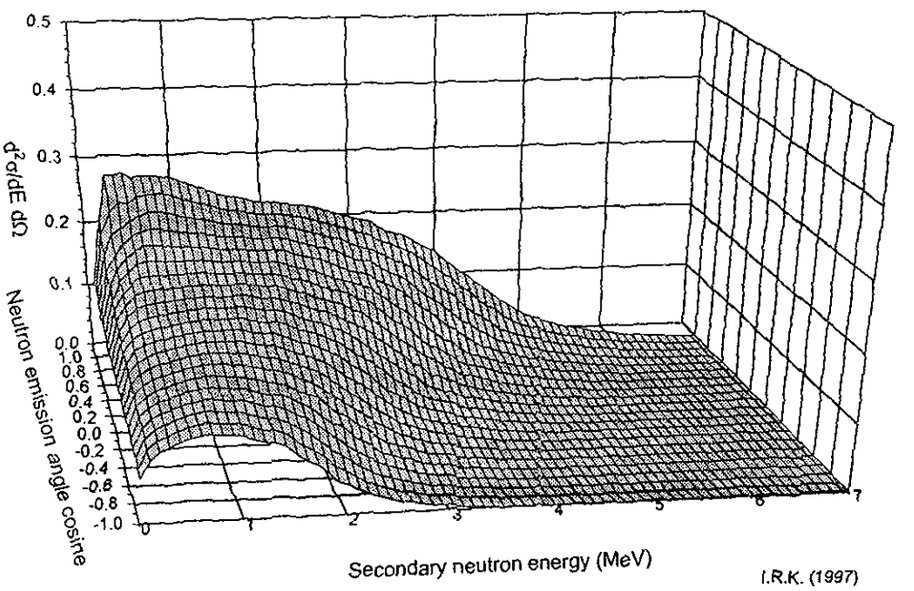

Figure 36: Energy-angular distribution of ^{9}Be(n,2n) secondary neutrons

Incident neutron energy 14.1 MeV, reaction component: (n,n'$_{11}$)

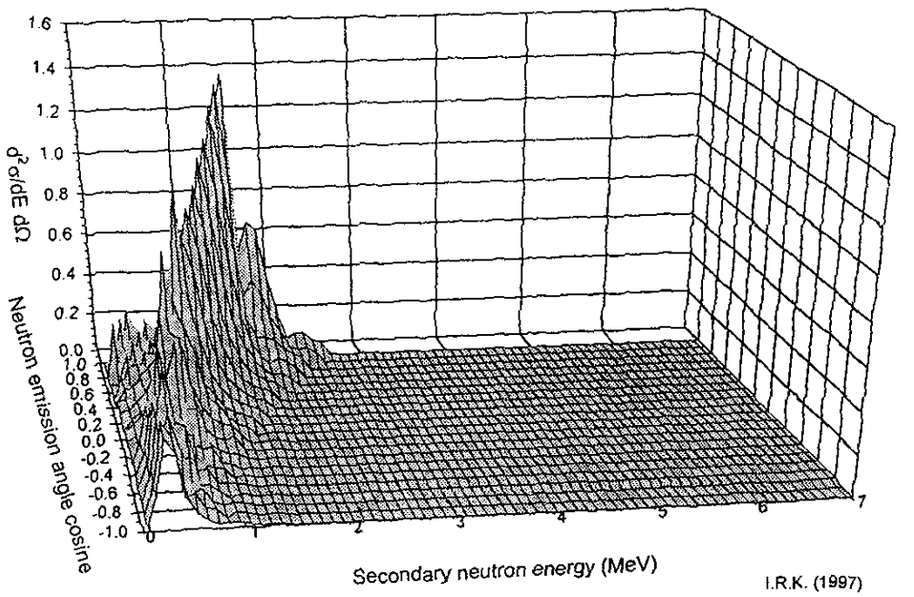

Figure 37: Energy-angular distribution of ^{9}Be(n,2n) secondary neutrons

Incident neutron energy 14.1 MeV, reaction component: (n,n'$_{11}$ (n"$_{0}$ ^{8}Be))

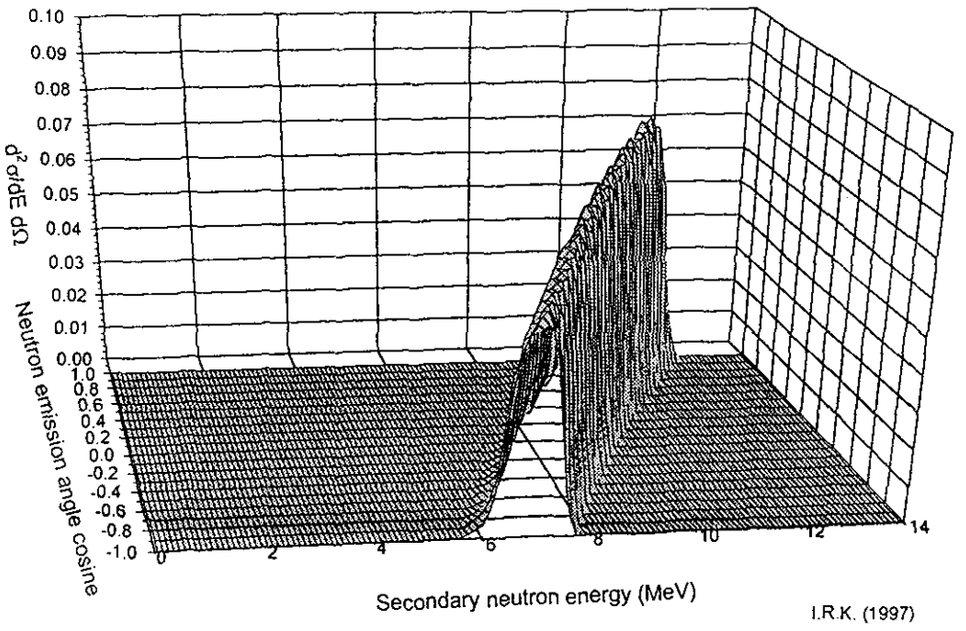

Figure 38: Energy-angular distribution of ^{9}Be(n,2n) secondary neutrons

Incident neutron energy 14.1 MeV, reaction component: (n,n'$_{11}$ (n"$_{1}$ ^{8}Be))

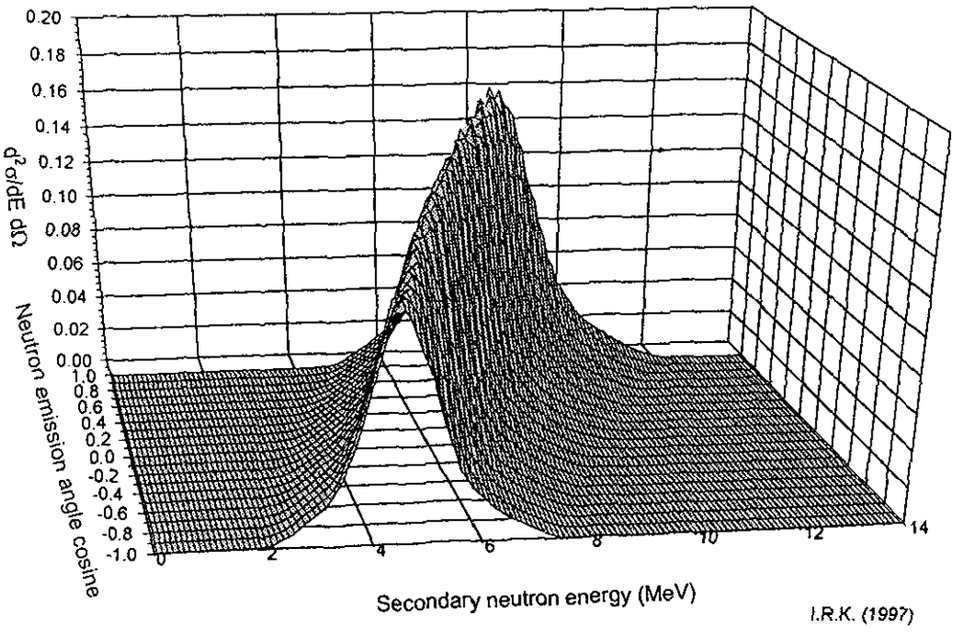

Figure 39: Energy-angular distribution of ^{9}Be(n,2n) secondary neutrons

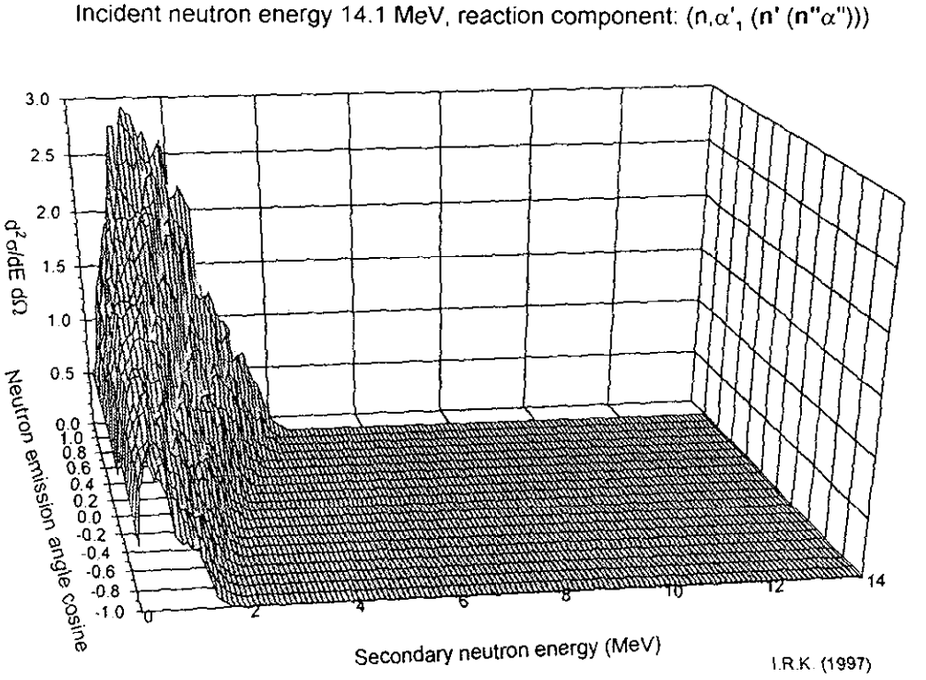

Figure 40: Energy-angular distribution of ^{9}Be(n,2n) secondary neutrons

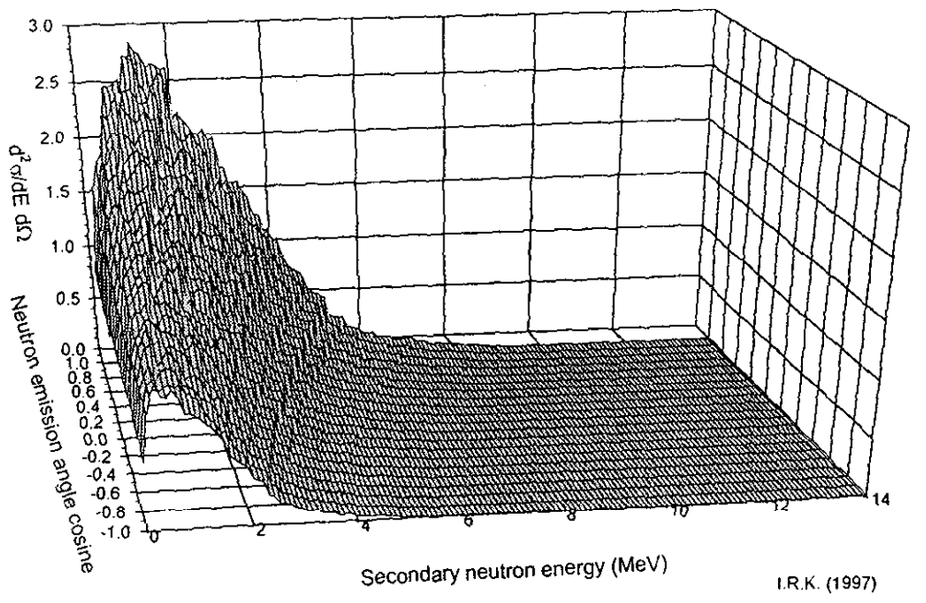

Figure 41: Energy-angular distribution of ^{9}Be(n,2n) secondary neutrons

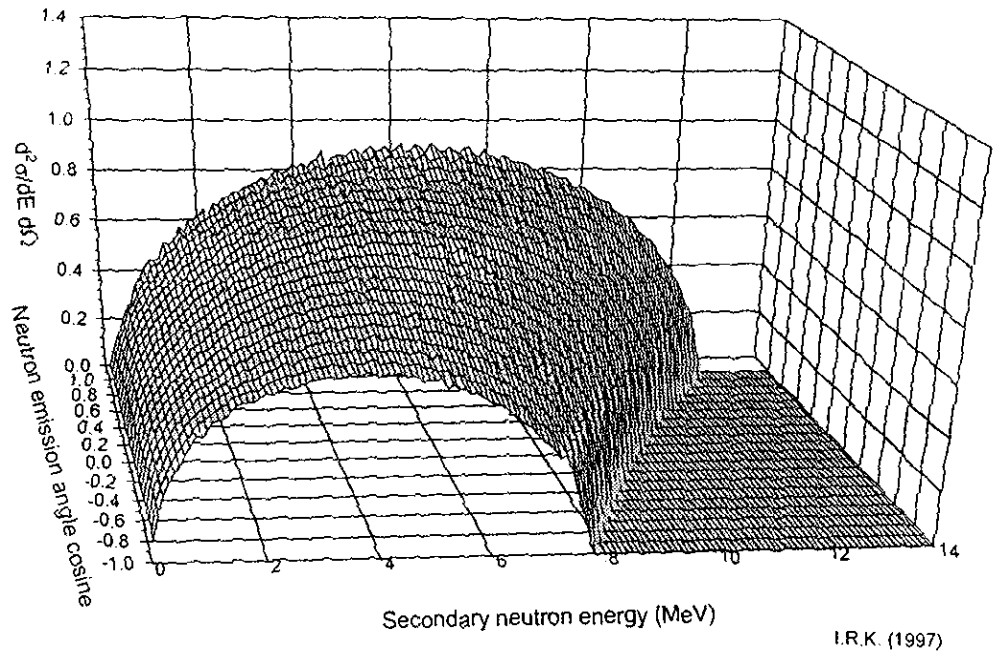

Figure 42: Energy-angular distribution of ^{9}Be(n,2n) secondary neutrons

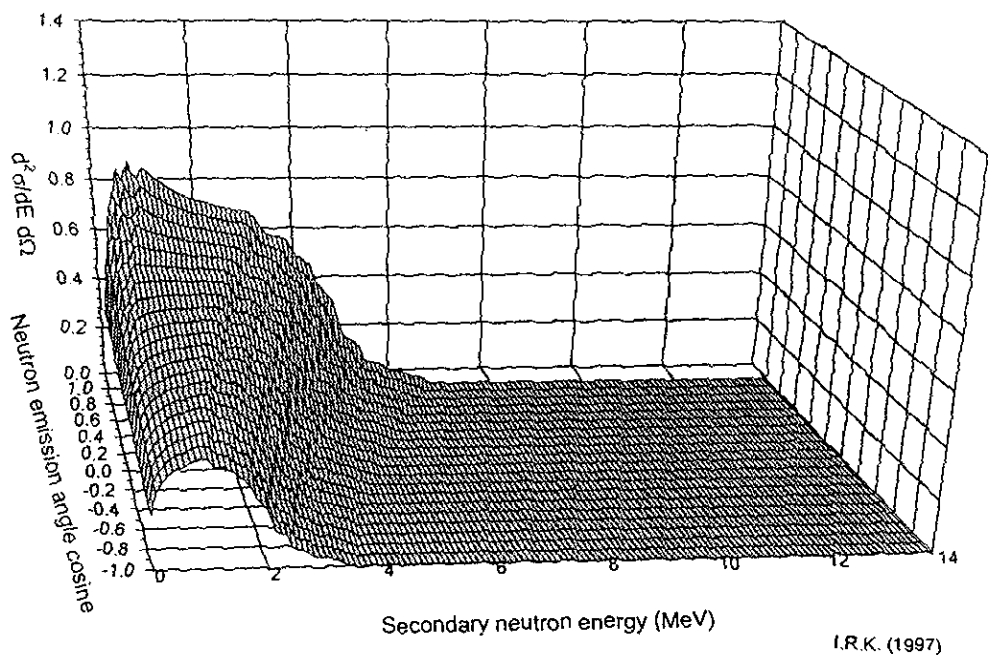

Figure 43: Energy-angular distribution of ^{9}Be(n,2n) secondary neutrons

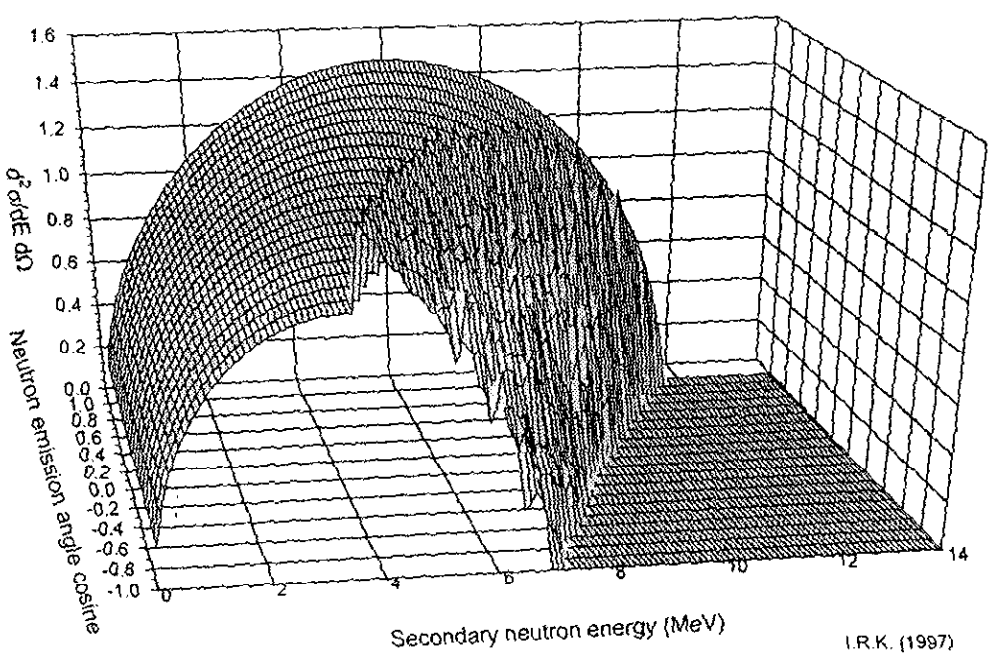

Figure 44: Energy-angular distribution of ^{9}Be(n,2n) secondary neutrons

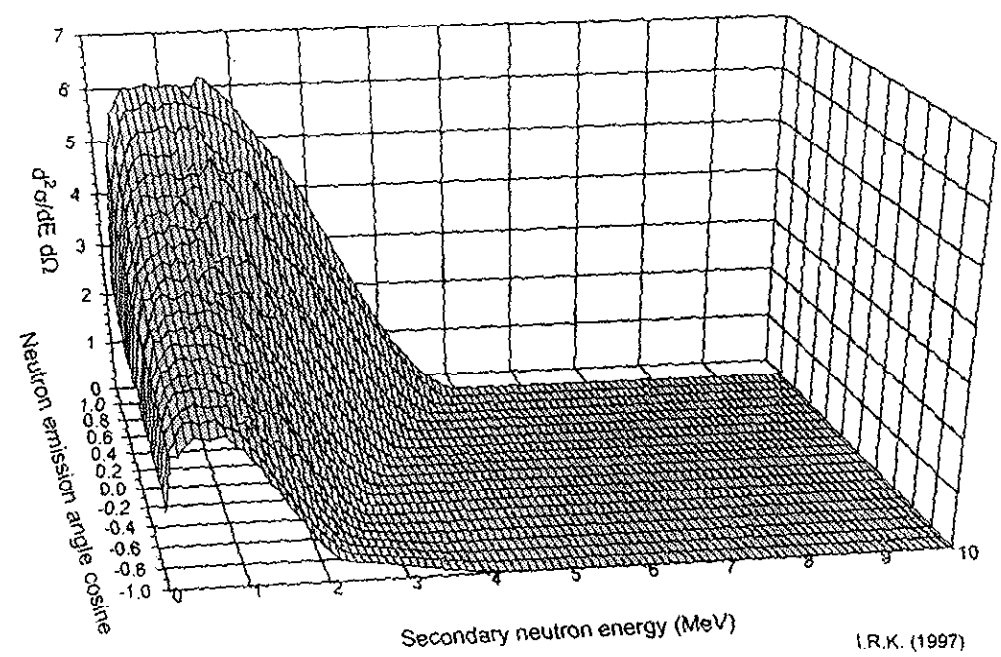

Figure 45: Comparison GLUCS results versus experimental data

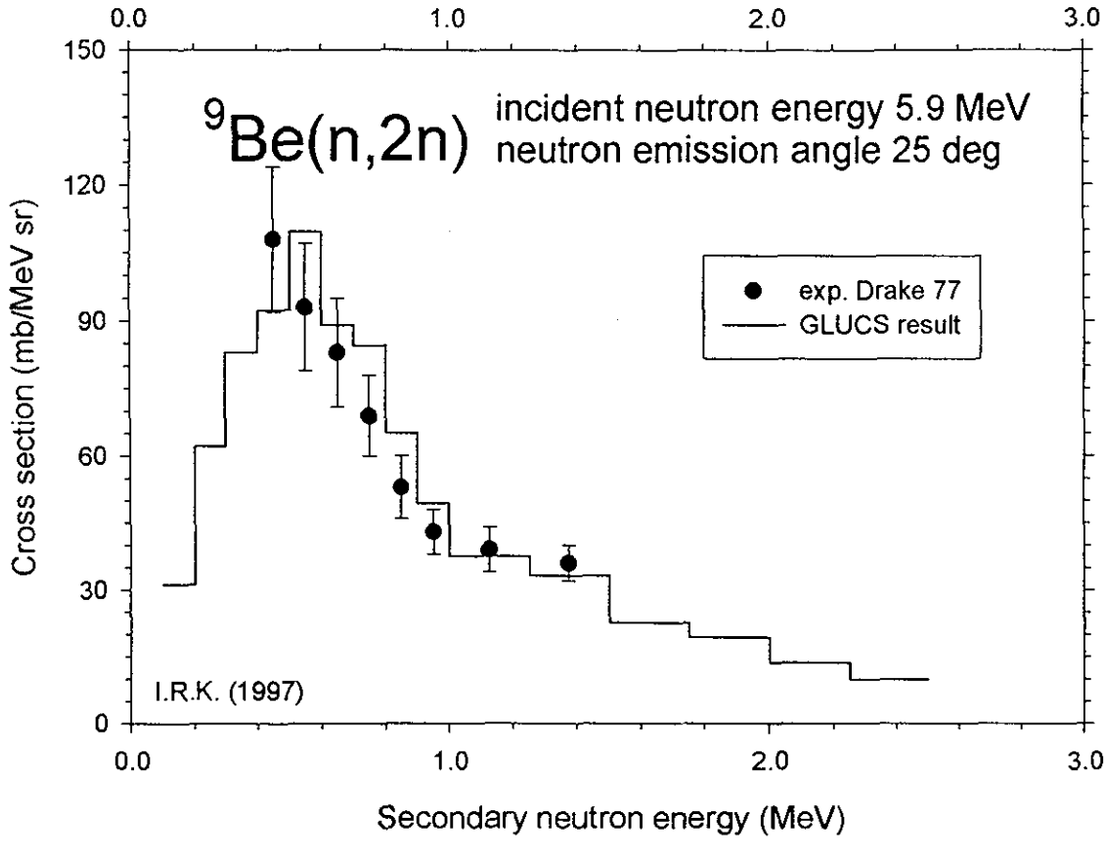

Figure 46

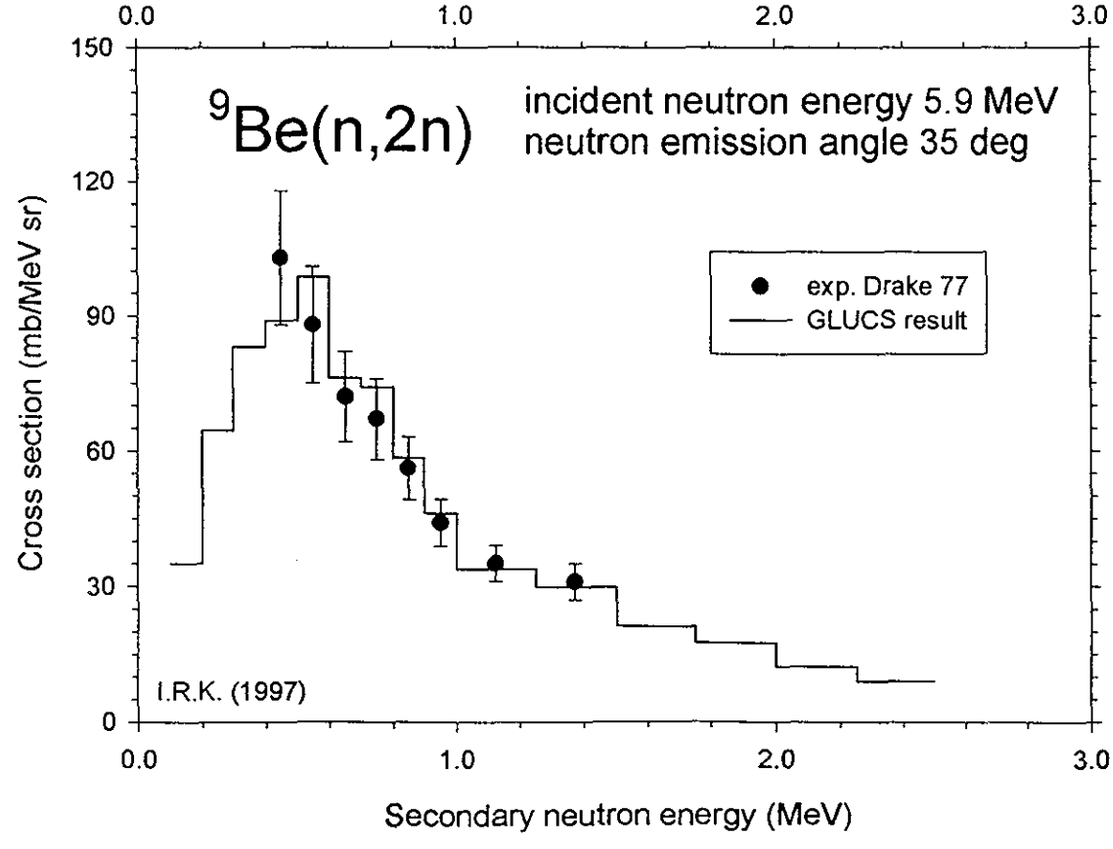

Figure 47: Comparison GLUCS results versus experimental data

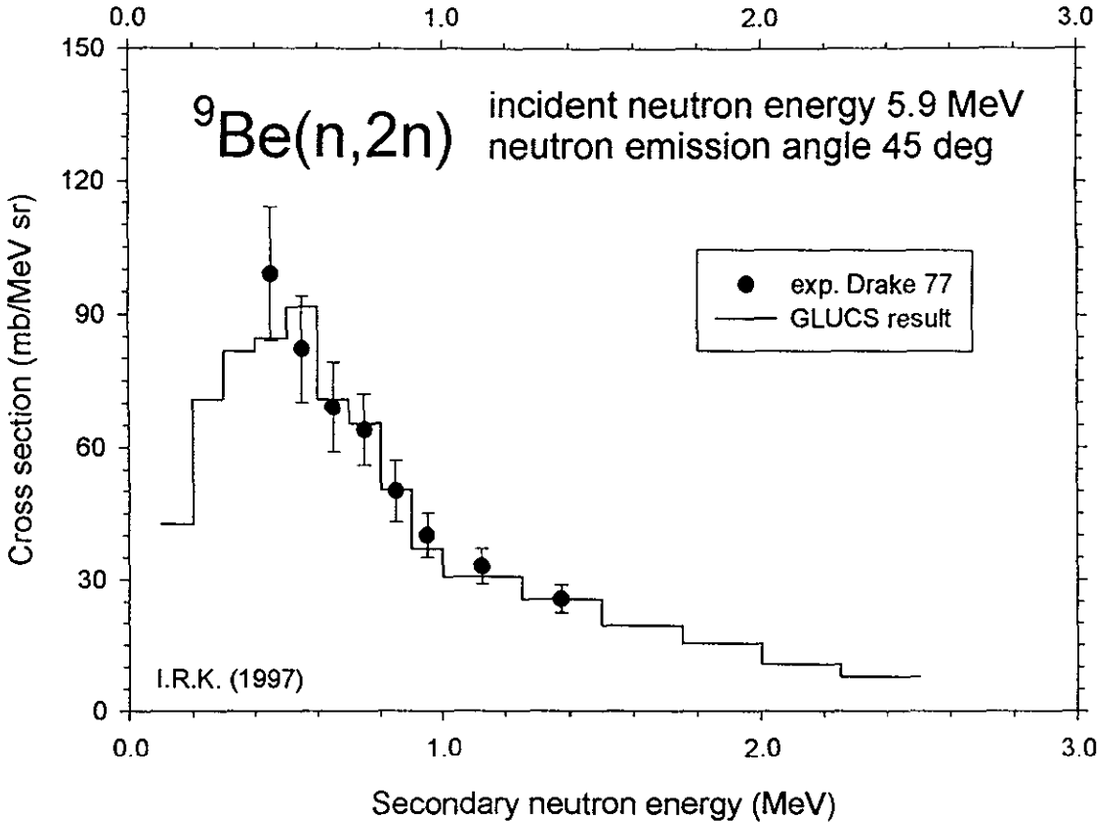

Figure 48

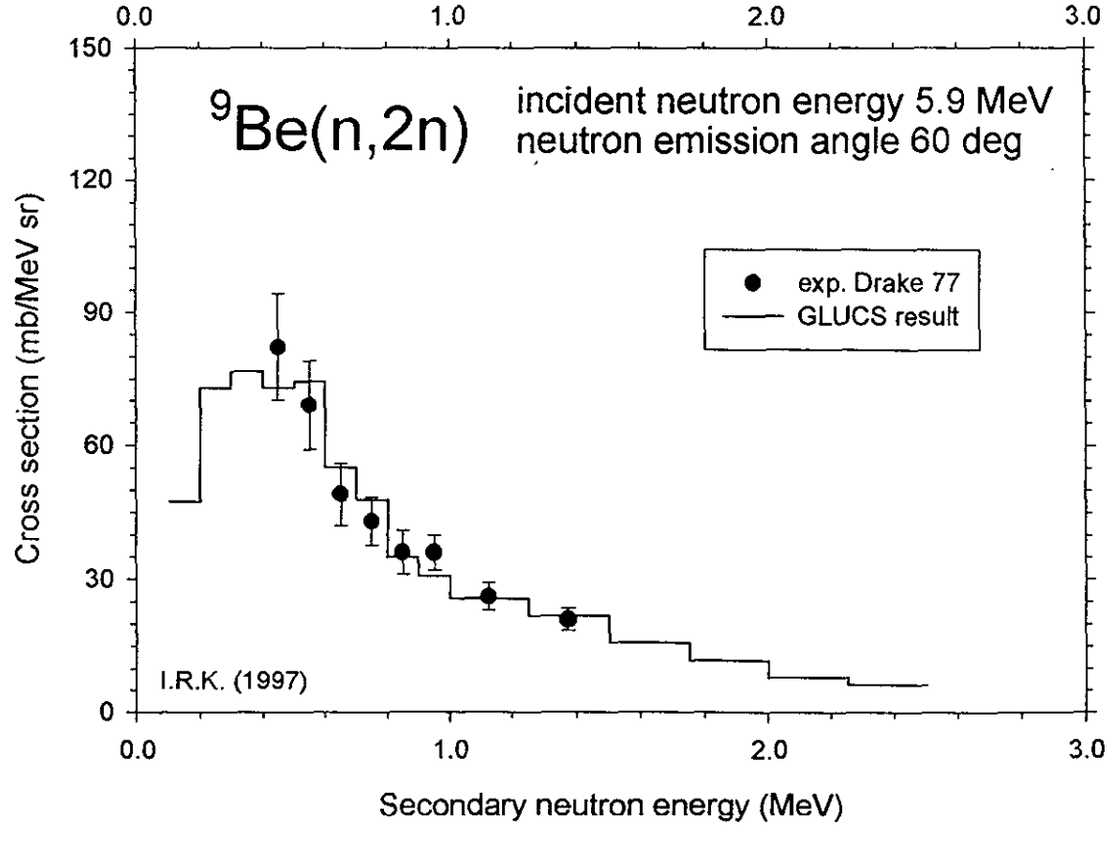

Figure 49: Comparison GLUCS results versus experimental data

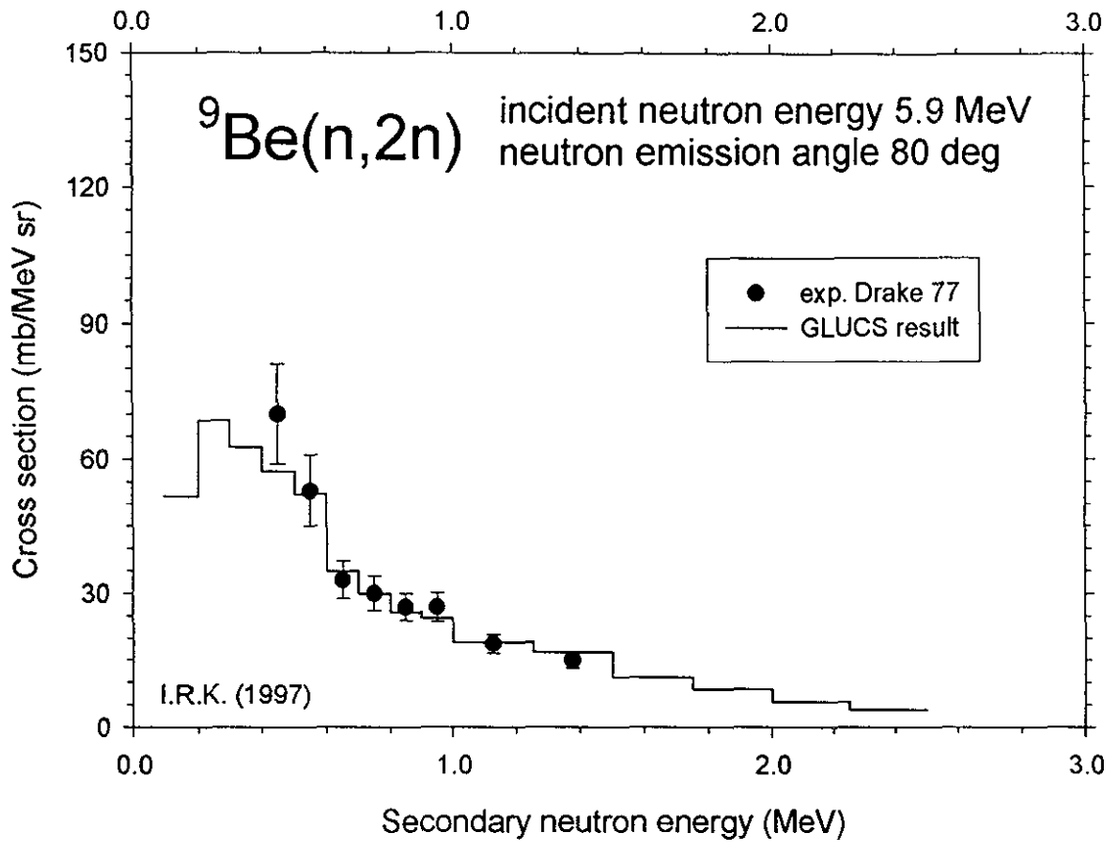

Figure 50

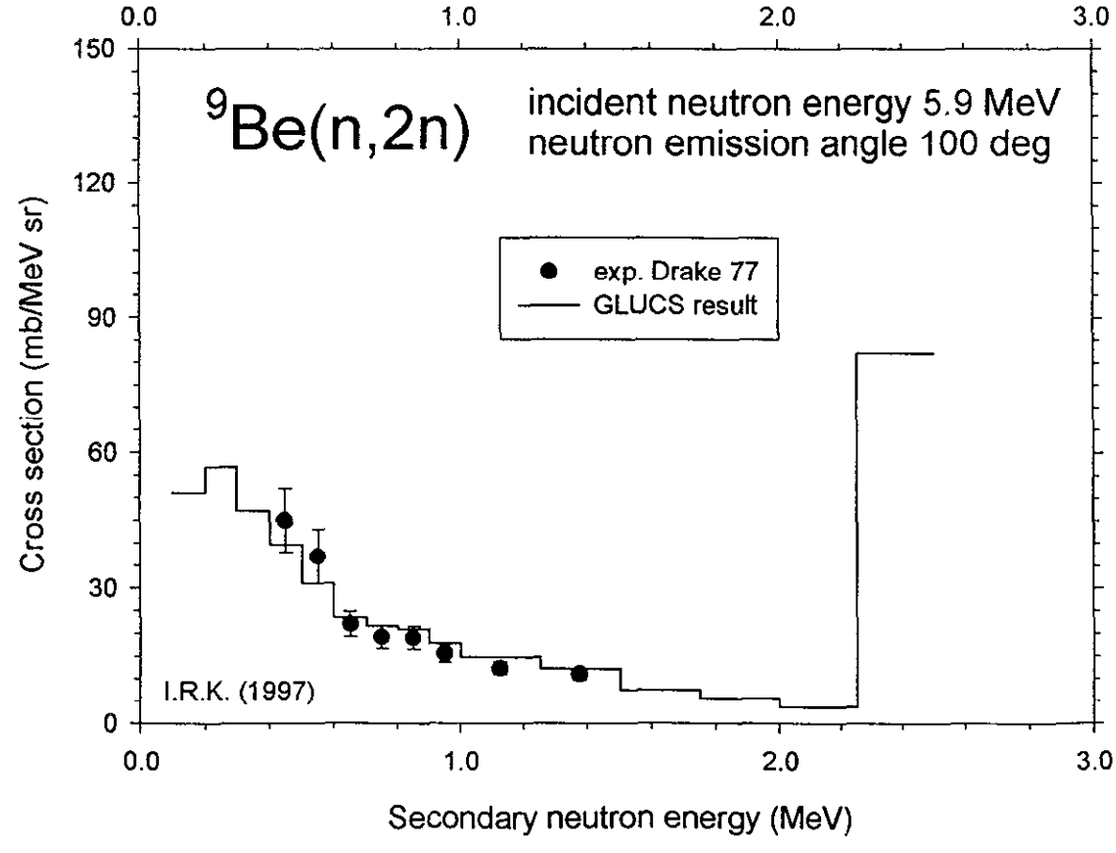

Figure 51: Comparison GLUCS results versus experimental data

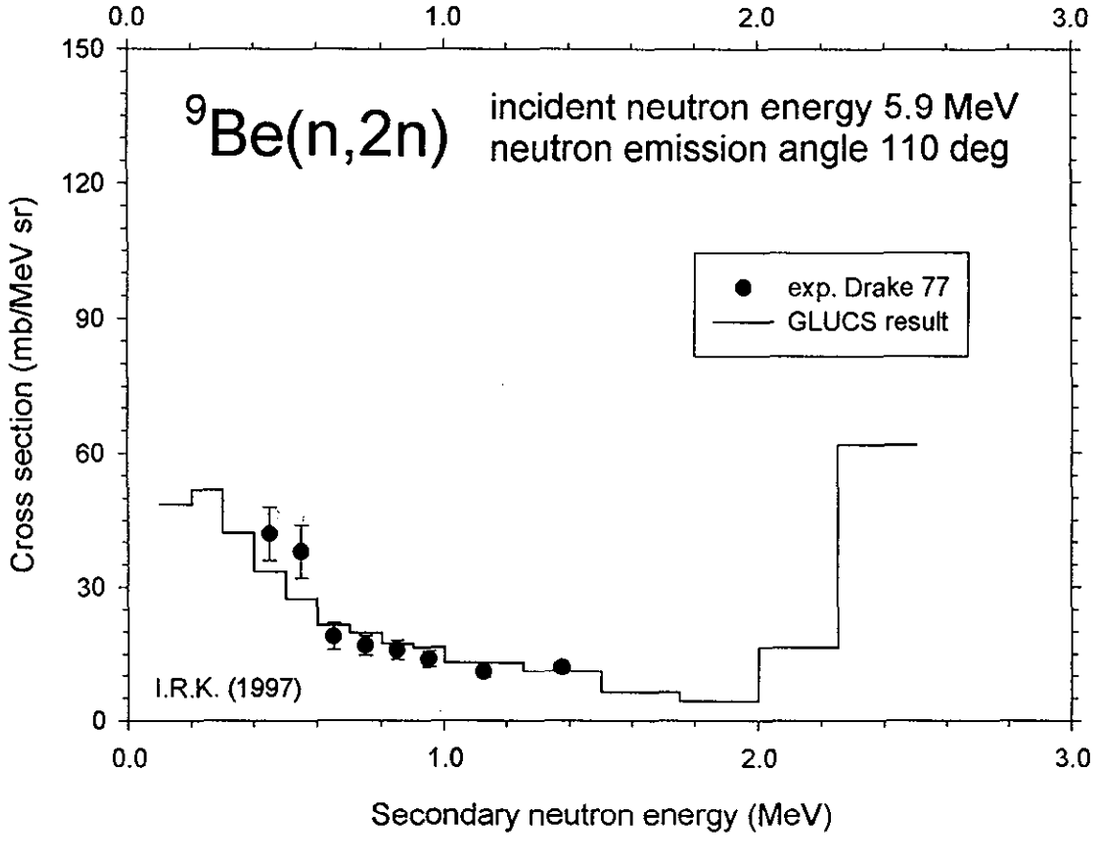

Figure 52

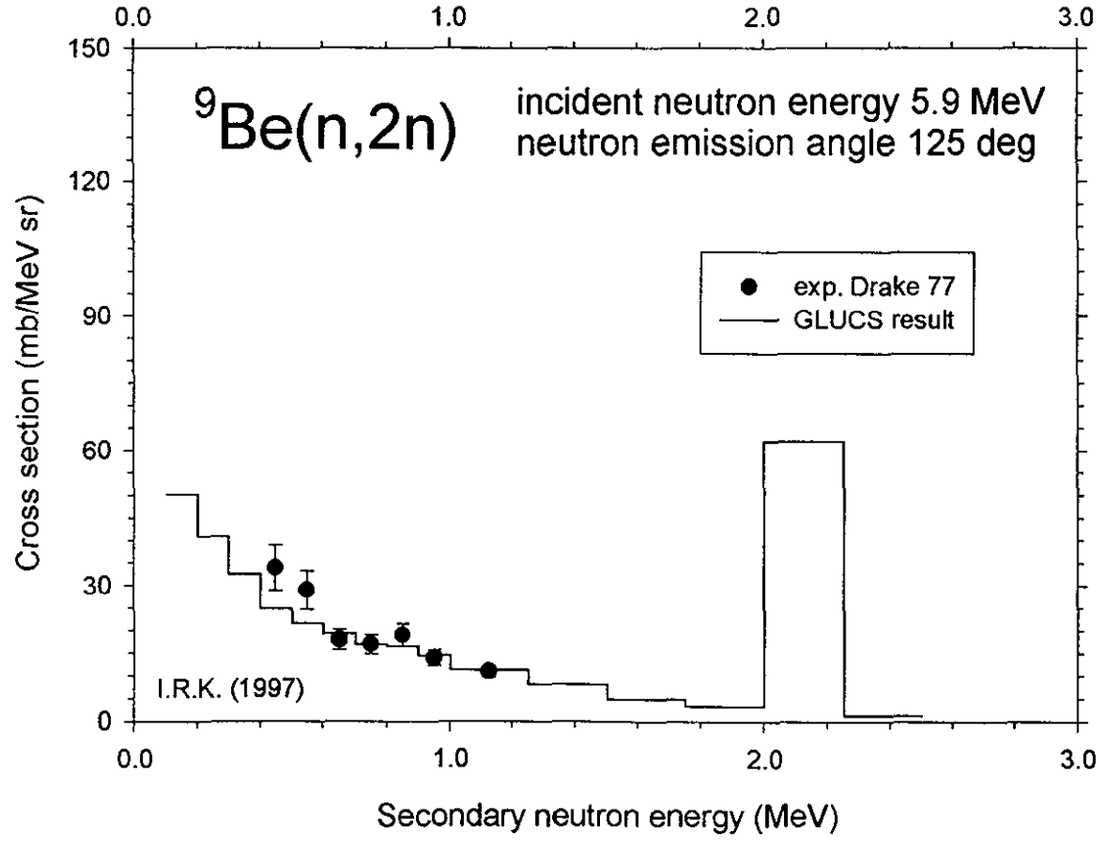

Figure 53: Comparison GLUCS results versus experimental data

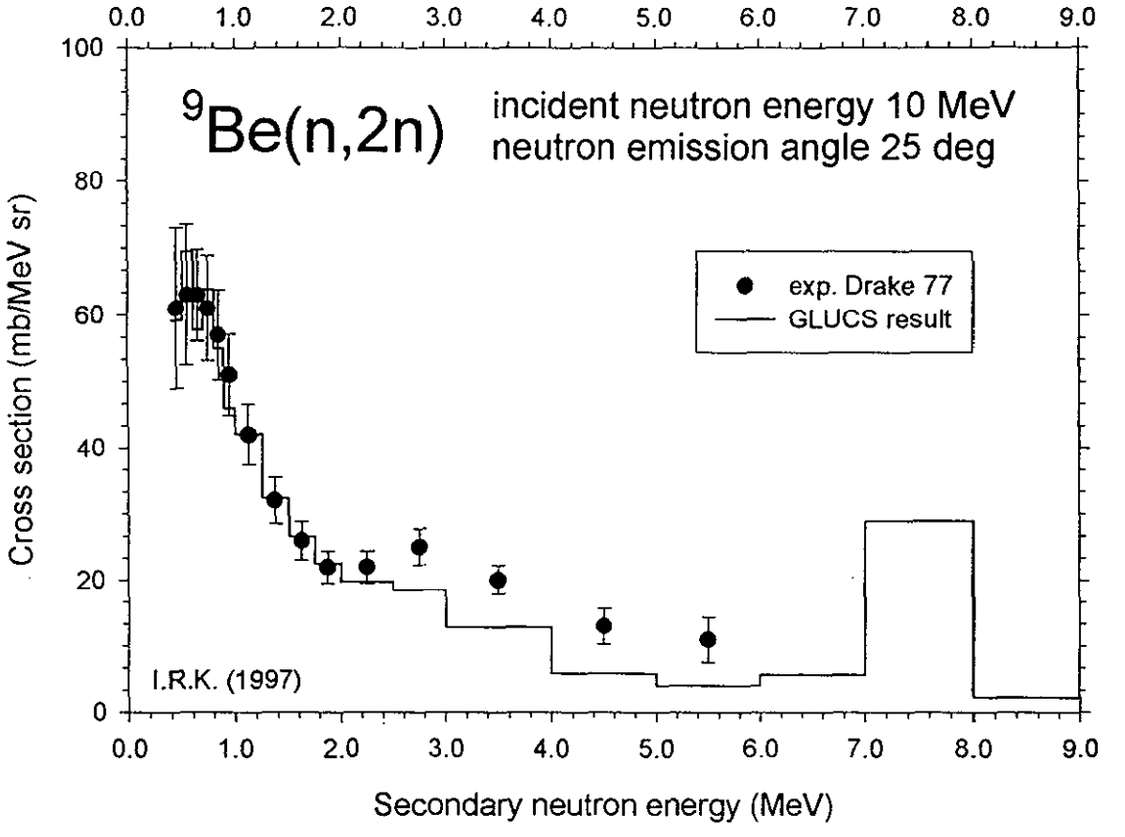

Figure 54

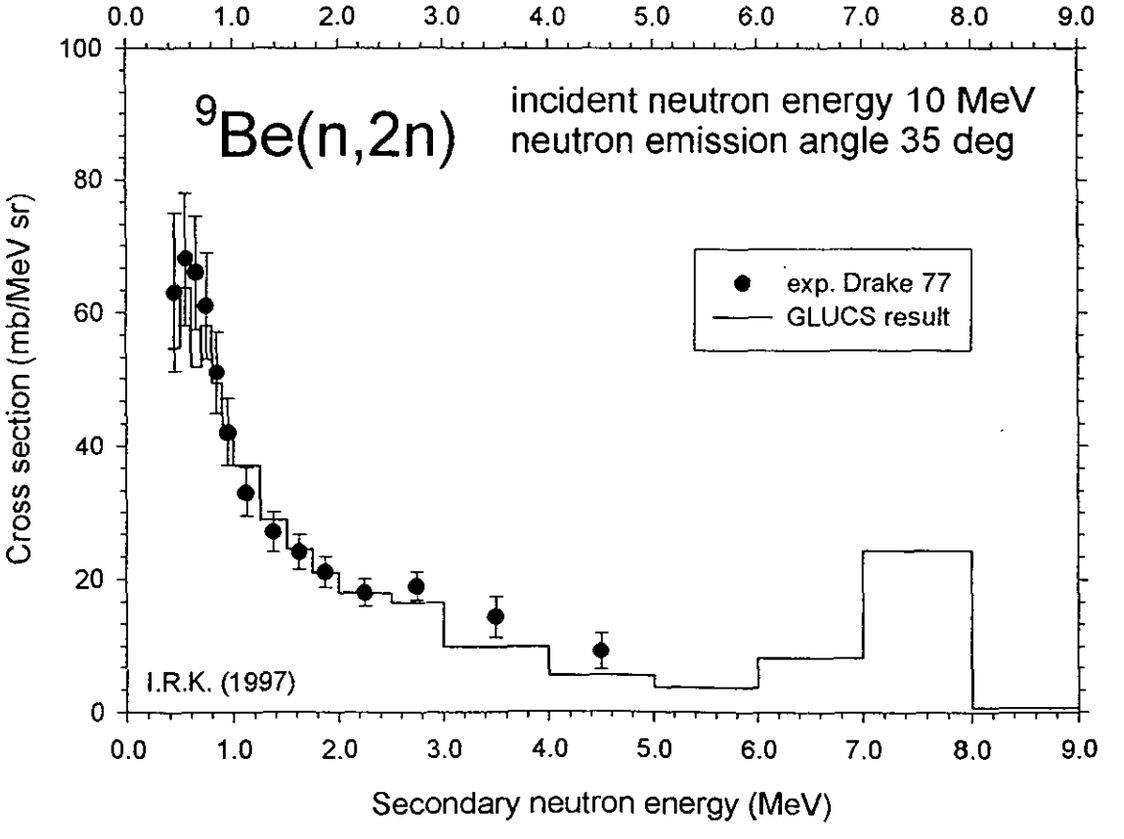

Figure 55: Comparison GLUCS results versus experimental data

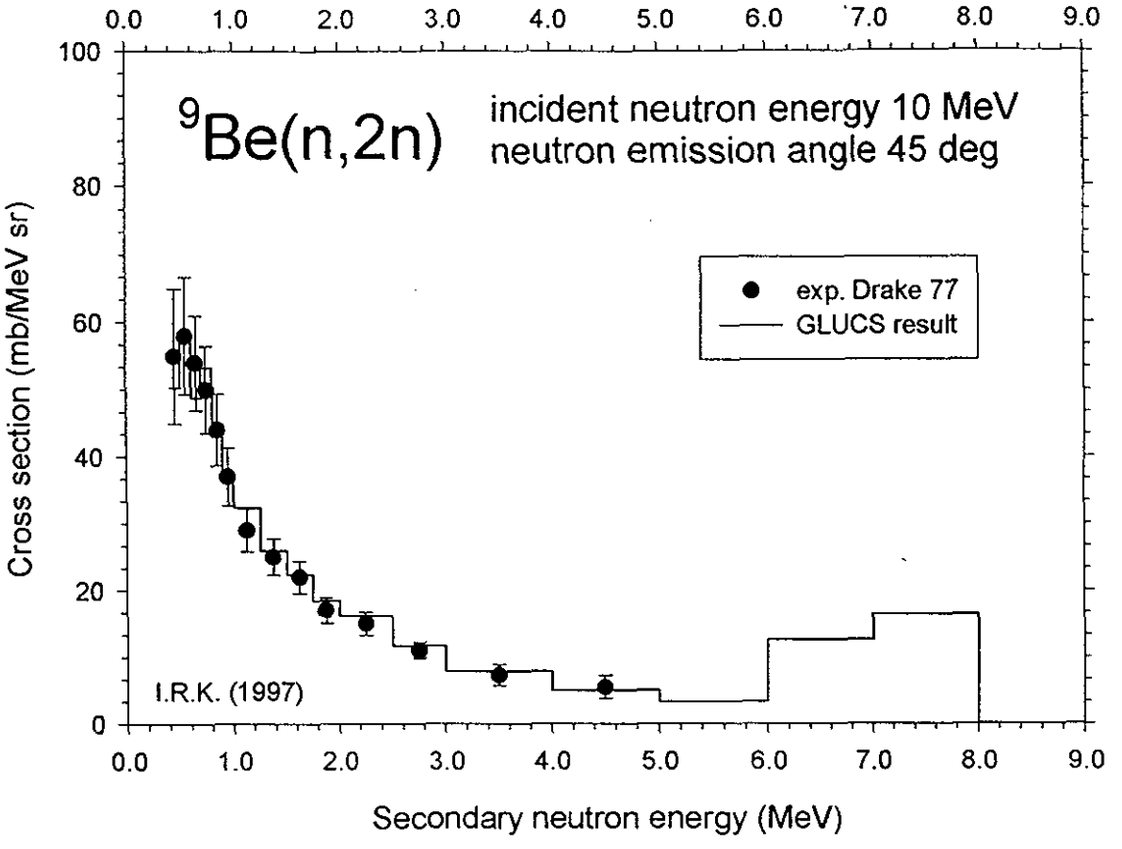

Figure 56

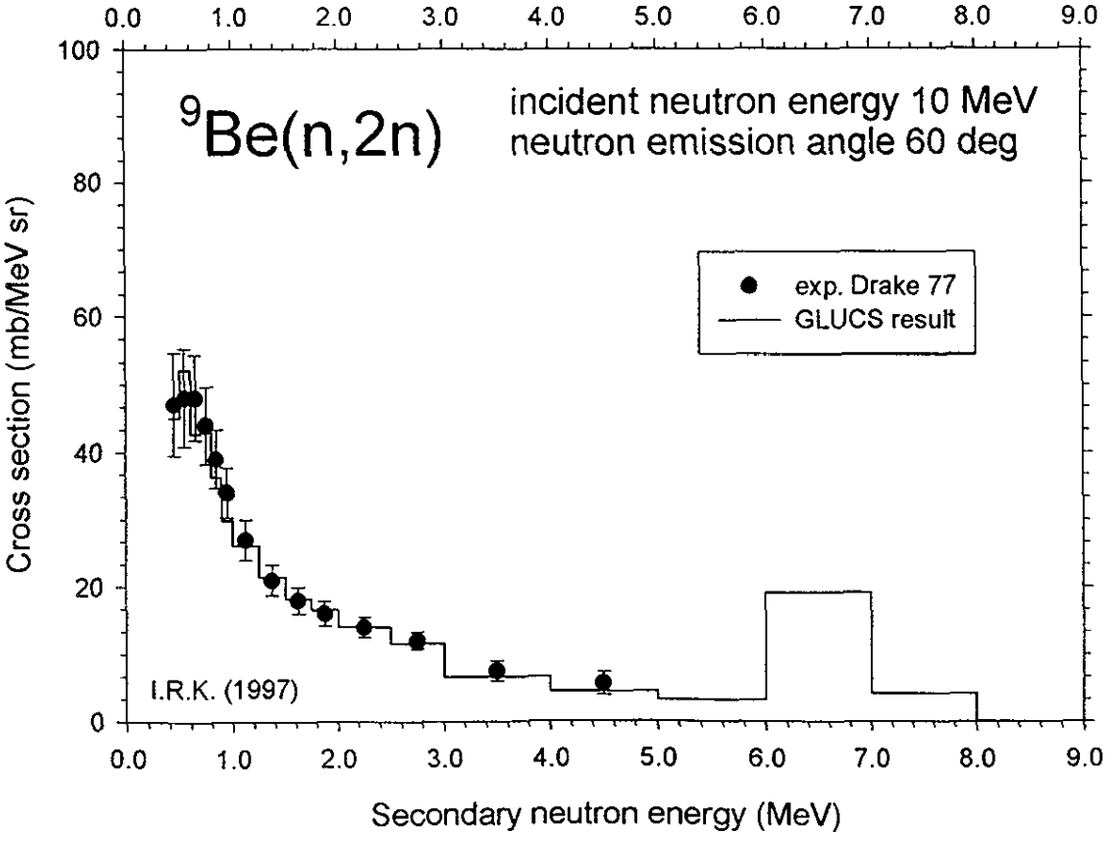

Figure 57: Comparison GLUCS results versus experimental data

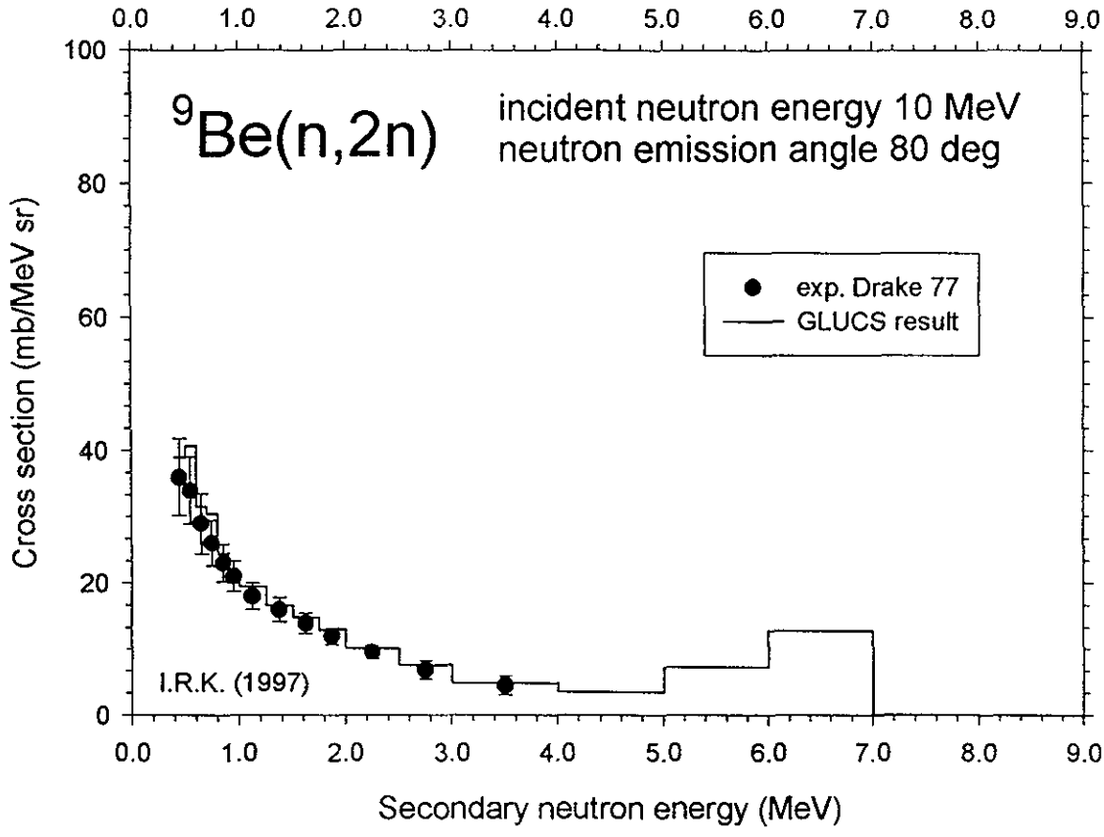

Figure 58

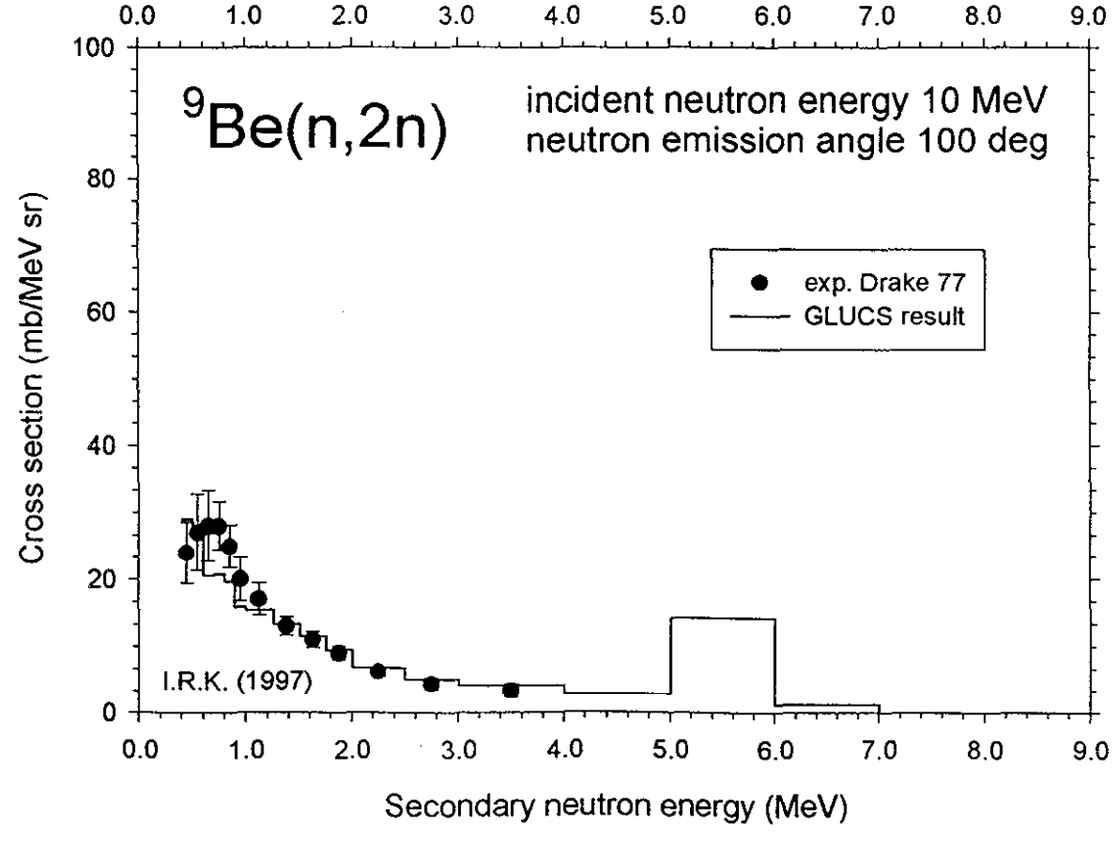

Figure 59: Comparison GLUCS results versus experimental data

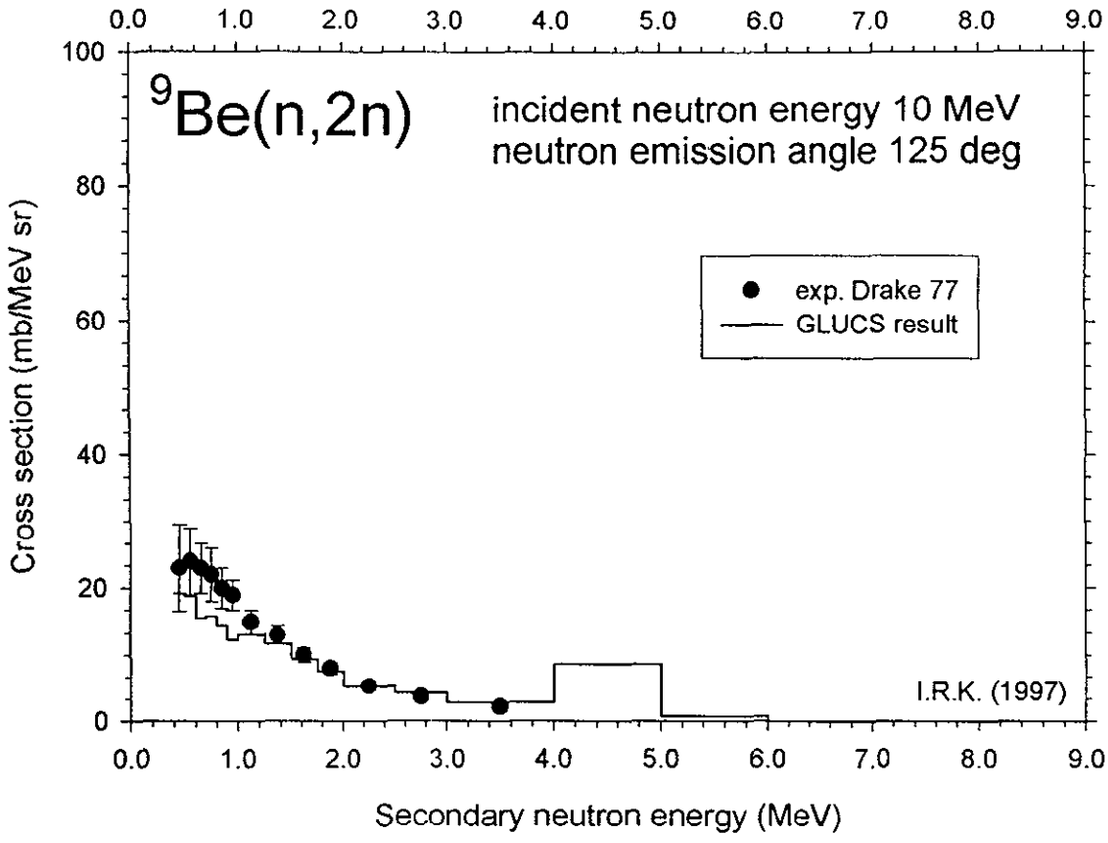

Figure 60: Comparison GLUCS results versus experimental data

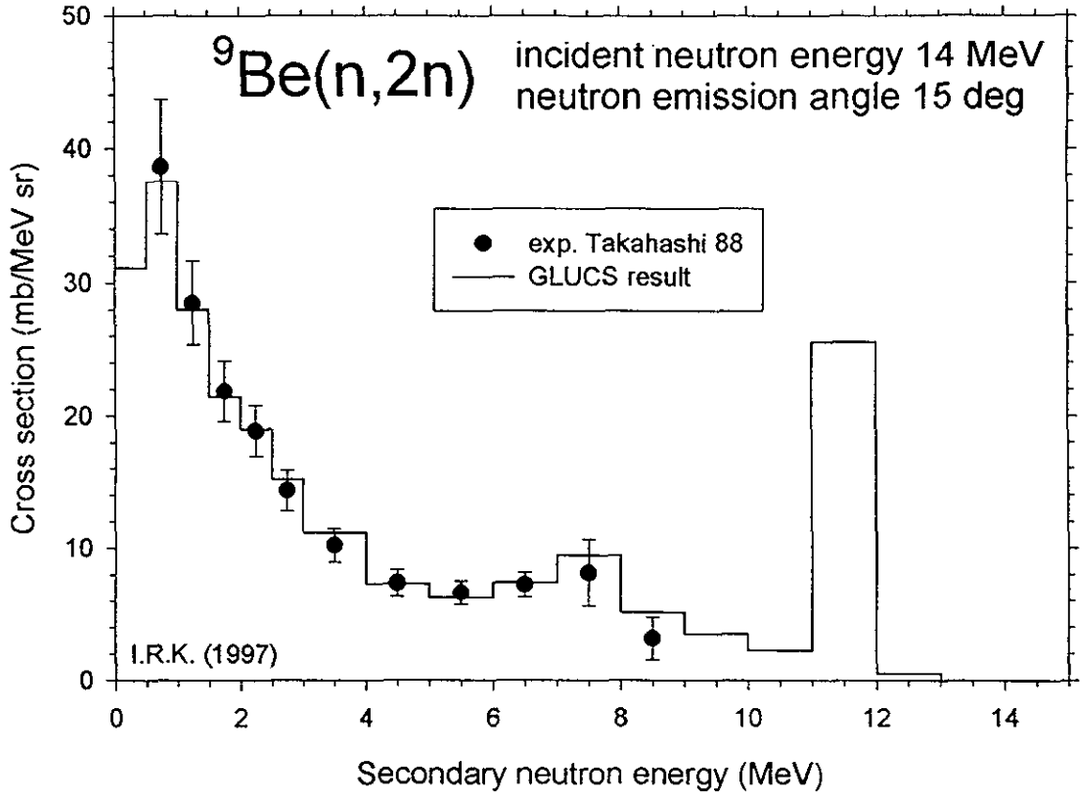

Figure 61

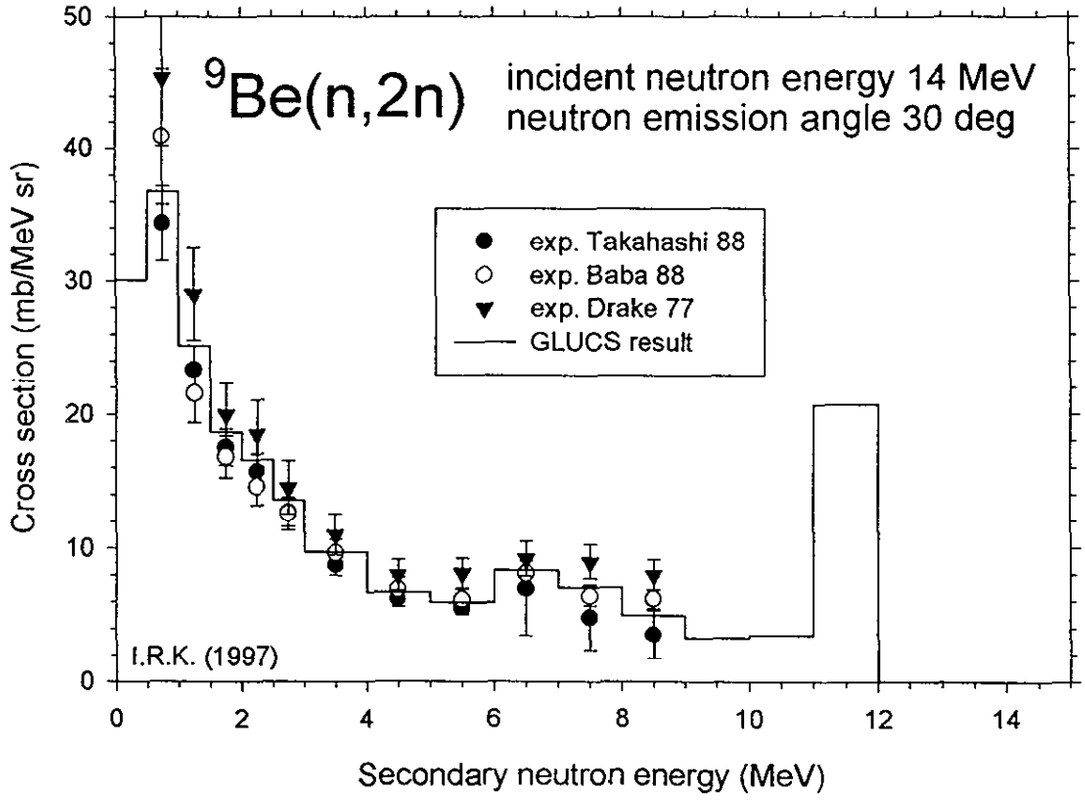

Figure 62: Comparison GLUCS results versus experimental data

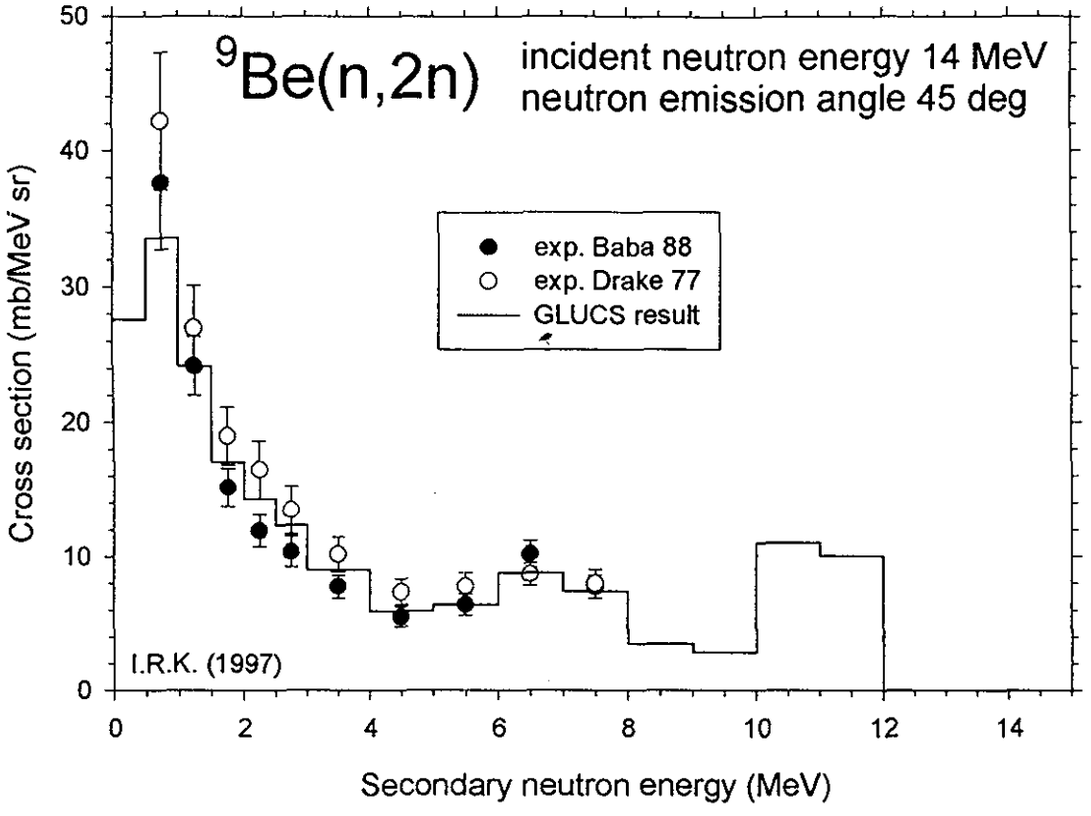

Figure 63

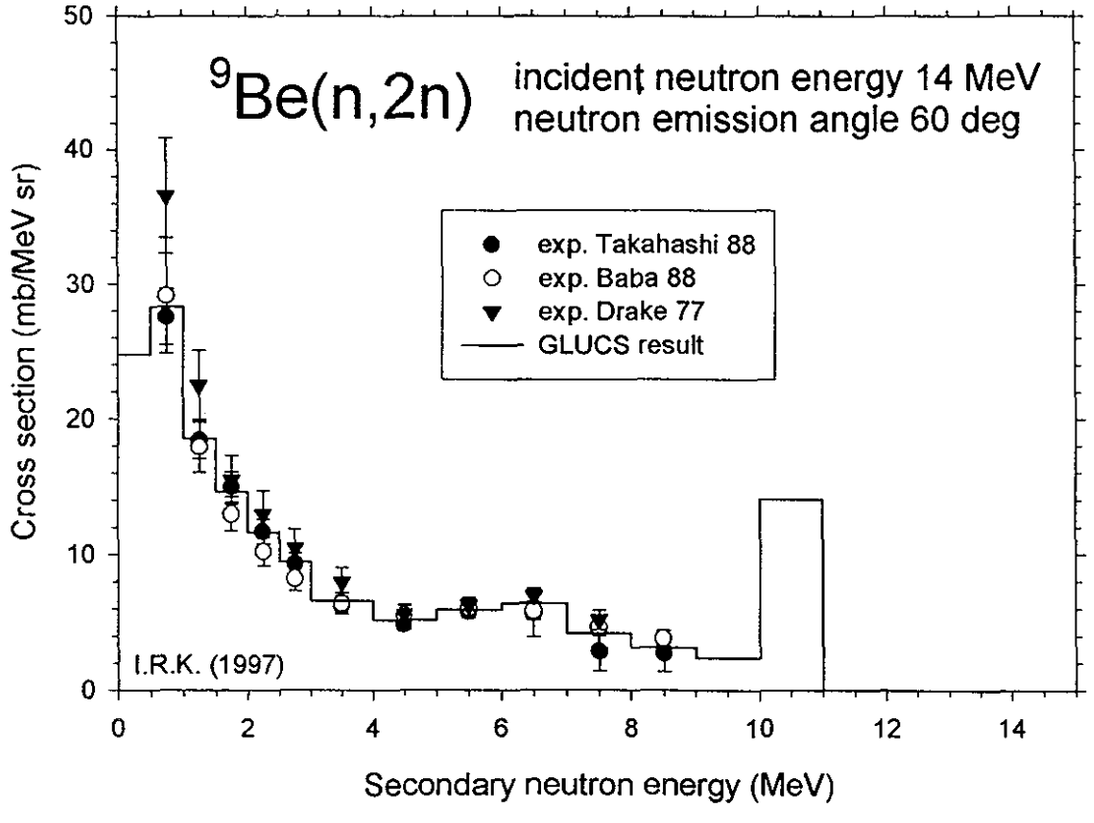

Figure 64: Comparison GLUCS results versus experimental data

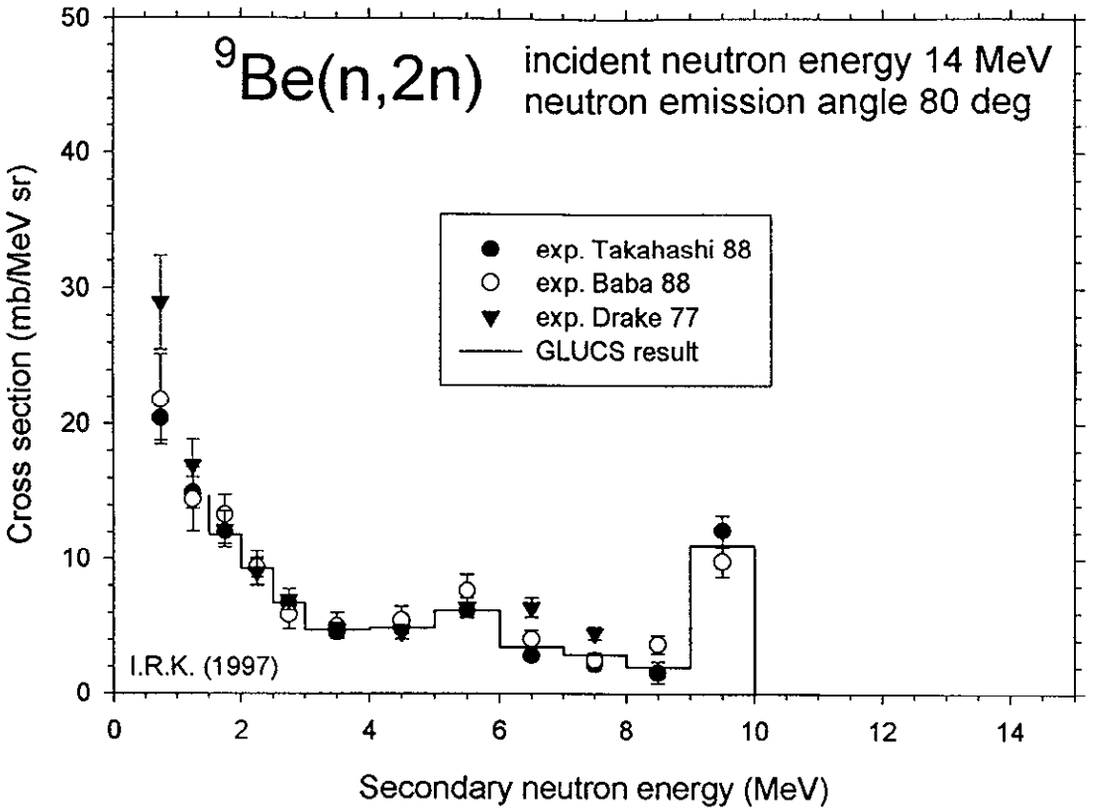

Figure 65

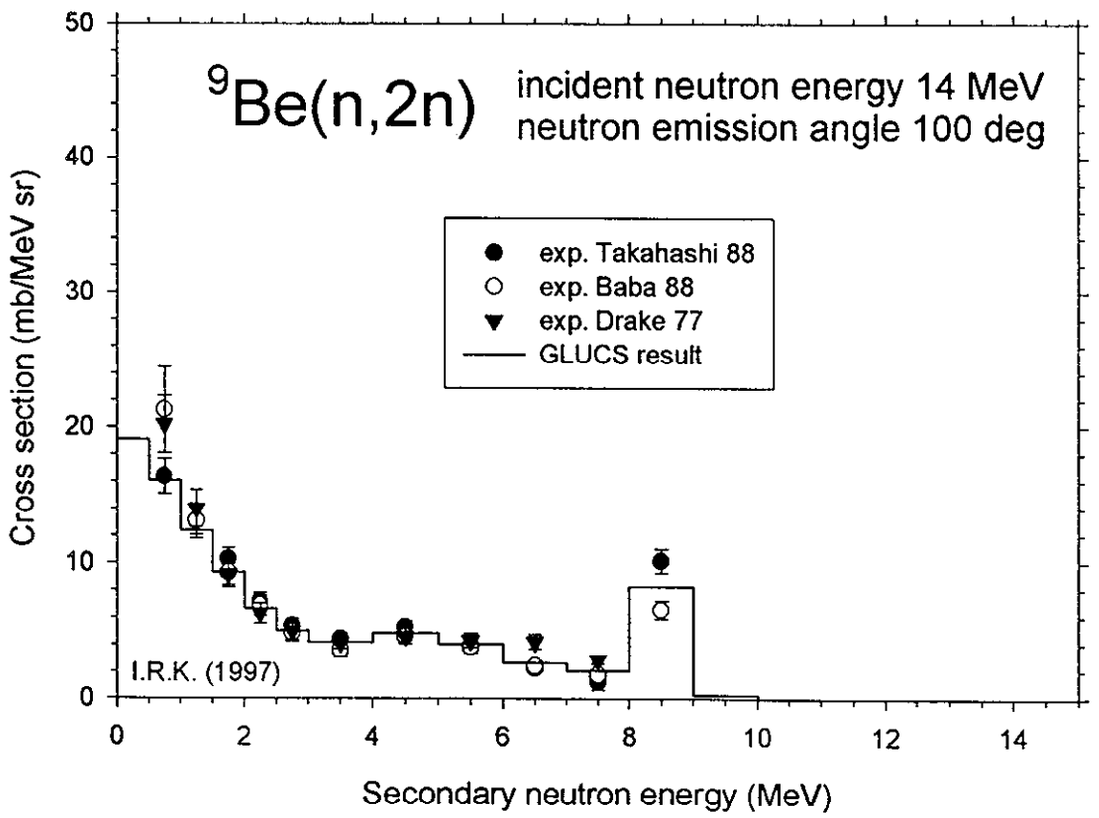

Figure 66: Comparison GLUCS results versus experimental data

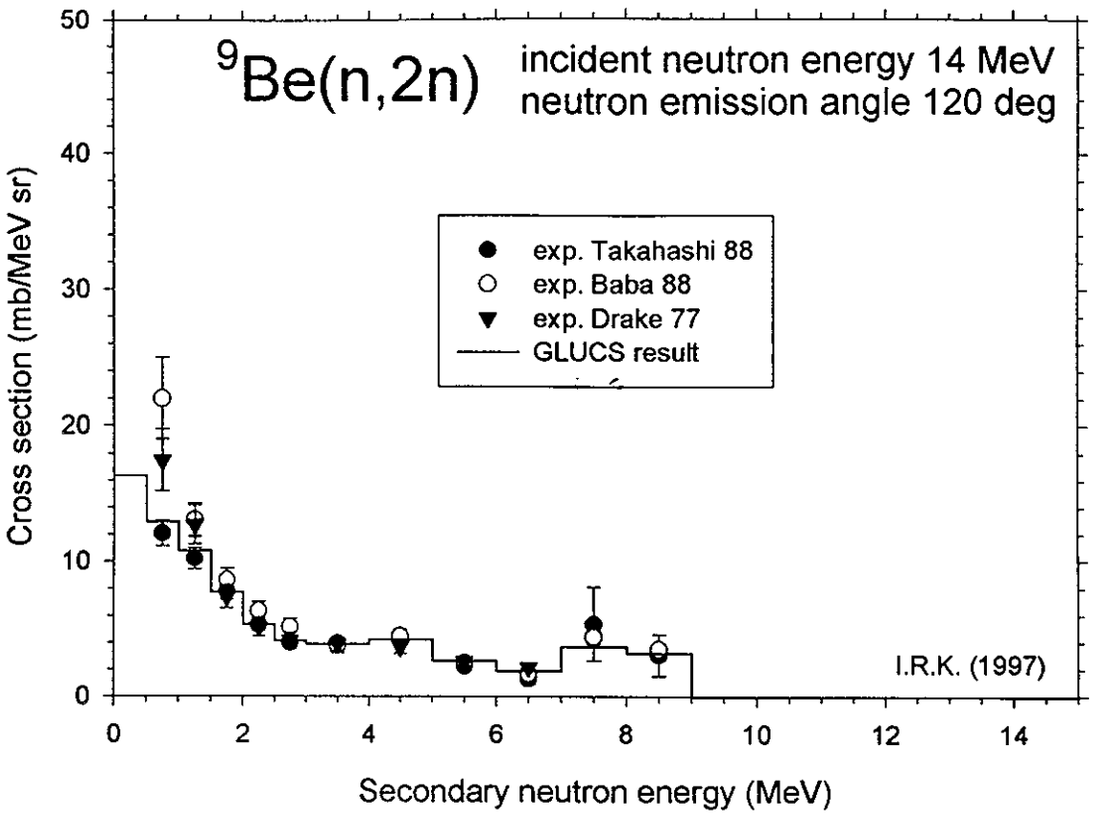

Figure 67